An Innovative Approach to Heat Extraction from a Salinity Gradient Solar Pond to Enhance Overall Efficiency

A thesis submitted in accordance with the regulations for the degree of Doctor of Philosophy

Yusli Yaakob

M.Sc. (Mechanical)

B.Eng. (Mechanical and Manufacturing)

School of Aerospace, Mechanical and Manufacturing Engineering

RMIT University, Melbourne, Australia

August, 2013

Declaration

I certify that except where due acknowledgement has been made, the work is that of the author alone; the work has not been submitted previously, in whole or in part, to qualify for any other academic award; the content of the thesis is the result of work which has been carried out since the official commencement date of the approved research program; any editorial work, paid or unpaid, carried out by a third party is acknowledged; and, ethics procedures and guidelines have been followed.

Yusli Yaakob

Date : 26 /8/ 2013

Acknowledgements

First and foremost, I offer my utmost gratitude to Allah, the most gracious, the most merciful, for guiding me to a straight path, strength and importantly a good life to me and my family over the years.

The journey of seeking knowledge was never straight and smooth. Great contributions of experts and lovely peoples around me have made these efforts possible.

I would like to express my gratitude to my fatherly primary supervisor Professor Aliakbar Akbarzadeh for his expertise, guidance, continuous support, and patience throughout my research work. He has shared so many valuable things not only in the areas of solar ponds and heat transfer, but also the way to become a good person in life.

Sincere thanks to my second supervisor, Dr. Abhijit Date for his fastidious review of my work and writing and encouragement throughout the study period.

I would like to thanks all my fellow researchers from the Conservation And Renewable Energy (CARE) groups for their friendship, advice and help.

I would like to acknowledge the technical support and help I received from the School of Aerospace, Mechanical and Manufacturing Engineering (SAMME) workshop staff: Don Savvides, Patrick Wilkins, David Goodie, Julian, Jean, Sebastian and many more involved direct and indirectly.

Special thanks to University Technology MARA, Malaysia for providing a scholarship for my study.

I would like to dedicate this thesis to my lovely mum, who passed away in January 2011. The love she laid the prayer she made and restless inspiration she conveyed was priceless towards achieving my objectives.

Finally, special love and appreciations to my wife Dzullijah Ibrahim, my growing sons Muhammad Arif, Muhammad Hakim and Muhammad Nabil for their understanding and patience without which these efforts are impossible.

Table of Contents

List of Figures

List of Tables

Nomenclature

$\dot{m}_c$ Cold water mass flow rate, kg s^{-1}

$\dot{Q}$ Heat extracted/lost, W

C_p Specific heat, J/kg.^oC

ρ Density, kg/m^3

β Thermal expansion, K^{-1}

μ Dynamic viscosity, N.s/m^2

v Kinematic viscosity, m^2/s

α Thermal diffusivity, m^2/s

k Thermal conductivity, W/m. ^oC/ Entry and exit loss factors

g Gravitional force, m^2/s

ΔP Pressure difference, kPa

f_1 Losses due to friction inside thermosiphon pipe

f_2 Losses due to friction inside the heat exchanger coil

Pr Prandtl number

Re_1 Reynolds number through the thermosiphon pipe

Re_2 Reynolds number through the heat exchanger coil

Re_{ct} Reynolds number inside the cooper tube

Ra_{Dhx} Rayleigh number through the heat exchanger coil hydraulic diameter, m

Nu_i Nusselt number inside the copper tube

Nu_o Nusselt number outside the copper tube

A_1 Cross sectional area of thermsiphon pipe, m^2

A_2 Cross sectional area on heat exchanger coil side, m^2

D_1 Diameter of themosiphon pipe, m

D_{ct} Diameter of copper tube, m

D_{co} Outer diameter of heat exchanger coil, m

D_{ci} Inner diameter of heat exchanger coil, m

D_{hx} Heat exchanger coil hydraulic diameter, $\frac{4(A_1-A_2)}{P_w}$, m

P_w Wetted perimeter normal to flow on coil and shell, $\pi(D_1 + D_{co} + D_{ci})$, m

H_1 Height of the thermosiphon pipe, m

H_2 Height of the heat exchanger coil, m

L_{ct} Length of the copper tube, m

V Velocity through heat exchanger coil and shell, m/s

u Velocity in thermosiphon pipe, m/s

T_{hi} Hot Temperature inlet ,^{o}C

T_{ho} Hot Temperature outlet, ^{o}C

T_{ci} Cold Temperature inlet, ^{o}C

T_{co} Cold Temperature outlet, ^{o}C

T_s Heat exchanger coil surface Temperature, ^{o}C

h_i Convection heat transfer coefficient inside the copper tube, W/m^2.^{o}C

h_o Convection heat transfer coefficient outside the copper tube, W/m^2.^{o}C

List of Acronyms

HEX Heat exchanger

Abstract

A solar pond is a simple and low-cost solar collector with long-term thermal storage. It utilizes a large body of salinity gradient water to absorb radiation from the sun and stores it in the form of heat at the bottom of the pond with temperature between 70-90^{o}C. The pond consists of three different layers. The cold thin upper layer is known as the upper convective zone (UCZ) and consists of low salinity water and has temperature close to the local average ambient temperature. The second layer is the gradient layer known as the non-convective zone (NCZ), where salinity increases from the top of the NCZ to the bottom of the NCZ. The bottom layer or lower convective zone (LCZ) has homogenous high salinity water which absorbs and stores solar thermal energy which reaches the bottom of the pond.

Conventionally, heat has been successfully extracted from the LCZ. This study concerns an attempt to extract the absorbed heat from the NCZ using external heat exchangers with the aim of enhancing the overall efficiency of the solar pond. External heat exchangers were fabricated and installed to extract heat from different levels in the NCZ. The process used a 12V pump to withdraw hot brine from the NCZ and re-inject it to the same level. Cold brine from the UCZ was used as a cold heat transfer fluid to extract heat from each of the heat exchangers. The results show that by extracting heat from the NCZ, the thermal efficiency of a solar pond could potentially be improved to 50% as compared with the conventional heat extraction method from the LCZ only.

An adverse effect associated with active heat extraction from the NCZ was the development of instability in the salinity gradient layer. Optimisation of the technique for withdrawal and re-injection of the cooled brine into the NCZ is essential to overcome this issue. It needs to be addressed as a future study.

The other part of the present study was the investigation of a semi-passive thermosiphon heat extraction system for heat removal from the NCZ or LCZ of a solar pond. The thermosiphon heat extraction system relies on buoyancy effects to remove heat by the effect of temperature difference. Theoretical governing equations have been

developed based on principles of conservation of energy and mass. Theoretical analysis revealed great potential for this system to be implemented in solar ponds. Experimental results from a single thermosiphon heat extraction system have been presented for various cooling water mass flow rates. The experimental and theoretical performance estimates were compared and the results showed a good agreement. The experimental findings showed that a thermosiphon heat exchanger has the potential to minimize the use of pumps in heat extraction from solar ponds.

Chapter 1 - Introduction

1.1 Background and Motivation

In October 2011, the world population reached seven billion people. This number is expected to grow rapidly over the next 50 years and has added to a situation where the demand for energy continuously increases. At the same time rapid growth of developing countries is another key factor in the rapid increase in energy demand. Fossil fuels are the major contributors to current world energy consumption, with oil, natural gas and coal contributing more than 80% of world energy demand.

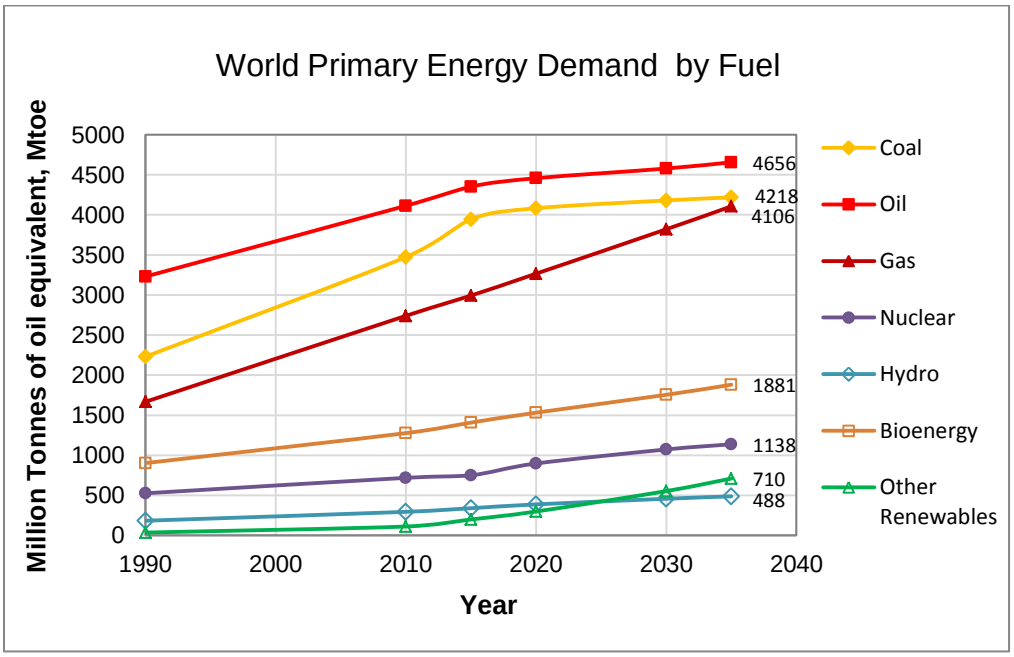

Figure 1.1: World primary energy demand in new policies scenario (Green, Joyce et al. 1987)

Figure 1.1 shows the rising trend of global energy demand from 1990 to 2010, and the projection of global energy demand from 2010 to 2035. Overall, the energy demand is projected to increase by 35% between 2010 and 2035, rising from the present 13,000 million tonnes of oil equivalent (Mtoe) to approximately 17,000Mtoe in 2035 (Green, Joyce et al. 1987). Fossil fuels account for 59% of the overall increase in energy demand. Oil remains the most demanded fuel, followed by coal and natural gas and is projected to reach more than 4,000Mtoe in 2035. World demand for natural gas is projected to increase by more than 50% from the present demand and it is expected to replace the use of coal.

The depletion of fossil fuel reserves globally and serious environmental effects arising from carbon dioxide (CO_2) emission have made fossil fuels unfavourable for future generation usage. According to the IEA, emission of CO_2 from burning fossil fuels increased by 10% in parallel with the world gross energy production from 2004-2008 (IEA 2010). The trend shows a yearly rise of concentration of greenhouse gases in the atmosphere and that it could intensify global warming over the next 50 years.

New types of abundant, less expensive and environmentally friendly energy sources must be developed. A possible option is to tap energy from natural resources. Sun, wind, water, geothermal and even biomass can produce clean non-polluting renewable energy as an alternative to current energy sources. Development and use of renewable energy in the long term will secure energy supplies as well as contributing to the reduction of the global environmental impact and possibly being commercially attractive (Asif and Muneer 2007). Many developed countries including the USA, Germany, Spain, Australia and Japan have introduced variations of policies and incentives to promote the application of renewable energy in domestic, commercial, industrial and transportation sectors (Dincer 2011, Solangi, Islam et al. 2011).

Table 1.1 Renewable energy sources, annual production and global demand (Silvi 2001)

Sources	Annual production (TJ)	Global Demand (%)
Solar thermal	228720	0.532
Solar thermal (electric)	1200	0.003
Photovoltaic	630	0.001
Geothermal	128060	0.292
Geothermal (electric)	151390	0.345
Wind	35760	0.082
Tidal	2160	0.005
Total	547920	0.806

Table 1.1 shows the production of renewable energy compared with global demand in 2001. The highest global demand in 2001 was for solar thermal. It was higher by more than 50% than the global demand for solar thermal producing high temperature for generating electricity. In 2008, solar thermal combined with geothermal energy contributed 2% of the total renewable energy production and contributed 27% of the global demand for heat (Seyboth, Matschoss et al. 2012). Distribution of energy consumption indicated that approximately 13% of industrial applications including dairy, tinned food, textiles, paper, chemical, meat processing, beverages and many others require low temperature thermal energy at up to 100^{o}C (Mekhilef, Saidur et al. 2011). Electricity in advanced societies accounts for less than 20% of consumption against 80% in the form of fuel and heat, where the greatest share of heat is consumed at low temperature (Silvi 2008). Evacuated tubes and flat plates are two popular methods of producing low grade temperatures for solar thermal hot water systems, but, they are

limited to small scale applications. Consequently, intensive research is needed to exploit the sourcing of low temperature energy from the sun.

1.2 Solar energy

The sun is the most abundant energy source available on earth. The total solar energy absorbed by the earth's atmosphere, oceans and land masses is approximately 3,850,000 exajoules (EJ) per year (Smil 2006). The value of the solar constant for the earth's surface is 1373 W/m^2 with a probable error 1-2% (McVeigh 1977). The solar constant is a term used to define the rate at which solar radiation is received outside the earth's atmosphere perpendicular to the solar beam, at the earth's mean distance from sun. The amount of energy provided by sun in one hour is more than human civilization uses every year (Morton 2006).

Solar thermal technology can be used to collect solar energy and store it in the form of low temperature heat (< 100^oC) or at high temperature up to 500^oC. Non-concentrating collectors can be used to supply low grade heat for domestic hot water supply, space heating for residential, commercial and institutional building and for industrial process heat. Concentrating types of solar thermal collector can provide high grade heat to operate heat engines.

The solar pond is another type of collector for producing large amounts of low temperature heat inexpensively. Solar pond technology existed more than 50 years ago. It has the ability to store heat from sun at between 70^oC and 90^oC, for long periods as demonstrated in El Paso Texas (Swift, Reid et al. 1987). The next section provides a basic description of a solar pond.

1.3 Solar pond

A salinity gradient solar pond (SGSP) simply uses a large body of salty water as a medium to collect and store heat from the sun. Physically, it consists of three different layers as shown in Figure 1.2. The cold thin upper layer is known as the upper convective zone (UCZ) and consists of low salinity water (2-3% saline). The temperature of the UCZ follows the daily average ambient temperature. The second layer is the gradient layer known as the non-convective zone (NCZ), where salinity increases from the top of NCZ to the bottom of the NCZ. The associated density gradient helps to suppress heat loss by natural convection. The bottom layer or lower convective zone (LCZ) has homogenous high salinity water which absorbs and stores solar thermal energy which reaches the LCZ in form of radiation.

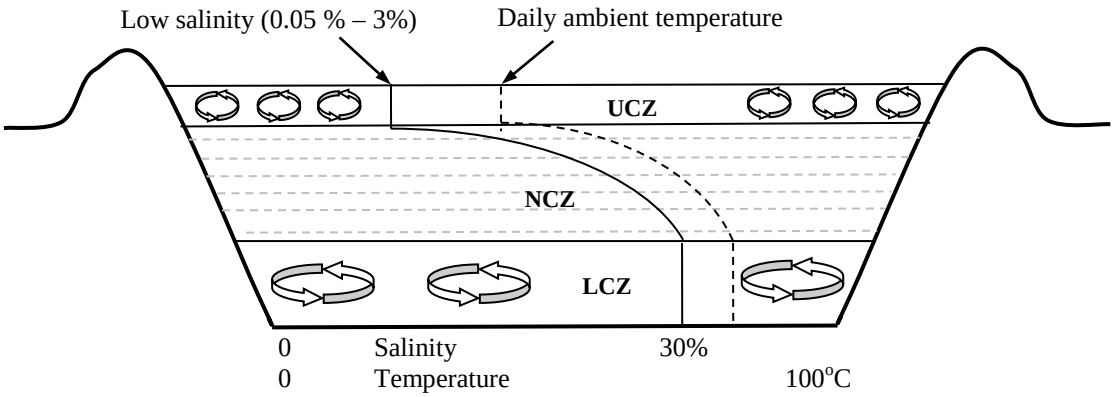

Figure 1.2 Schematic of salinity gradient solar pond

Conventionally heat is extracted from the LCZ of a solar pond by an in-pond or external heat exchanger. The uses of heat from solar ponds include space heating, greenhouse heating, industrial process heat, water desalination, and chemical process heat and power generation. The main concern with solar ponds technology is low efficiency which averages 11% to 15% when delivering heat (Weinberger 1964, Tabor 1981). Solar pond

efficiency is defined as the ratio of the total amount of heat extracted to the amount of solar radiation received at the surface of the pond.

Heat extraction is the process of collecting the stored heat from the LCZ of the solar pond. The current research is concerned with exploring a new method of heat extraction from the NCZ to increase the overall efficiency of solar ponds to up to 50% when delivering heat. Heat extraction was commonly carried out in an active mode using a pump. This research investigates the possibility of eliminating the pump by using the passive mode of a thermosiphon heat exchanger which is similar to a concept used in flat plate solar heat collectors. A solar pond with improved efficiency and without the need for a pump in the heat extraction system will be commercially more attractive and can benefit many sectors globally.

1.4 Objectives, research questions and scope of study

The current study has the following objectives;

i. To investigate the feasibility of heat extraction from the gradient layer (NCZ) using an external heat exchanger to enhance the overall efficiency of the solar pond.

ii. To develop a thermosiphon based heat exchanger for passive heat extraction from solar pond.

The research questions that arise from the above objectives are;

i. Is it feasible to implement heat extraction from the NCZ using an external heat exchanger?

ii. How much efficiency improvement can be achieved?

iii. What would be the effect of heat extraction from NCZ on the stability of a solar pond?

iv. Would it be possible to eliminate the use of pump in a conventional heat extraction system?

To answer the research questions and subsequently to achieve the research objectives, the following activities / tasks are followed,

i. Literature survey to understand previous and current developments of solar ponds.

ii. Feasibility study on the RMIT solar pond by monitoring its thermal performance for a year and learning good practice for maintaining a working solar pond.

iii. A further literature survey relating to attempts to improve thermal performance of solar ponds and investigating previous work on extracting the heat from the NCZ.

iv. Investigate and understand theoretically the penetration of solar radiation into clear water, to verify the amount of heat entering the LCZ and the remaining heat available in the NCZ.

v. Theoretical investigation of active heat extraction based on the performance of each heat exchanger to be installed.

vi. Design and development of an active system for extracting heat from the NCZ by introducing multi-layer brine removal with re-injection to the same level.

vii. Fabrication, installation and experimental investigation of an active heat extraction system from the NCZ at the RMIT solar pond.

viii. Investigating the effect of heat extraction from the NCZ on the stability of the salinity gradient.

ix. Theoretical investigation of passive heat extraction using a thermosiphon heat exchanger.

x. Experimental validation of the theoretical model for a thermosiphon heat exchanger.

xi. Conclusion & future work

1.5 Methodology

Comprehensive literature review is carried out to improve understanding of the working of solar ponds. This includes the theory of solar pond technology and previous works related to solar pond operation. The latter concentrates on works related to heat extraction and improvement on solar pond thermal efficiency which have been published in peer-reviewed journals and also from previous MSc and PhD theses. At the same time, familiarisation with solar pond operation is essential in order to have better understanding of solar pond practice. The emphasis is on routine maintenance to maintain solar pond stability, clarity control, wave suppression and monitoring techniques using appropriate instrumentations.

The works in this stage consisted of theoretical analysis, designing and construction of heat exchanger prototype to prove the concept experimentally. The initial task at this stage is to analyse the passive method of using a thermo siphon. Considering natural convection and buoyancy effects due to temperature difference, sixteen equations with sixteen unknowns must be solved to re-establish the theory with an assumption that the system is properly sealed and there is no heat is loss to the surrounding. The model is solved by using an Excel spread sheet, with a rational assumption of hot water velocity in order to generate the programme. The prototype of the thermo siphon heat exchanger is constructed using a 4-inch diameter PVC pipe and a 6m length of 9.52mm x 0.91mm coiled cooper tube as a condenser. It is fabricated and tested in RMIT laboratory. The

result showed the system is workable with low temperature difference, which is suitable with RMIT solar pond condition which has an average temperature difference of 20^{o}C to 30^{o}C.

A series of heat extraction system consisted of seven heat exchangers has been installed in RMIT solar pond for experimental work. This is an active method system of heat extraction from multi-layer of NCZ using a 12V pump to draw out hot brine through external heat exchanger shell and re-injected it back to the same level. Simultaneously, cold water from UCZ is pumped through the heat exchanger coils to collect heat in stages from difference level of NCZ. The volume flow rate of hot brine was carefully controlled, to minimise the mixing effect on NCZ salinity gradient. The system was run for 24 hours for certain period of time in the particular month. The experiments have been done in summer, autumn and spring of 2012. The results obtained was analysed to determine the amount heat that have been extracted and the effectiveness of the system and the overall efficiency of solar pond Basically, the whole project consisted of three stages, begun with feasibility study, followed by theoretical analysis and finally, end experimental work was carried out.

1.6 Structure of the thesis

The thesis is divided into seven chapters including the introduction, and the remaining chapters are as follows:

Chapter 2 describes the concept of solar pond technology, starting from the discovery of natural salt lakes to the development of artificial solar ponds globally and their applications. The chapter includes design criteria, site selection, construction methods and lining installation, establishing a salinity gradient and maintaining pond stability. The chapter also addresses routine maintenances including salt management, clarity

maintenance, wave suppression and manual monitoring of salinity, temperature and pH level.

Chapter 3 presents a description of the RMIT solar pond. It describes the physical characteristics of the pond including size and volumetric capacity, the heat extraction system, the salt charger and the automatic monitoring system. This chapter also presents a manual method to monitor the stability of a solar pond and the routine processes to maintain its stability and water clarity including the management of the required instrumentation.

Chapter 4 presents an analysis of temperature development in the gradient layers (NCZ) of solar ponds and operation of multi-layer heat extraction from the NCZ using external heat exchangers in the RMIT solar pond. A previous attempt to tap available heat from the NCZ to improve overall thermal performance of solar pond is described. The main content of this chapter is the theory and design of the heat exchanger, coiling of the associated copper tubing and installation of the heat exchanger system in the RMIT solar pond. This chapter includes description of the experimental procedure and theoretical performance analysis of an individual heat exchanger.

Chapter 5 presents theoretical and experimental assessment of a thermosiphon-based heat exchanger to passively extract heat from a solar pond. The chapter presents analysis of an active external heat exchanger for performing heat extraction from the LCZ and describes in detail the fabrication and installation of the proposed heat exchangers system and the associated experimental procedure.

Chapter 6 presents the results from, and discussion of, both experiments. The first section presents results of heat extraction from the NCZ of solar ponds. The second section presents the results of the thermosiphon heat exchanger experiment. The outcomes from both experiments are analysed and discussed in detail.

Chapter 7 concludes the analysis of the proposed multi-layer heat extraction from the NCZ to enhance overall thermal efficiency of solar ponds and the introduction of a passive heat extraction method from the LCZ using a thermo siphon heat exchanger. In addition, some recommendations for future work and suggested research directions are presented.

1.7 Publications

1.7.1 Journals

1. **Yaakob, Y**., et al. (2011). "Heat extraction from gradient layer using external heat exchanger to enhance the overall efficiency of solar ponds." International Journal of Renewable Energy Research **1**(1): 1-6.

2. Gasulla, N., **Yaakob, Y**., et al. (2011). "Brine clarity maintenance in salinity gradient solar ponds." Solar Energy **85**(11): 2894-2902.

1.7.2 Conferences

1. **Yaakob, Y**., et al. (2010). Heat extraction from salinity gradient solar ponds using external heat exchanger. The AUSES 48th Annual Conference. Canberra, Australia, Australian Solar Energy Society.

2. **Yaakob, Y**., et al. (2011). Heat Extraction from gradient layer using external heat exchangers to enhance the overall efficiency of solar ponds. 2011 IEEE First Conference on Clean Energy and Technology. Kuala Lumpur, Malaysia, University of Malaya Kuala Lumpur Press.

3. **Yaakob. Y**, Date. A, Akbarzadeh. A (2013), Introduction of multi-layer heat extraction from non-convective zone of solar ponds. AEDCEE 2013, Alternative

Energy in Developing Countries and Emerging Economies, Bangkok, 30-31 May, 2013

Chapter 2 - Background and overview of solar ponds

2.1 Natural salt lakes

The concept of a solar pond originates from the occurrence of natural salt lakes in many places on earth. Naturally, salt in saline water migrates to the bottom of the lake and fresh water supplied from a river or less salty water from sea will float above it. This phenomenon establishes a salinity gradient, where the salt concentration increases with depth. This results in a corresponding temperature gradient with higher temperature at the lake bottom.

Early researches on these lakes were conducted by biologists. The first scientific report on a natural solar lake was presented by Von Kalecsinsky (1902). His data show a maximum bottom temperature of 70^{o}C at 1.32m depth at the end of summer in the natural salt lake, Medve Lake. The lake lies in the foothills of the Carpathian Mountains, in north central Romania at a latitude of 46^{o} 35' S, 25^{o} 6' E. He has analyzed water samples from the lake and found that the lake was stratified into three non-mixing layers as elaborated by Bolon (Bolon 1981). This created a significant temperature difference with the top surface close to the ambient temperature of 26^{o}C during early spring. Based on this finding, Kalecsinsky has suggested the use of artificial solar ponds to harness inexpensive solar heat for energy applications.

Another discovery was in Antarctica at a latitude of 77^{o} 32' S, 161^{o} 34' E. Lake Vanda, which is 8km long and 1.6 km wide, traps heat naturally with a temperature of approximately 25^{o}C at its 66m deep bed even when its surface is covered with ice and with a mean ambient temperature of approximately -20^{o}C (Wilson and Wellman 1962). Twelve holes were drilled in two lines along the length and across the width at 300m intervals for scanning purposes. The temperature and conductivity of the water were

scanned vertically at 1.5m intervals. It was concluded that radiant energy from the sun was the only possible heat source for the saline water in the lake. A similar finding from Lake Bonney was reported by Shirtcliffe and Benseman (1964) at 77^{o} 43' S, 162^{o} 26' E. Their measurements in January 1963 showed a maximum temperature of approximately 7.5^{o}C at a depth of 10m to 15m. This phenomenon was attributed to the existence of a salt gradient and to radiation that penetrated the ice cover. There were other lakes in different continents which exhibited similar behaviour including hot lakes in the state of Washington (Anderson 1958) and Lake Mahega in western Uganda, Africa (Melack and Kilham 1972). A small natural solar lake of size 140m x 50m was found near the coast of Sinai which is separated from the sea at the Gulf of Aqaba by a 60m natural barrier as reported by Cohen et. al (1977).

2.2 Artificial solar ponds

The discovery of the thermal behaviour of natural salt lakes prompted the development of artificial solar ponds in the late 1950s. The concept of an artificial solar pond is to use salt (usually Sodium Chloride) solution to suppress natural convection by creating increasing concentration with depth (Fynn and Short 1983). This will keep the heat trapped at the bottom part of the pond and the concept has attracted the interest of many researchers around the globe primarily for research and development facilities. The findings and experience gained from experimental ponds have led to the capability of constructing productive solar ponds based on reliable design criteria. They also provide useful information for better sizing of future solar ponds. Overviews of working solar ponds are presented in Sections 2.5 and 2.6.

2.3 Construction

Fundamental aspects of sizing a solar pond are the surface area, the pond depth and the wall slope. The basic requirement to size a solar pond is related to the demand for heat in

its application, the local climate and the geographic conditions. For example, characteristics of a solar pond to supply hot water at 35°C for building space heating will be very different from those of a solar pond to generate electricity. For power generation, sustained performance at higher temperatures of 80°C or above is essential. The solar pond must be located as close to its application as possible (Akbarzadeh, Andrews et al. 2005). In order to match thermal output of a solar pond to the energy and temperature required by end users, it is very important that the temperature of the lower convective zone is maintained between 3°C and 5°C above the end use temperature. If the LCZ temperature is much higher than the delivery temperature, heat loss will increase thus resulting in increased economic penalties.

2.3.1 Site selection

Site selection is very important for a solar pond in order for the construction work and operation to be at minimum cost. An ideal site should have ample flat land to minimise earth moving costs and should not be cultivable. The site should have easy access to salt and fresh water for pond establishment and surface washing. The soil must be appropriate for building a strong wall and the ground water table must be deep enough to minimise bottom heat loss. The site should have a high level of incident solar radiation as this will directly affect the performance of the solar pond. The performance of a solar pond will also depend on local evaporation rates. High evaporation and a shallow water table would impair the pond performance as heat is easily lost to the surroundings. Other aspects which must be considered are low prevailing wind speeds to minimize wave-induced mixing and the depth of the top mixed zone, which can reduce the thickness of the NCZ hence affecting the pond performance. Low wind speed reduces the amount of debris falling into the pond, thereby assisting in maintaining cleanliness. The last and the most important aspect of site selection is the solar pond proximity to the end users of the energy produced.

2.3.2 Pond design

A solar pond is significantly different from a normal water retention pond. It must have the ability to collect and store solar energy efficiently. Particularly, it needs to be compact in shape and have uniform depth to maximise heat energy collection. A critical issue that arises is to minimise shading effects inside the pond. Ideally a solar pond should be built in a circular shape to reduce the shading effect. However, this shape may be less practical in relation to excavation work compared to a square or a rectangular shape for a large scale solar pond (10,000 m^2).

Most solar ponds have been built in rectangular shapes as with the ones constructed in El Paso, Bhuj and in Margherita Di Savoia. For a rectangular shaped pond, the long axis should be perpendicular to the prevailing wind to reduce surface mixing. The land is excavated beforehand, and the excavated soil is used to build the side walls of the pond with a slope of approximately 1:2 (Hull 1989). The newly exposed pond floor is compacted with heavy rollers and small sharp stones and dried soil clusters are removed before laying the liners. The liners are then covered thinly with a layer of locally available clay.

2.3.3 Lining and salt

2.3.3.1 Liner

Liners are very important components of a solar pond to prevent saline water from leaking into the soil underneath the pond and endangering the local ground water. Hot brine leaking from a pond will carry away with it salt and heat, which is environmentally unacceptable and will seriously reduce the thermal performance of the solar pond. It is essential that the soil below and surrounding the pond is as dry as possible to avoid formation of an air gap underneath the liner. An air gap can also cause leaking problems as experienced in the Bhuj solar pond (Kumar and Kishore 1999).

The liner material should be robust and able to withstand high temperature close to the boiling point of water, be resistant to ultraviolet radiation and be unaffected by the salty environment (Lu, Swift et al. 2004). Various types of lining material have been used previously for solar ponds. There were numbers of lining failure occurred for the past sixteen years in the El Paso solar pond (Swift and Lu 1996). The El Paso pond had a PVC coated polyester fabric liner known as XR-5 which was installed for initial operation of the pond. However, in 1992 a failure occurred and it was decided that the entire lining system needed to be changed. Compacted plastic clay lining (CCL) was introduced as an alternative to improve the lining system. Figure 2.1 shows the lining system is being installed in the bed of the El Paso solar pond in May 1994. It is important that the liners have long lifetime and be cost effective. Failure of liners has been one of the main problems encountered when working with solar ponds.

Figure 2.1 Installation of lining system at El Paso solar pond

More environment friendly liners for solar ponds can be made from compacted clays. However, not all clays are suitable to be used as natural liners for solar ponds. This is because hot NaCl brine can cause some clay to become more porous and lead to the release of unwanted gases from the ground. For ponds which can operate effectively unlined, costs can be significantly lower as lining is one of the main cost components as

demonstrated in the Laverton solar pond (Hull, Nielsen et al. 1989). However, in many locations pond lining is necessary, for both environmental as well as performance reasons (Almanza and Castaneda 1993).

Various polymeric liner materials can be used for lining a solar pond. Low-density polyethylene (LDPE) and high-density polyethylene (HDPE) are often used along with natural clay for solar pond lining. Covering them with a thin layer of soil or sand will protect LDPE and HDPE liners against ultraviolet radiation. Small solar ponds can utilise the commercially available 10m wide standard liners. However, large solar ponds with surface areas of a few hundred hectares require their liners to be joined on site by heat sealing in order to achieve the desired width and to reduce cost. The best liner laying practice is to make sandwich layers of clay and polymer liners as demonstrated in Bhuj (Kumar and Kishore 1999). This is considered the best leak proofing practice for a solar pond (Almanza and Castenada 1993, Akbarzadeh, Andrews et al. 2005).

2.3.3.2 Candidate salts

Dissolved salt and water are the main components required to establish a salinity gradient solar pond. Any kind of salt as well as any natural brine can be used as long as it meets the following criteria;

i. It must have an adequate solubility to form the salinity gradient profile and have strong temperature dependency to minimise the effect of diffusion.

ii. Good transparency to allow penetration of solar radiation for better thermal storage at the solar pond bottom.

iii. Easily available and inexpensive, where proximity to a bulk supply of the salt will be a definite advantage.

iv. Non-hazardous to people and the environment, particularly during handling and disposing. Appropriate procedures must be strictly followed to prevent pollution.

Sodium Chloride (NaCl), often referred to as common salt is currently the most commonly used salt worldwide for salinity-gradient solar ponds to establish the salinity gradient. Magnesium Chloride ($MgCl_2$) is the second most common salt used to establish a solar pond. The by-product of a NaCl salt production factory, which is known as bittern, consists mainly of $MgCl_2$ and potassium chloride KCl, is also suitable for use in a solar pond.

The density of a NaCl solution can be increased up to 1300 kg/m^3. However, this density can be increased to more than 1500 kg/m^3 if the salt used is mainly $MgCl_2$. The solubility of sodium chloride is fairly constant with temperature, while that of magnesium chloride increases with temperature. The use of refined NaCl produces greater brine transparency which provides the significant advantage of reducing the clarity maintenance cost.

The use of bittern has incurred a clarity issues as reported in the Atlit solar pond near Haifa, Israel and the Laverton solar ponds in Victoria, Australia. The main reason is that bittern is a waste product of salt production and it normally mixes with dirt and is often highly coloured (Tabor and Matz 1965) by algal and bacterial populations (Hull, Nielsen et al. 1989). Despite of its poor water clarity, the Atlit solar pond has recorded a maximum temperature of 70^{o}C. A similar situation was reported in the Margherita Di Savoia solar pond, where a maximum temperature of 71^{o}C has been recorded despite water clarity issues arising from algae bloom in the bittern brine (Folchitto 1997). Conversely, the Laverton solar pond water clarity issue has affected its thermal performance such that the maximum temperature reading did not exceed 60^{o}C.

A solar pond can be an ideal integral part of a commercial salt production facility where the residual salts can be used as brine, saving the more valuable sodium chloride for salt

making. Simultaneously, it will create pollution-free environment and be more economical to use. Both NaCl and bittern satisfy the listed criteria, but ultimately the choice is influenced by availability and cost.

2.4 Salinity gradient establishment and maintenance

The key to success of an operational solar pond depends is the establishment and maintenance of the stratified region that act as transparent insulation on top of the storage zone (Zangrando 1991). This layer contains stratification of temperature (*T*) and salinity (*S*) in parallel, where both of *T* and *S* increase with depth. The salinity gradient must be established artificially whilst the temperature gradient is formed naturally after a period of time following absorption of solar radiation. The salinity component of density which is greater at the bottom acts as counterbalance to the temperature component which is less on top, in order to maintain stability.

2.4.1 Salinity gradient establishment

There are a number of different methods for setting up the salinity gradient in a solar pond as described by Zangrando (1979). These methods are each explained in Sections 1.4.1.1 to 1.4.1.3.

2.4.1.1 Natural diffusion

This is among the earliest methods and was proposed by Tabor (1963) as a means of creating the salinity gradient. The procedure is to half fill the pond with water, and then add and mix the salt with it. A pump is used to stir the water to dissolve the salt thus creating highly concentrated brine. Finally the upper half of the pond is filled with fresh water. Diffusion will naturally create a salinity gradient over a certain period of time depending on the pond size. This is the simplest method but represents the longest time

taken to establish the gradient layer. It is only suitable for application if the pond is very large (more than 1 km^2).

2.4.1.2 Stacking

In this method, a mixture of highly concentrated brine is introduced to the pond to form the desired storage layer. Then the pond is filled with less concentrated brine in stepwise concentrations, ranging from the lower concentrated brine layer to the fresh water layer at the top. The density changes will smooth themselves through diffusion and partly because of the kinetic energy from the injected fluid flow. This technique has been used to established the salinity gradient at the University of New Mexico solar pond (Zangrando 1979). However, this method has two major drawbacks if it is to be implemented for a large solar pond. Firstly, it requires a large mixing tank and secondly, during the filling process, the layer may be exposed to surface wind which may cause uneven mixing. Therefore, this method is only suitable for small scale solar ponds.

2.4.1.3 Redistribution

This method is commonly used worldwide to establish the salinity gradient in solar ponds. It was developed by Zangrando (1980). This method requires the pond to be filled with highly concentrated brine to a depth equal to the storage layer thickness plus half of the remaining depth, which is equivalent to half of the salinity gradient layer. Fresh water is added through a diffuser to create a thin horizontal flow in order to minimise the mixing. The diffuser is initially positioned on top of the storage layer and moves upward continuously or in a stepwise manner. The recommended steps should not exceed 5cm. The brine above the diffuser will be progressively diluted as the water level rises. The timing should be controlled such that the diffuser will reach the top surface at the same time as the water level. Hence, the rate of diffuser movement must correspond to twice the water flow rate. As an example, for each 5cm water level rise, the diffuser must move upwards 10cm. A stepped salinity gradient will be created at the end of the process, and

it may take some time to linearize the gradient depending on the diffusion rate. The entire process may be performed automatically or manually with a continuous or intermittent mode. In most cases, a circular diffuser has been used and placed at the middle of the pond to distribute the flow equally in all directions. Figure 2.2 shows a schematic diagram of the redistribution technique for establishing a salinity gradient in a solar pond.

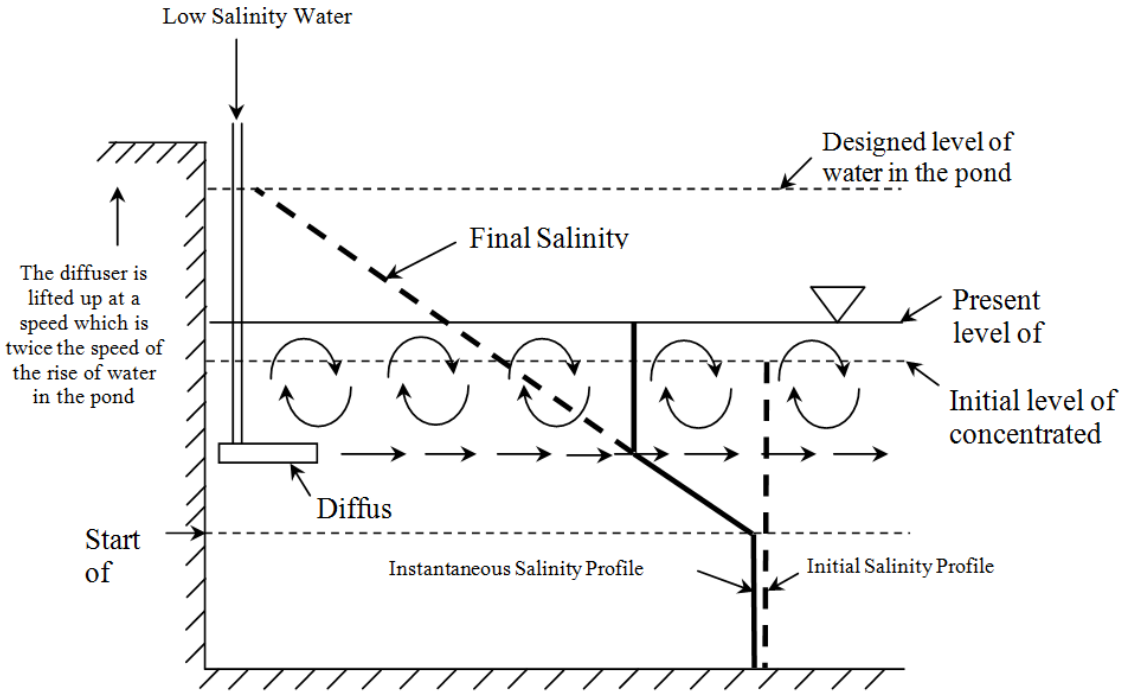

Figure 2.2 Schematic diagram of gradient establishment using Redistribution technique (Date 2012)

2.4.1.4 Froude Number

The Froude number, Fr is a dimensionless value comparing the ratio of the inertia to the gravitational forces. The Froude number is important parameter in analysing the level of mixing when fluid is being injected into fluid environment. The Froude number is defined as;

$$Fr = \left[\frac{\rho v^2}{(g\Delta\rho B)}\right]^{1/2} \quad (2.1)$$

Where ρ is the density of the surrounding fluid, v is the injection velocity, g is the gravitational force, $\Delta\rho$ is the density difference between the injected fluid and the surrounding fluid and B is the diffuser gap.

The Froude number needs to be maintained at 18 as the mixing of the two fluids occurs at and above the diffuser level (Liao, Swift et al. 1988). If the Froude number is smaller than this value, the injected fluids will rise by the buoyancy effects. If the value is larger than this value, the injected fluids will fall below the diffuser level. It is important to monitor closely the entire process of gradient establishment in order to adjust the flow rate or other parameters to keep the Froude number as close as possible to the recommended value. During the gradient establishment in the Bhuj solar pond, the slit width of the diffuser was adjusted seven times to maintain the critical Froude number (Kumar and Kishore 1999).

2.4.2 Stability of solar pond

The efficient operation of solar ponds depends on their stability with respect to vertical motion of the salt (Weinberger 1964). In the rising solar pond, salt transported from the highly concentrated zone to the low concentration zone is predominantly due to natural molecular diffusion as described by the upward diffusive salt flux equation (Anati 1987, Hull and Nielsen 1989):

$$\Gamma = -\kappa_s \left(\frac{dC}{dz}\right) \quad (2.2)$$

where Γ is the salt flux in kg/m^2.s^1, z is the vertical direction which is positively downward because $\frac{dC}{dz}$ is negatively upward in a solar pond, C is the salt concentration in kg/m^3 and κ_s is the solution diffusivity as a function of temperature and salinity.

Zangrando (1991), has established a best fit equation for to calculate κ_s for a NaCl solution as;

$$\kappa_s = (0.58 + 0.030T + 0.0002T^2 + 0.001S^2) \times 10^{-9} \quad (2.3)$$

Operational salinity gradient solar ponds require an adequate salinity gradient to maintain internal hydrodynamic stability. The salinity gradient solar pond is an artificial entity wherein brine is injected to the lower part of the pond to support the upward movement. The net local density, ρ (kg/m^3) across the layer with the effect of difference in salinity and temperature components can be expressed in the following equation (Hull, Nielsen et al. 1989, Zangrando 1991);

$$\rho = \rho_0[1 - \alpha(T - T_0) + \beta(S - S_0)] \quad (2.4)$$

where T is temperature in ^{o}C, S is salinity in % by weight, α is the coefficient of thermal expansion in $(^{o}C)^{-1}$, β is the coefficient of expansion of water associated with salinity in $(\%)^{-1}$ and subscript 0 refers to a reference point. Both α and β are functions of T and S. Salinity S (kg salt over kg of solution as %) is selected instead of concentration C (kg of salt over m^3 solution) whenever T is not constant because the salinity does not change as a function of temperature unlike the concentration (Zangrando 1991). To maintain the static stability the effect of salinity on the density at any depth must be equal to or greater that the effect of temperature. Hence, many researchers have used the term density stability ratio as;

$$R_\rho = \frac{\beta(\partial S/\partial z)}{\alpha(\partial T/\partial z)} \quad (2.5)$$

where z is the depth positive downward from the surface in meters. To satisfy the static stability requirement, the effect of salinity must be stronger than the effect of temperature at any depth inside the NCZ, $R_\rho \geq 1$. The increase of temperature results in decrease of

density. To counter this condition, substantial salinity stratification must be maintained so that each layer inside the NCZ is more saline than the layer above it.

Solar pond stability monitoring includes both interface and internal stability as functions of height (Lu, Swift et al. 2004). This is essential activity for keeping a stable solar pond. At the El Paso solar pond, the boundary positions are determined by using the temperature and salinity data using "four points methods" at 5cm interval was implemented (Lu 1994). The internal stability in NCZ layer is performed by monitoring the local "stability margin number" (SMN) (Xu, Golding et al. 1987). It is defined as the ratio of the measured stability coefficient to the calculated stability coefficient to satisfy the dynamic stability. This method has been successfully implemented in El Paso solar pond (Lu, Swift et al. 2004) and in laboratory studies at The Ohio State University (Xu 1990). The SMN is mathematically expressed as;

$$SMN = \frac{(dS_a/dz)}{(dS_i/dz)} \tag{2.6}$$

where dS_a/dz is the measured salinity gradient (%/m). The dS_i/dz indicates the theoretical salinity gradient (%/m) required to meet the stability criteria for the measured temperature profile in NCZ at height, z expressed as;

$$\frac{dS_i}{dz} = \frac{\alpha}{\beta}\left(\frac{\nu+K_T}{\nu+K_S}\right)\frac{dT}{dz} \tag{2.7}$$

where dT/dz is the temperature gradient, ν is the kinematic viscosity in m^2/s and K_T and K_S are thermal and solutal diffusivity in m^2/s respectively.

By incorporating equation (2.7) into equation (2.6), the SMN can be written as;

$$SMN = \frac{\beta}{\alpha}\left(\frac{\nu+K_S}{\nu+K_T}\right)\frac{\Delta S_a}{\Delta T} \tag{2.8}$$

To sustain the local stability, the SMN must be equal or greater than one. It was reported for the El Paso solar pond that, the gradient breakdown will occur when the SMN value goes below 1.6 at specific depth (Xu, Golding et al. 1991). At the El Paso solar pond, the SMN has been set at 2.5 as a control limit. It is important, so that any necessary corrective measure can be taken when the SMN approaches this number (Lu, Swift et al. 2004).

2.4.3 Salinity gradient maintenance

Maintaining salinity gradient is essential to keep a solar pond operating over a long period of time. The salinity gradient requires both routine and corrective maintenance. Routine maintenance is to replace salt which continuously diffuses upwards from the high concentration salt in the storage zone to the low concentration salt at the surface. The corrective maintenance is to rectify any instability found within the gradient zone from development of the convective layer.

2.4.3.1 Routine maintenance

The important aspect here is to ensure the stability of the salinity gradient in relation to the effects of diffusion. Because of the large salinity different between the highly concentrated brine in the lower convective zone and the low salinity brine in the upper convective zone, there is upward salt diffusion. To accommodate this, the top layer of the pond is continuously washed with fresh or low salinity water with a flow rate of at least twice the evaporation rate (Akabarzadeh, Andrews et al. 2005), while salt is added to the storage zone. An alternative approach to prevent the salt from polluting the environment and for cost saving is to recycle the washed salt. It can be done by collecting, evaporating and re-injecting the concentrated brine back into the lower convective zone. An evaporation pond that is at least equal to the total pond surface area should be constructed next to the solar pond for this purpose as demonstrated by Alagao et al. (1994) at RMIT University, Melbourne.

Salt is added to the lower convective zone in the following ways;

i. Salt charger: A salt charger normally of cylinder shape is attached vertically to the pond wall so that it extends above the top surface and the bottom end is open at the lower boundary layer. A salt (normally coarse salt) is replenished into the salt charger and controlled to be at the same level as the pond surface.

ii. Diffuser: A salt is mixed with low salinity brine or fresh water to obtain high concentration brine. This is normally done in an evaporation pond or by using a mixing tank. The high concentration brine is then pumped or siphoned into the lower convective zone through a diffuser. The injection rate should be controlled so that the critical Froude number is in between 14 to 16.

Figure 2.3 below shows the application of both methods as installed in the Pyramid Hill and RMIT solar ponds.

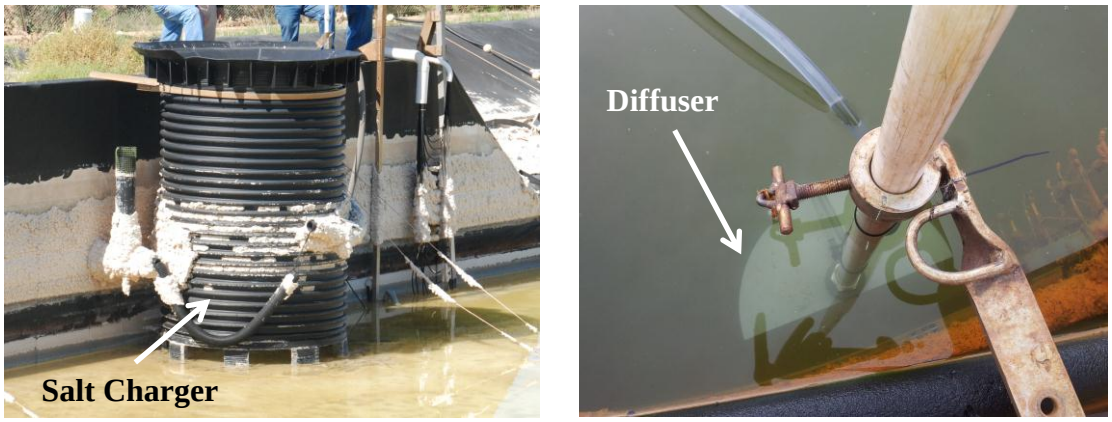

Figure 2.3 Salt charger at Pyramid Hill (left) and semi-circle diffuser at RMIT (right)

An alternative method called the falling pond method was suggested by Tabor and Matz (1965) to control the effect of diffusion in solar ponds. Hot brine from the lower convective zone is extracted and passed through a flash evaporator to produce steam and concentrated brine. The steam can be used for applications such as for space heating

while the reduced volume of highly concentrated brine is returned to the lower convective zone. This process will lower the pond water level, and fresh water is added to the surface to recover the original level. If the volume of water drop matches the diffusion rate, the salt actually remains stationary and the gradient remains undisturbed without the need to add more salt and without surface washing.

2.4.3.2 Corrective maintenance

The breakdown of salinity gradient caused by the development of the convective layer needs immediate attention. Xu, Swift et al. (1992) reported that, in three hours, a small step of 5 cm breakdown had developed into a further three steps breakdown at the same thickness. The breakdown of the gradient will result in increased heat transfer rate upward from the storage zone to the surface.

For small breakdowns less than 5 cm, the gradient normally restored itself. Beyond that, correction by scanning injection, as described in the redistribution techniques, needs to be done (Zangrando 1979). The procedure is to use cold and low salinity brine from the surface or hot and high concentration brine from the storage zone and inject them into the affected region of gradient where the convective layer has developed. It was suggested by Zangrando (1979) that if the gradient above the instabilities is strong, brine from the surface is used, but if the gradient below is weak, high concentration brine from storage zone is used. This technique is found to be efficient and least time consuming for restoring the gradient.

2.5 Wave suppression

Waves above 10 cm in height in the solar pond surface will increase the thickness of the upper convective zone and penetrate into the gradient layer. This occurrence is caused by strong wind across the surfaces of larger ponds. It is important to find a way of reducing wind velocity across the water surface in order to minimise the water motion (Schladow

1984). A grid structure of floating foam barriers was used in early solar pond experiments to protect from wind as reported by Hull et. al (1989). Instead of a dedicated structure, fencing can also provide a significant wind breaking technique as demonstrated in Miniasburg, USA. The best technique known to suppress the waves is by using floating rings made of PVC as used at the Pyramid Hill solar pond and shown in Figure 2.4. The floating rings act as dividers on the surface area of the pond into small isolated cells to limit the turbulent motion of the waves (Chyng, Lee et al. 2003). It was found that the use of floating rings helped to maintain the desired thickness of the gradient layer, keep its stability and minimise upward heat loss.

Figure 2.4 Wave suppression by floating ring at Pyramid Hill solar pond

2.6 Clarity maintenance

Clarity is one of the important factors for achieving good thermal performance. It is important to maintain the brine above the lower convective zone as clear as possible to maximise light penetration to the bottom. The salt concentration level does not have a significant influence on solar radiation penetration, but the suspended particles, dust and debris can seriously reduce the amount of solar energy reaching the lower convective zone (Wang and Yagoobi 1995). Another aspect that contributes to the transparency

problem is the growth of microbial and algal substances(Gasulla, Yaakob et al. 2011). Acidification of the pond provides a simple and reliable maintenance method for preventing or inhibiting algal blooms and maintaining high transparency. The pH level of the pond should be monitored and hydrochloric acid added to keep the level between 3-4 as demonstrated in El Paso (Lu, Swift et al. 2004). However, the disadvantage of using HCl is associated with metal corrosion. A more environmentally friendly approach is to add brine shrimp to the pond to feed off and hence control the algae level (Wang and Seyed-Yagoobi 1995, Malik, Date et al. 2011). The use of copper sulphate to treat algae growth has also proved to reduce the rate of metal corrosion (Gasulla, Yaakob et al. 2011).

2.7 Heat Extraction

There are two methods whereby heat can be extracted from LCZ of a solar pond. The first method is to circulate fresh water as a heat exchanger fluid using a pump through an in-pond or submerged heat exchanger in LCZ. In this method heat is harvested only by natural convection in the brine and the heat transfer area needs to be determined according to the application demand. To avoid corrosion and be more cost effective, a non-metallic material may be used for the heat exchanger pipes as was demonstrated in the 3000 m^2 solar pond in Pyramid Hill (Leblanc, Akbarzadeh et al. 2011) as shown in Figure 2.5. The heat extraction rate is quantified by the following equation;

$$\dot{Q} = \dot{m}\, C_p dT \tag{2.9}$$

Where $\dot{m}\ is$ the mass flow rate in Kg/s, Cp is the fluid specific heat in J/Kg^{o}C and dT is the temperature difference in degree Celsius.

The efficiency of solar pond as stated in section 1.3 was defined as follow:

$$\eta = \frac{The\ amount\ of\ heat\ extracted\ (W/m^2)}{The\ amount\ of\ radiation\ received\ at\ pond\ surface\ (W/m^2)} \tag{2.10}$$

Figure 2.5 In-pond heat exchanger at Pyramid Hill solar pond

The second method is to withdraw hot brine from top part of the lower convective zone by pumping it through an external heat exchanger after which the cooler brine is returned to the bottom part of the lower convective zone. In this second method, less heat exchanger surface area is required, but the distribution system needs to be designed carefully to avoid erosion of the gradient zone. Both methods have been tested in solar ponds around the world and have shown satisfactory outcomes. However, the most common method used is withdrawing the brine through the external heat exchanger. This method proved to be a trouble-free system and cost effective as practiced in the El Paso and Bhuj solar ponds as shown in Figure 2.6. The cooler brine returned to the bottom area of the pond can help reduce heat loss to the ground (Lu, Swift et al. 2004).

Figure 2.6 The external heat exchanger at Bhuj solar pond

Recent investigations revealed that heat extracted from both the gradient zone and the storage zone can improve overall efficiency of solar ponds. However, in-pond heat exchangers for heat extraction from the gradient zone are only effective for small ponds. To extract heat from the gradient zone of large solar ponds, a selective withdrawal method should be used. This method requires hot saline water from different depths to be extracted and passed through successive external heat exchangers wherein the heat transfer fluid is preheated using the gradient zone (Andrews and Akbarzadeh 2005, Leblanc, Akbarzadeh et al. 2011, Yaakob, Date et al. 2011).

2.8 Monitoring and instrumentations

Reliable monitoring systems and procedures are very important to ensure optimum operation and steady performance of a solar pond. Physical parameters such as temperature and salinity profiles in the pond should be routinely monitored. It is also very important to monitor the water clarity and for this, measurement of turbidity of water is essential and at the same time the water pH should be monitored. Control of algae growth is critical to the efficient performance of a solar pond as discussed previously. The temperature, density, turbidity and pH of the solar pond should be monitored once every

two weeks. Failure to do this will lead to decrease in the thermal efficiency of the solar pond. Temperature and salinity profiles help to check the stability of the gradient zone of a solar pond.

The simplest method of monitoring these parameters is by using a sample extraction device as shown in Figure 2.7 (top). This device can be made from a 3.5m long 25mm diameter plastic tube. The sampling tube is used to withdraw brine samples from equally spaced different levels in the pond. Thermocouples are connected to the inlet of the tube such that the temperature at the point in the pond from which the sample has been withdrawn can be measured. The automated sampling system as shown with a schematic in Figure 2.7(bottom) would be more practical for large solar ponds.

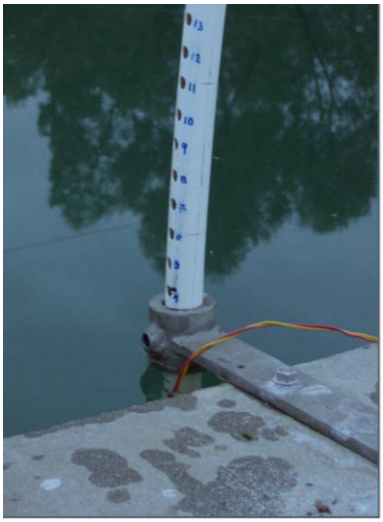

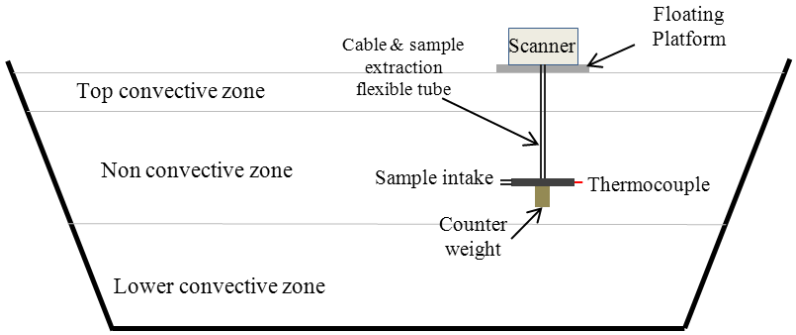

Figure 2.7 Sample extraction device (top) and automated sampling system (bottom)

It is also useful to monitor the total global solar radiation incident upon a horizontal surface near the pond surface to keep records of solar energy input for calculation of the solar pond thermal efficiency. Inspection of temperature and salinity profiles is a direct and simple way to locate the depths of the gradient zone, the surface zone and the storage zone, as well as detecting the presence of any convective layers.

2.9 Applications of solar ponds

Solar ponds can be environmentally friendly and economical when constructed at a suitable location and using local resources. For these situations solar ponds are much cheaper than any other large-scale solar thermal collectors. The main advantage of the solar pond compared with other solar thermal collectors is that they have an integrated thermal energy storage system so that they can supply a substantial amount of thermal energy on continuous basis. Solar ponds are particularly useful for remote areas as an alternative to diesel power generators. In the past three decades, application of solar ponds has been successful for industrial process heating, space and water heating, desalination, power generation, aquaculture and chemical production.

2.9.1 Industrial process heat

Solar ponds can be economically viable for industrial process heating, including manufacturing processes which require low-temperature heat, aquaculture and drying applications, at sites where land and water (brackish or sea water) are available, and solar radiation is high. Solar ponds for heating are more economical in areas where natural gas is not available and the only alternative fuels are LPG or oil, and they may even compete with natural gas where the price of the latter is high. Furthermore, the key benefit of a solar pond is that it is a zero-greenhouse-emissions source of heat. In 1985, the El Paso solar pond became the first solar pond in the world to supply process heat to industry,

where 350 x 10^6kJ of thermal heat has been delivered to a food canning plant (Reid, McLean et al. 1985, Swift, Reid et al. 1987). The 6000m^2 Bhuj solar pond has supplied a total of over 15,000m^3 of hot water to a dairy plant at an average temperature of 75^{o}C since September 1993 to April 1995 (Kumar and Kishore 1999). During its seven years of operation since June 2001, the 3000m^2 Pyramid Hill solar pond in northern Victoria has supplied process heat to the Pyramid Salt Pty Ltd to produce a high grade salt (Leblanc, Akbarzadeh et al. 2011).

2.9.2 Space and water heating

A solar pond is a low temperature heat collector as well as providing long term storage. The easiest and most efficient way to utilise the trapped heat is to use it in direct space or water heating. A solar pond has the capability of storing summer heat for winter applications, which is very suitable for heating buildings (Tabor 1981). This is practical when other solar heating approaches are impossible during winter. Rabl and Nielsen (1975) have suggested that solar ponds could be used for a single house, where the pond area is approximately the same area as the floor area. A solar pond is so practical, even at high latitudes and with less sunlight such as in London in the United Kingdom, that it is still possible to be used as building space heating (Bryant and Colbeck 1977). For a 155m^2 Wooster solar pond in Ohio, a dynamic computer model of its energy collection and storage has shown that the peak temperature gained in late summer could be used for house space heating (Shah, Short et al. 1981). Apart from space heating, solar ponds have shown potential for water heating. A 2000m^2 pond in Mimiasburg, Ohio was constructed by the city municipal council to heat the community swimming pool and recreational building in winter (Fynn and Short 1983). In Singapore, a 14m^2 and 1.5m depth fibreglass solar pond was constructed to supply heat for a catering facility at Changi Airport (Kho, Hawlader et al. 1991), where an average load of 54m^3 of hot water at a temperature of 60^{o}C is required for daily operation with continuous demand on a 24-hour basis.

2.9.3 Desalination

Brackish water is a groundwater with a level of salinity between freshwater and seawater. In many places in the world brackish water appears naturally, for example in most parts of Victoria in Australia. Desalination is a means of transforming the unpleasant brackish water to drinkable water and simultaneously overcoming the shortage of fresh water supply. It is the process of removing salt and impurities from groundwater using heat to produce fresh water. Thermal desalination by using a salinity gradient solar pond is one of the promising solar desalination technologies (Lu, C. Walton et al. 2001). It has been studied at the El Paso solar pond since 1987, where a 19,000L/day 24 stage flash evaporation system was installed and demonstrated as an environmentally friendly concept with zero emission and pollution (Lu, Swift et al. 2004). Thermal desalination processes such as multiple effect evaporation or a multistage flash process use heat from solar ponds to desalinate the brackish ground water to produce fresh water and salt which can be recycled to the solar pond (Leblanc, Andrews et al. 2010). A 25,000m^2 salinity gradient solar pond was constructed in southern Italy to desalinate seawater, where it has the capability of producing 10m^3/day of fresh water with a maximum temperature from the solar pond of 60^oC (Folchitto 1997).

2.9.4 Power generation

The quest for alternative energy to produce electricity is a key point behind the development of solar pond technology. A solar pond produces low temperature solar heat between 70^oC and 90^oC making it less attractive for electricity generation compared with conventional fuel or coal fired power plant. However, a large area solar collector such as a solar pond could be competitive as a power generator if compared with a diesel powered generator for producing electricity in remote areas. The best practice is to couple the solar pond to an Organic Rankine Cycle (ORC) engine to convert the low temperature heat supply to electricity using low boiling organic liquid, such as Freon, as the working

fluid. The first concept solar pond power station (SPPP) was constructed in Ein Bokek in 1977, where a 150kW ORC engine with approximately 13% Carnot efficiency was installed next to a 7000m^2 solar pond to produce power at approximately 20kW (Tabor 1981). In 1982, a 5MW ORC engine was installed to generate power from a 250,000m^2 solar pond in Beith Ha'rava on the Dead Sea shore (Tabor and Doron 1990). A 2000m^2 solar pond in Alice Spring as shown in Figure 2.8 has demonstrated 15kW power generation using an ORC engine from 1981 to 1989 (Collins and Frederiksen 1989). The 100kW ORC in the El Paso solar pond produced 70kW electricity and 15kW was successfully connected to the grid (Hull, Nielsen et al. 1989).

Figure 2.8 ORC engine installed in Alice Spring solar pond

2.9.5 Salinity mitigation

Salinity is a major environmental problem, where salt accumulates on the soil surface because of the rise of the groundwater level, rendering the land infertile and preventing plant growth as shown in Figure 2.9. In the year 2000, it was estimated that over 1 million hectares of land in Australia was affected by the salinity problem costing approximately at $50 million per year in lost production (Lu 1994). A number of salt

interception schemes were introduced, where saline groundwater was pumped into evaporation basins. The water was evaporated by solar heat and the salt remained.

Figure 2.9 Died trees in salinity affected land in north Victoria

Integrating a solar pond into a salinity mitigation scheme is a rational solution to this problem. It provides simultaneous support for a potential application such as process heat. If evaporation ponds are established in a chain as in a salt production line, the first few ponds in the chain provide ideal opportunities for creating solar ponds (Akbarzadeh, Johnson et al. 2009).

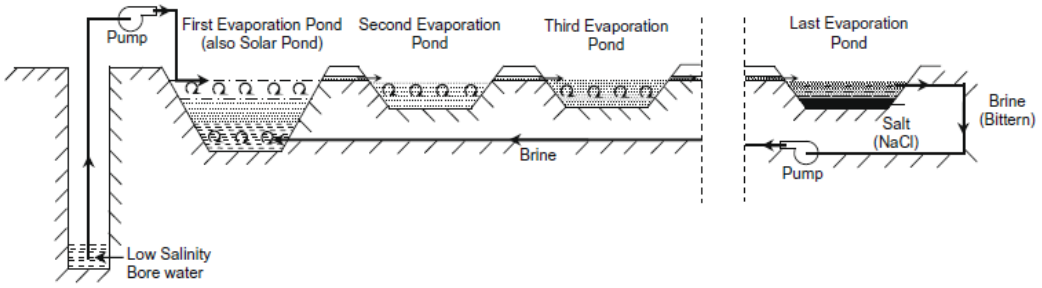

Figure 2.10 Integration of solar pond in salinity mitigation scheme (Akbarzadeh, Johnson et al. 2009)

Figure 2.10 shows the first of a chain of evaporation ponds acting as a salinity gradient solar pond to trap the solar heat. The solar pond normally has 3m to 3.5m depth, whilst the other ponds can be as shallow as 0.5 m depth. Low salinity bore water is pumped into the solar pond for surface washing. The overflow from the first pond goes to the second pond and gravitates. The process continues for a number of ponds in the chain. The salinity is progressively increased from one pond to the next by evaporation. Finally, the highly dense solution in the last pond with specific gravity of 1.3 crystallises and produces salt and magnesium chloride. This solution can be pumped to the bottom of the solar pond to maintain the salinity gradient.

2.9.6 Chemical production

Solution mining uses low temperature heat for extracting minerals from mines. A by-product of such mining operations is a large amount of high salinity or brackish water. One of the major requirements for constructing a solar pond is a large continuous supply of saline water and in return the solar pond can continuously supply a large amount of low temperature heat. It is economical to integrate a solar pond with a solution mining site.

Lesino et. al (1990) have reported the commercial use of four equal sized 400m^2 salinity gradient solar ponds for sodium sulphate (Na_2SO_4) production in a region 3500m above sea level. The sodium sulphate solution dissolves at 40^oC, making the solar pond a useful component of the process. The application of a solar pond can provide substantial cost saving when it replaces the function of a conventional boiler. A square 2500m^2 experimental solar pond was constructed near to the Zabuya salt lake for lithium carbonate (Li_2CO_3) production (Nie, Bu et al. 2011)approximately 110 km southeast of Lhasa at 4422m above sea level. The Zabuya Lake is a carbonated salt lake rich with lithium (Li), boron (B) and potash (K). When the natural brine is heated, lithium

carbonate is produced as shown in Figure 2.11 and sodium chloride is left as waste, which can be returned to the solar pond.

Figure 2.11 Workers collecting lithium carbonate (left) and the harvested lithium carbonate (right) at the Zabuya salt lake in Tibet

2.10 Overview of solar ponds worldwide

2.10.1 Israel's solar pond

The earliest work on artificial solar ponds was initiated by a group of researchers led by Harry Tabor in Israel at the beginning of 1958 following the idea of Dr. R Bloch. The main motivation was to develop low cost power production technology to harvest energy from the sun on a large scale with built-in storage (Tabor 1981).The project began with a laboratory set-up of several small tank ponds filled with sodium chloride, $NaCl_2$ followed by moderately sized experimental field ponds (Hull 1979).

2.10.1.1 The Ein Boqek solar pond power plant (SPPP)

Work on solar ponds resumed when the energy crisis arose in 1973 to 1974. The first solar pond power plant (SPPP) of 6250m^2 was set-up at Ein Boqek on the shores of the Dead Sea in 1977 (Tabor and Doron 1986). Temperatures between 85^{o}C and 90^{o}C were recorded at the bottom layer (LCZ). The solar pond was coupled to an Organic Rankine

cycle (ORC) turbo generator of 150kW for power production. The method of using an ORC to convert the low temperature heat into electricity using a low boiling point organic liquid such as Freon was developed by the Ormat company (Bolon 1981). Electricity produced by this method was successfully transferred to the national grid in December 1979. However, its annual pond thermal efficiency is 17% and heat converted by the ORC was approximately 11% below the expected level because of heavy ground heat loss (Tabor 1981). The operation ran for seven years until 1986 to power nearby resorts.

2.10.1.2 The Beith Ha'rava solar pond power plant (SPPP)

The experience gained from the Ein Boqek solar pond power plant has led the way for installing larger scale solar pond power plant. In 1982 210,000m^2 and 40,000m^2 solar pond power plants were built in Beith Ha'rava at the north part of the Dead Sea which aimed for 5MW power production (Tabor and Doron 1990). The capacity of the Beith Ha'rava SPPP project was based on 5% conversion efficiency of the ORC engine to convert the heat from 1km^2 of pond with 20% thermal efficiency from annual solar radiation received at 2000kWh/m^2 (Tabor 1980). The actual annual pond efficiency was 16% instead of the expected 18%. The thermodynamic efficiency obtained was 5.5% leading to overall efficiency of conversion from sun to electricity of less than 1% to yield 5.89GWh annually. This is because the 5MW ORC was designed for 1km^2 capacity, but the necessary heat exchangers and cooling facilities were incomplete because of financial constraints. The Beith Ha'rava SPPP as shown in Figure 2.12 was running for five years from 1984 to 1989.

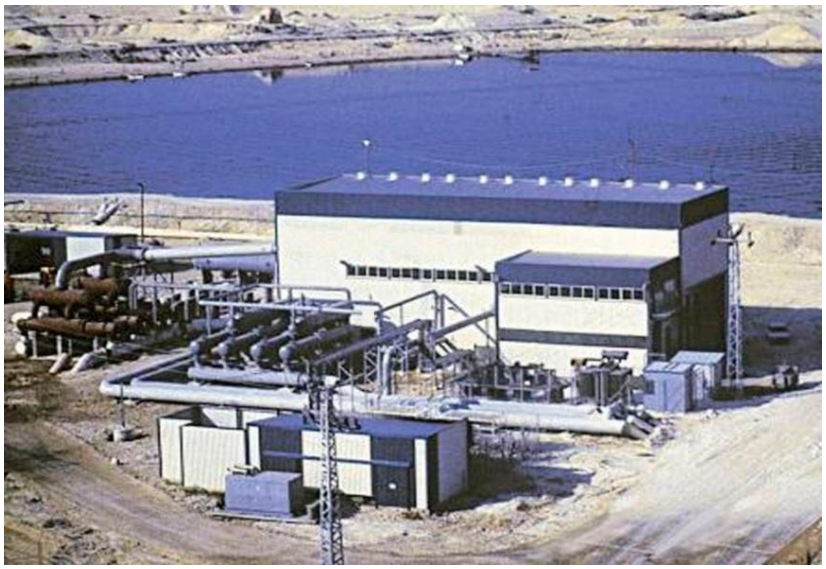

Figure 2.12 The Beith Ha'rava solar pond power plant (SPPP)

2.10.2 Solar ponds in the USA

2.10.2.1 Solar ponds in Ohio

Research on solar ponds in the USA was initiated by Prof Nielsen in 1974 at the Ohio State University who has interest in long term energy storage (Barg 1987). A theoretical study was carried out by Rabl and Nielsen (1975) to investigate the attenuation of solar radiation which influences temperature rise in solar ponds. They have extended Weinberger's theoretical work to develop a precise one dimensional mathematical model based on the heat equation. A larger prototype solar pond with $200m^2$ surface area has been constructed at the Ohio State University and commenced operation in summer 1975 (Nielsen 1975). Maximum temperatures of 62^oC and 69^oC were achieved in June 1976 and August 1977 respectively. Later, a $400m^2$ solar pond was built to provide reliable and efficient data for mathematical model validation (Nielsen 1980). The absorption of radiation was measured and an energy balance has been calculated as a comparison to the theoretical modelling and it shows reliable accuracy.

A 156m^2 solar pond was built at the Ohio Agriculture Research and Development Centre (OARDC) at Wooster to heat a greenhouse starting in winter 1977 (Fynn and Short 1983). Hull (1979) reported that the pond was able to obtain a maximum temperature of only 46^oC because of heat loss to underground water. Shah et al. (1981) have introduced a brine-sourced electrical power driven heat pump which can operate between 5^oC to 40^oC to be incorporated into the solar pond heat extraction system. It has enabled the pond to heat the greenhouse to a temperature above 40^oC over an extended period during winter.

In 1978, a solar pond was built by the City of Miamisburg to heat a community swimming pool and recreational building (Fynn and Short 1983) with surface area of 2020m^2. The maximum temperature reached was 51.1^oC in summer and reduced to 28^oC in winter (Bryant, Bowser et al. 1979). It began to supply heat to the city swimming pool in summer 1978 with initial heat of 40,000kWh.

2.10.2.2 Solar pond in New Mexico

The University of New Mexico in Albuquerque has built a 175m^2 circular shaped experimental solar pond in the fall of 1975. It was built mainly to supply 33MWhr per year of useful heat to meet the requirements of a single house in Albuquerque as reported by Barg (1987). The pond reached a maximum temperature of 93^oC in August 1977. Heat extraction began on November 1977 and continued through 1978. Zangrando (1991) has investigated the hydrodynamic issues that affect the performance of solar ponds in order to obtain a general approximation useful for operational guidance.

2.10.2.3 Solar pond in El Paso, Texas

The El Paso solar pond as shown in Figure 2.13 is a research, development, and demonstration facility operated by the University of Texas at El Paso and is funded by the Bureau of Reclamation and the state of Texas. The project was initiated in 1983,

located on the property of Bruce Foods Inc, a food canning company. The existing unused lined water storage pond with a surface area of approximately 3355m^2 has been converted into a salinity gradient solar pond (Reid, McLean et al. 1985). The operation begun in July 1985 after completing the initial gradient establishment in June, and a pond temperature of 72^oC was recorded.

Figure 2.13 The El Paso solar pond

The El Paso solar pond became the first solar pond in the world to supply industrial process heat, where 350 x 10^6kJ of thermal heat has been delivered to the adjacent food canning factory (Swift, Reid et al. 1987). It also became the first solar pond electrical power generating facility in the USA in September 1986, when equipped with 100kW ORC engine. From September 1986 to September 1987, the engine has operated for approximately 540 hours and generated a gross total of 23,000 kWhr for an average power of 43kW (Swift, Reid et al. 1988). In September 1987, the El Paso solar pond became the first experimental solar pond powered desalination facility in the USA. It has produced 17.3m^3/day of desalinated water using 24-stages in a falling film low temperature desalination unit.

2.10.2.4 Solar pond in Illinois

A 2000m^2 salinity gradient solar pond has been constructed at the University of Illinois (UI) in May 1987. The UI solar pond was constructed mainly to supply space heating to a swine research facility, which is located 25m away (Newell, Cowie et al. 1990). The pond experienced a maximum temperature of 70^oC at the end of July 1988 as well as temperatures below freezing during winter, when 10cm of ice covered the surface. Based on experience gained from the UI solar pond, the same system can be replicated for drying grain from corn farms in Illinois.

2.10.3 Solar ponds in India

2.10.3.1 Solar pond in Bhavnagar

In India the first solar pond with a surface area of 1200m^2 was built in The Central Salt and Marine Chemicals Research Institutes, Bhavnagar in 1970, and is filled with bittern as reported by Srivinasan (1993). Another solar pond with surface area of 1600m^2 was built by the same agency in 1980 at the Institute's experimental salt farm some eight km away (Mehta, Pathak et al. 1988). The pond was filled with sea bittern up to 1m and the rest of the pond was filled with sea water in April 1981. The maximum temperature obtained at the LCZ was 75^oC compared to the intended 80^oC.

2.10.3.2 Solar pond in Bangalore

A circular shaped experimental solar pond of diameter 11.5m with surface area of 100m^2 and depth of 2m was built at Pondicherry for the Institute of Science in Bangalore (Patel and Gupta 1981). The pond's floor consisted of reinforced concrete and the pond had a brick wall. The pond was filled with sodium chloride at 30^oC and was able to reach a temperature of 70^oC after 87 days. That was the maximum temperature gained by the pond, as signs of leakage occurred in summer 1980.

A second experimental solar pond of 240m^2 was built at the Indian Institute of Science, Bangalore and operated for five years commencing in 1984 (Srinivasan 1990). During its operation, the temperature gained in the LCZ was between 50^oC and 70^oC. This performance implied that a small solar pond in a tropical climate is sufficient to supply heat below 50^oC. Erosion of the gradient zone in the pond occurred from January to July 1985, when the internal convective zone was formed, even with a thicker depth of NCZ. This phenomenon could be due to influence of intense side wall heating as described by (Akbarzadeh and Manins 1988).

2.10.3.3 Solar pond in Karnataka

A solar pond with surface area of 400m^2 has been constructed in Masur, Karnataka to serve its rural community. A second pond with surface area of 300m^2 has been built to supply hot water for the engineering college student hostel at Hubli, Karnataka as reported by Srinivasan (1993).

2.10.3.4 Bhuj Solar pond in Gujerat

The largest solar pond built in India so far of 6000m^2 is located in the premise of the Khuj Dairy in Bhuj, Gujerat mainly to supply process heat (Kumar and Kishore 1999). Construction started in July 1987 and was completed by May 1991. The pond has achieved a maximum temperature of 99^oC in May 1991, but heat removal was not carried out at that time because of delay in heat exchanger installation. The fully operational Bhuj solar pond is as shown in Figure 2.14.

Figure 2.14 The 6000m^2 Bhuj solar pond

From September 1993 to April 1995, a total of over 15,000m^3 of hot water was supplied to the dairy plant at an average temperature of 75^oC. The dairy daily demand of an average of 25m^3 was only 31% of the pond capacity. The dairy has saved approximately 935MT of lignite each year through continuous use of solar pond heat. This equates to a monetary saving of US$19,444 per year and the simple payback period is estimated to be less than five years. The success of the Bhuj solar ponds in providing process heat for two and a half years improved the future prospects of this green technology.

2.10.4 Solar ponds in Australia

Solar pond projects in Australia were inspired by the success of solar pond projects in the Dead Sea area of Israel. The high insolation and availability of land as well as locally available saline water has made Australia a favourable site for solar ponds. The main motivation was to provide an alternative power supply to diesel powered electricity generation especially in remote areas where fuel prices are very high.

2.10.4.1 Aspendale solar pond

The first solar pond project in Australia was initiated by the Commonwealth Scientific and Industrial Research Organisation (CSIRO) in 1964 (Davey 1968). A square solar pond with surface area of 44m^2 and depth of 0.86m charged with sodium chloride (NaCl) was built in Aspendale, Victoria. The pond operated for two years and recorded a maximum temperature of 63^oC, and the efficiencies achieved were between 15% and 25%. However, the pond was affected by heavy wind, which increased the thickness of the surface layer and created mixing which reduced the thickness of the gradient zone.

2.10.4.2 Laverton solar pond

Two solar ponds of size 900m^2 each of 2.6m depth were built side by side in 1981 at the Cheetham Salt Works in Laverton, Victoria (Golding 1985). One pond was lined and insulated by slabs while another was unlined to compare their performances. The unlined pond was left unfilled until late 1982 to observe the inflow rate of ground water as reported by Hull et al. (1989). In January 1983, a pile of insulation slabs below the liner floated to the surface and the pond needed to be emptied to repair the damage. It was refilled in March 1983 to continue the operation and research work. The unlined pond was less vulnerable even though it showed a maximum seepage of 40m^3/week corresponding to 10mm per day in midwinter.

2.10.4.3 Alice Spring solar pond

The Alice Spring solar pond of size 2000m^2 at Northern Territory started as a demonstration project in 1980, and the operation began in late 1981 (Collins and Frederiksen 1989). The immediate problem after the pond temperature reached 80^oC was the instability of the gradient layer which led to poor performance and maintenance difficulties. In March 1984, a new pond of 1600m^2 was built with vertical side wall to supersede the slopping wall pond as shown in Figure 2.15. By early March 1985, the

operating temperature has reached 85^{o}C, and in the same month an ORC engine has been successfully demonstrated. The Alice Spring solar pond operated from 1985 until 1989, with a range of temperatures from 80^{o}C to 85^{o}C. The ORC engine achieved 20% conversion efficiency with thermal to electrical efficiency of just over 1.5%. Sherman and Imberger (1991) have reported in summer 1988-1989 that the pond has maintained solar thermal efficiency of 12% to 15% during the heat extraction process from late January to March.

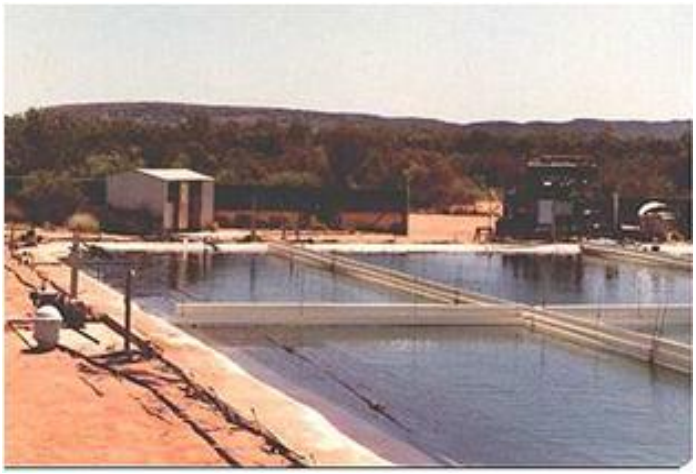

Figure 2.15 The Alice Spring solar pond

2.10.4.4 Pyramid Hill solar pond

A solar pond was constructed at the Pyramid Salt Ltd facility at Pyramid Hill in northern Victoria. It was a collaborative project between Geo-Eng Australia Pty. Ltd, Pyramid Salt Pty Ltd and RMIT University with the primary objective of evaluating the technical performance and economic viability of solar ponds to produce process heat for industrial purposes (Leblanc, Akbarzadeh et al. 2011). It has a surface area of 3000m^2 with 2.3m depth as shown in Figure 2.16. The construction began in February 2000, and the pond started to supply heat for commercial salt production in June 2001. A total of 48 heat extraction tubes were laid down just below the NCZ-LCZ interface across the pond, each

of 60m length. The heat exchanger fluid was plain water supplied from one end to collect the heat from the pond to be delivered to the salt production process. The heat exchanger was designed to produce 60kW of heat with a water flow rate of 174LPM. The inlet temperature to the process was 62^{o}C and the temperature dropped to 57^{o}C at the outlet. The heat extraction system has supplied heat at the approximate rate of 50kW in mid-December of 2001.

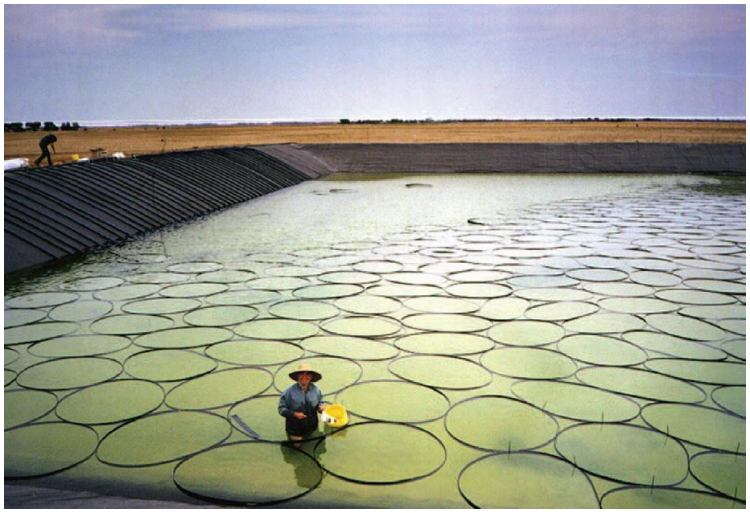

Figure 2.16 The 3000m^2 Pyramid hill solar pond

2.10.5 Solar ponds at other places

2.10.5.1 Puna, Argentina

Four equal sized 400m^2 prototype solar ponds have been constructed in 1981 in Puna, northeast of Argentina where a huge deposit of salt minerals existed. The ponds have been constructed in the premises of a mining company which produced sodium sulphate at 2400m above sea level (Lesino, Saravia et al. 1990). The raw salt mineral consisted of a mixture of 75% sodium sulphate dehydrate, 15% sodium chloride and 1% clay. Lesino et al (1990) have reported that the mineral dissolves at temperature around 40^{o}C, and is then precipitated under controlled conditions. For some processes in the

hydrometallurgical industry such as leaching and fractional crystallization, substantial amounts of heat energy are required (Lesino and Saravia 1991). A solar pond was chosen to produce this heat as an alternative to fossil fuel and also to provide a suitable processing environment. The introduction of solar ponds for mining has substantial cost saving. A conventional plant producing 120 tons per month costs approximately US$40,000, but the total cost for the same production using a solar pond is US$18,000. This finding showed that, solar pond technology is economically viable for implementation in the mining industry.

2.10.5.2 Margherita Di Savoia, Italy

A 25,000m^2 salinity gradient solar pond was constructed in the premises of a local slate work at Margherita Di Savoia, in the coastal area of the Apulia region of southern Italy (Folchitto 1997). The main purpose of this project was to operate an innovative and advanced thermo compression desalination unit that could perform at 60^oC. The hot water from the pond was supplied to the desalination unit which had capacity of producing 10 m^3/day of desalinated water. The performance of the desalination unit was recorded from June until November 1990. It showed that the desalination efficiency has increased since the first test and achieved an average production of 300litres per hour.

2.10.5.3 Tibet, China

A square 2500m^2 experimental solar pond was constructed near the Zabuya Lake at the Qinghai Tibet Plateau. The Zabuya lake is a carbonate type lake, where deposits of salt mineral with lithium (Li), boron (B) and potash (K) can be found on a large scale (Nie, Bu et al. 2011). Lithium carbonate (Li_2CO_3) precipitates when the natural brine from the lake is heated. The pond was filled with saturated brine of sodium chloride (NaCl), waste left when producing Lithium carbonate. The primary objective of the solar pond was to provide process heat for lithium carbonate production. The pond began operation on February 2002 and ended on June 2002. The maximum temperature of 39^oC was

recorded in early June 2002. But, the highest temperature difference was recorded in late April, when the LCZ temperature rose to 32^{o}C compared to an ambient temperature of 3^{o}C, leading to thermal efficiency of 31%. The experiment outcome showed potential for producing heat energy from solar ponds for mining works.

Chapter 3 - The RMIT Solar Pond

3.1 Introduction

In this chapter the RMIT experimental solar pond is described and its operation is explained in detail. The description includes the physical condition of the pond including its size and volumetric capacity, the heat extraction system, the salt charger and the 24-hour automatic monitoring system. The routine processes to maintain stability and manual monitoring of density, temperature, pH level and water clarity are addressed. Major maintenance including gradient repair and removal and refilling the pond are also explained in this chapter.

3.2 Pond description

RMIT University constructed in 1998 a 50m^2 experimental salinity gradient solar pond. The pond is situated in the Renewable Energy Park at the School of Aerospace, Mechanical and Manufacturing Engineering, Bundoora East Campus, Victoria. The pond has a circular shape to minimise shading effects and has a diameter of 8.2m and depth of 2.05m as shown in Figure 3.1. The vertical wall and floor of the pond were constructed using 0.2m thick reinforced concrete. As the pond is unlined, the concrete surface is coated with 1mm of epoxy resin for protection against corrosion and other chemical reactions. The pond was constructed 1.35m below ground level with a 0.7m wall erected above ground level. This enables the pond to be maintained easily and operated safely. The pond was designed to have a 0.56m thick storage zone, 1.34m gradient zone and 0.15m surface zone (Leblanc, Akbarzadeh et al. 2011). Figure 3.2 shows a schematic diagram of the pond including the salt charger, thermocouple arrangement and the insulation system.

Figure 3.1 The 50m^2 RMIT experimental solar pond at Bundoora

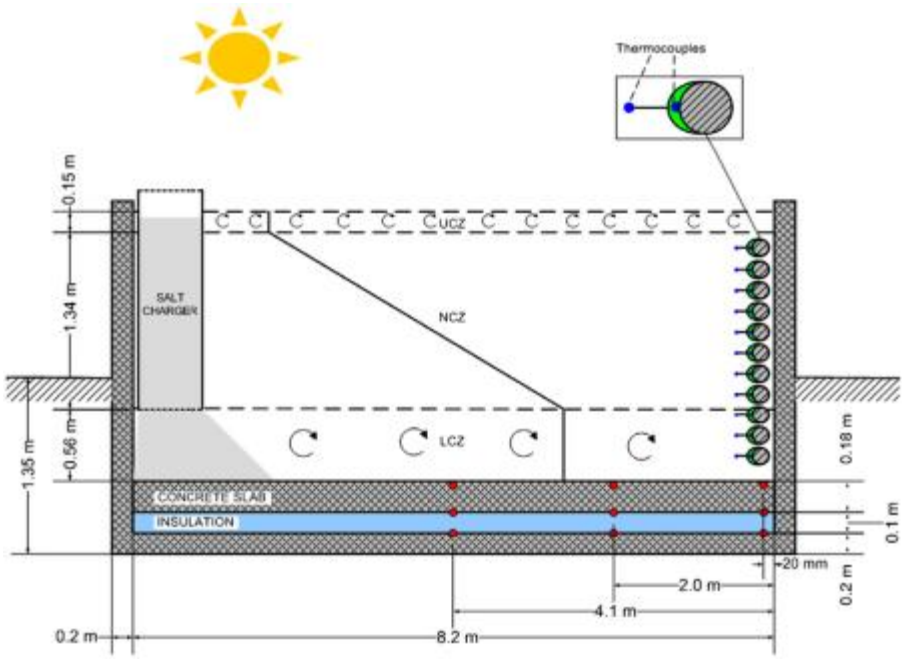

Figure 3.2 Schematic diagram of the RMIT solar pond (Leblanc, Akbarzadeh et al. 2011)

A dial thermometer was installed on top of the concrete wall as shown in Figure 3.3 to monitor ambient, top and bottom temperatures. An observation window made of 10mm thick glass of width 0.4m and height 1.5m is installed in the pond wall as shown in Figure 3.4(a). The purpose of this window is to monitor water clarity, the condition of the internal heat exchanger and to study the stratification layer in the pond. Granular potassium permanganate ($KMnO_4$) was used to visualize the stratification layer in the pond as shown in Figure 3.4 (b). The observations were carried out after the pond was filled with saturated brine prior to gradient establishment. The observations clearly show that 2/3 of the depth from the bottom consisted of constant concentration brine whilst in the upper 1/3 of the depth, mixing occurred with the appearance of irregular layer formation.

Figure 3.3 A Dial thermometer on top of the concrete wall

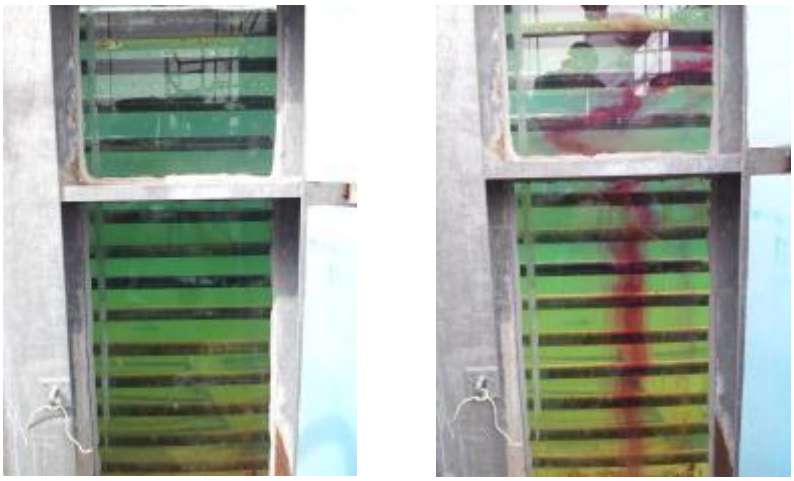

(a) (b)

Figure 3.4 (a) The observation glass window and (b) The visualisation of layers using potassium permanganate

3.2.1 Zone thickness and typical profiles

A working solar pond needs consistent zone thicknesses of the UCZ, NCZ and LCZ. Erosion caused by external forces such as strong wind, heavy rain or extreme ambient temperatures may expand the thickness of the UCZ. Similarly, the internal forces due to upwards salt transportation may cause the upper boundary to expand downwards and the lower boundary to move upwards. Both forces apparently will result in decrease of NCZ thickness, which will directly affect the performance of a solar pond. Consequently, in order to maintain the designated zone thicknesses, the UCZ brine needs to be diluted and salts need to be added to the LCZ. The details of this procedure are explained in section 3.2.1. Figure 3.5 shows the evolution of the UCZ, NCZ and LCZ thicknesses in the RMIT solar pond from 27 May 2011 to 26 April 2012. The effect of erosion can be seen in summer 2012 between January and March, where the thicknesses of the UCZ and LCZ increased thus reducing the thickness of the NCZ. This phenomenon is expected, as in summer the hot and dry conditions accelerate the rate of salt diffusion. However, the

thickness of each zone remained acceptable with an average of 0.15m for UCZ, 1.25m for NCZ and 0.65m for LCZ which do not differ greatly from the designated thicknesses.

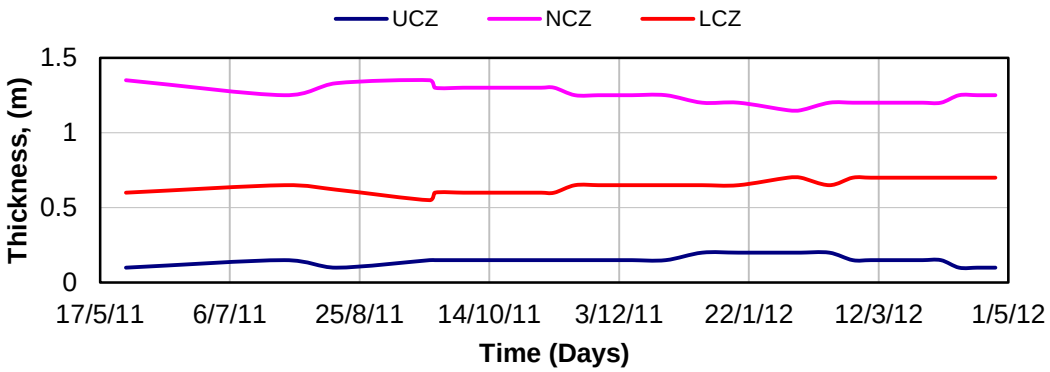

Figure 3.5 The evolution of UCZ, NCZ and LCZ thicknesses over twelve months

The density and temperature profiles of the RMIT solar pond in summer 2012 are shown in Figure 3.6 (a) and (b). Based on both profiles, the pond had a 0.6 m thick LCZ, 0.2 m UCZ and 1.25 m thick NCZ. The top surface consisted of low salinity brine with temperature close to ambient. Both density and temperature increased with depth towards highly dense brine of 1208kg/m^3 with a maximum temperature of 62^{o}C in the LCZ. The temperature difference between the LCZ and UCZ was 35.6^{o}C based on average monthly solar radiation of 279 W/m^2.

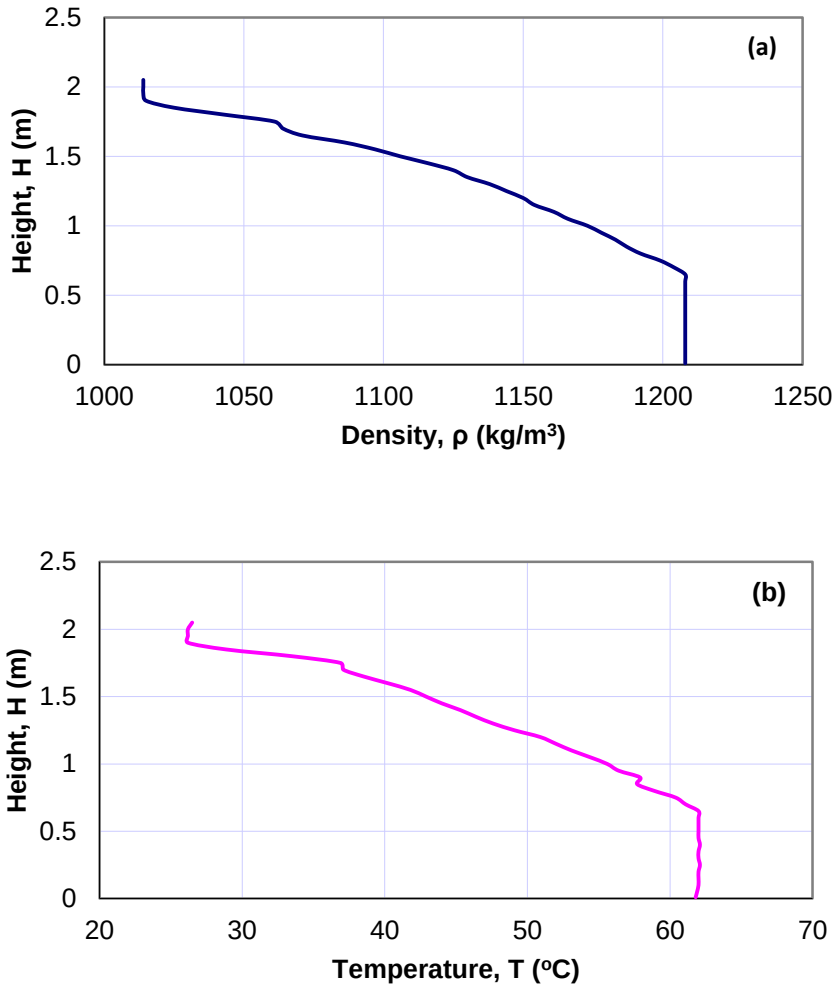

Figure 3.6 (a) Density and (b) temperature profiles taken on 18 Jan 2012

To ensure that the pond is always in good working conditions with profiles as shown in Figure 3.6, routine maintenance must be adhered to. The details of the maintenance procedure are explained in the following sections.

3.3 Maintenance

3.3.1 Salt charging

The pond was filled with 105m^3 of sodium chloride (NaCl) solution, with the concentration varying between 1005 kg/m^3 at the top surface and 1200 kg/m^3 at the bottom. A 0.6m diameter cylindrical salt charger made from polyethylene is fixed to the pond wall at approximately 0.56m above the floor for salt replenishment as shown in Figure 3.7. A livestock coarse salt supplied by Pyramid Salt was used for this purpose.

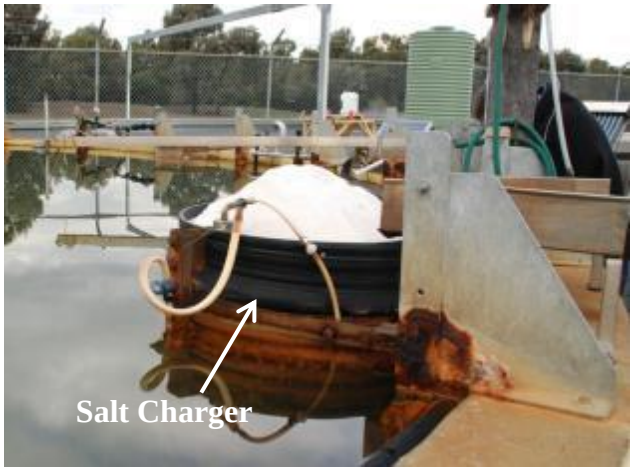

Figure 3.7 The Salt charger

Figure 3.8 shows the salt consumption at the RMIT solar pond from Mar 2011 to April 2012. It shows clearly that during summer, from December 2011 to February 2012, the salt consumption increased to twice the normal rate. The average consumption was approximately 87.5kg per month. Theoretically, based on equation 2.4 in Chapter 2, the estimated salt consumption was approximately 55kg per month. The measured data and estimated values are essential for a salt inventory analysis. A salt inventory analysis helps in budget planning as well as for detection of any leakage problems (Lu, Swift et al. 2004).

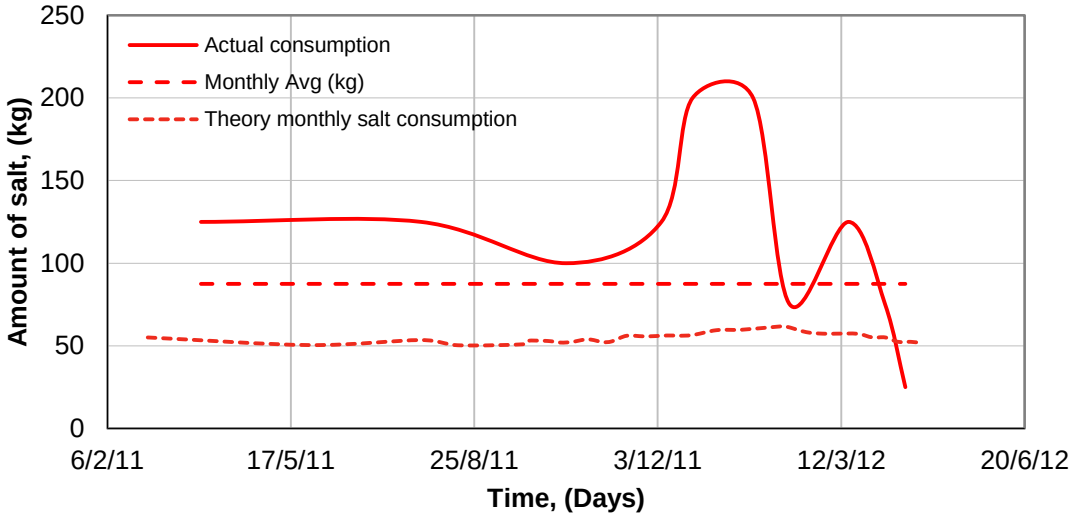

Figure 3.8 Salt consumption in the RMIT solar pond over twelve months

Fresh water is used continuously for surface flushing and to compensate for water loss by evaporation. The fresh water flow rate is set at approximately double the evaporation rate. There is an overflow system with three alternative water levels to ensure that the pond water is always at a constant level. Water levels indicators are (1: Low 2: Medium 3: High). Figure 3.9 shows the surface flushing and overflow systems.

(a) (b)

Figure 3.9 (a) Surface flushing and (b) Three levels of overflow system

3.3.2 Pond refurbishment

Pond refurbishment was carried out between June 2006 and December 2006. The main work was to install insulation for the pond to reduce heat loss to the ground and to its surroundings. A 100mm thick polystyrene insulation layer was installed on the pond bed, with density and thermal conductivity of 0.03w/m^{o}C and 35kg/m^{3} respectively. However, because of its low density, the insulation was exposed to a buoyancy force. Therefore a l80mm thick layer of concrete was poured on top of the insulation layer to overcome the upward buoyancy force. Similarly, the wall above the ground was insulated with a 100mm thick layer of polystyrene to reduced heat loss to the surroundings. Nine thermocouples were installed on top of and below the concrete floor to monitor the temperature variations as shown in Figure 3.2.

3.3.3 Salinity gradient repair

In early March of 2012, a convective layer of approximately 10cm thickness was detected at a location 1.2m above the floor. The extensive experimental activity to withdraw and inject brine to the NCZ was the main contributor to this problem. Initially, no remedial action was taken as it was hoped that natural diffusion would slowly eliminate the developed convective layer. Instead, by early June 2012 the convective layer expanded to 0.4 m thickness as shown in Figure 3.10. In the event of unintended convective layer development in the NCZ region, it will only restore itself if the thickness of the layer is less than 3cm or 4cm, otherwise some modification is necessary (Zangrando 1979).

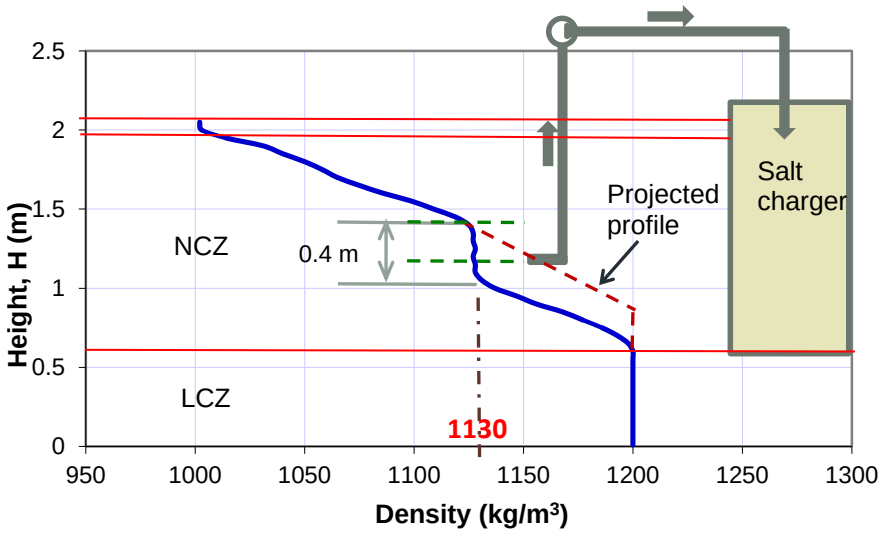

Figure 3.10 Schematic of gradient repair procedure

The scanning injection method, introduced by Zangrando and Bryant (2013) was employed to modify the damaged gradient. The same method has been successfully applied for gradient repair in the El Paso solar pond (Xu, Swift et al. 1992, Lu, Swift et al. 2004). The basic procedure is described in section 2.4.1.3 in Chapter 2. The following steps were taken at the RMIT solar pond to repair the affected gradient.

i. The diffuser was placed at the middle of the affected layer, and brine was transferred at a constant flow rate of 0.03 L/s into the LCZ through the salt charger as shown in Figure 3.10 to remove the layer below it.

ii. The brine density from the pump outlet was measured every four hours to ensure that the affected layer was removed completely.

iii. The diffuser was moved to the upper part of the affected layer as the density showed a higher reading than the affected layers, in this case 1130 Kg/m^3.

iv. Steps (i) to (iii) were repeated until the affected layer was removed.

The main objective of transferring the brine in the affected layer is to increase the concentration below it, in order to achieve the projected profile as shown in Figure 3.10. The density profile was measured daily to monitor the evolution of the salinity gradient within the four days of the process as shown in Figure 3.11. The process began at 10.30am on 24th July 2012 and stopped on the midday of 28th July 2012. The process resumed at 5.00pm on 30th July 2012, and stopped at midday 1st of August, 2012. The density measurement showed a reading of 1135Kg/m^3, and the plotted density profile was satisfactory as projected. There was an average of 2.1^{o}C temperature drop at the affected layer from 19th of June to 23rd of July when the ambient temperature drop showed only 0.4^{o}C as shown in Figure 3.12. After the gradient repair procedure was completed, the temperature gradient had been restored to the previous gradient reading around the affected layer, as on the 19th of June, while the temperature in the LCZ remains the same at approximately 2^{o}C less. This was acceptable as solar heat needs time to accumulate and increase the temperature of the LCZ. Overall, approximately 1.6 tons of salts were added progressively through the salt charger to maintain high concentration of brine in the LCZ and maintain the pond stability.

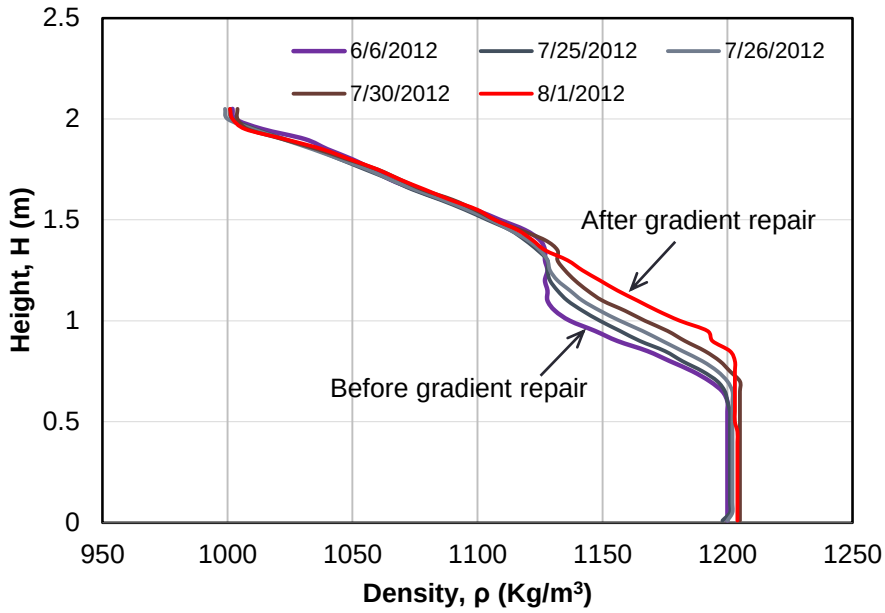

Figure 3.11 Density evolution during the gradient repair process

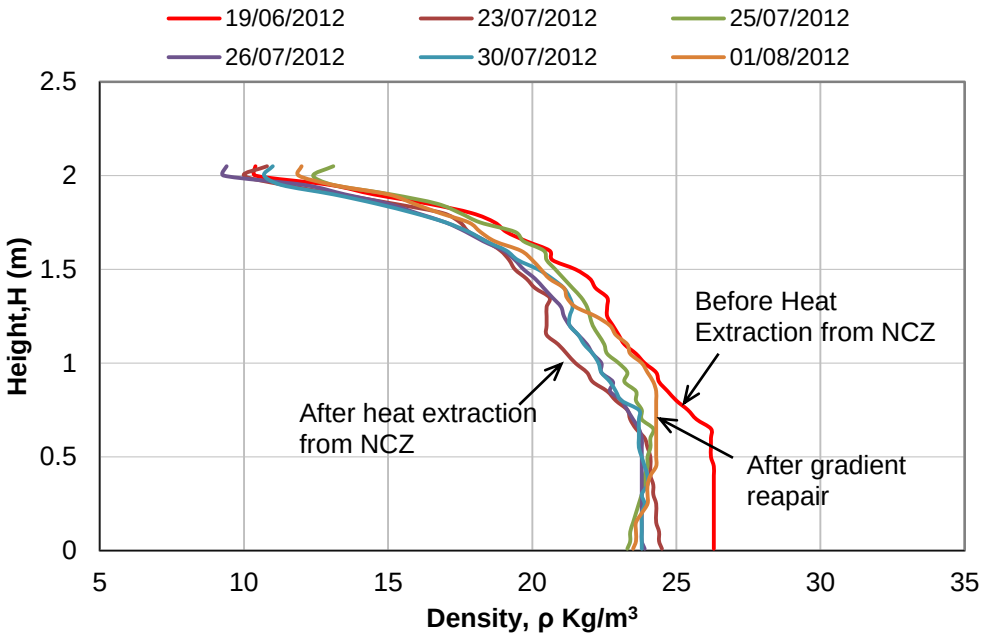

Figure 3.12. Temperature evolution during repair gradient process

A semi-circular diffuser made of PVC with a diameter of 350mm, an overall thickness of 25mm and a gap of 3mm as shown in Figure 3.13 was used during the process. It was fabricated using two PVC plates held apart by a 3mm spacer to create six horizontal channels along the gap. The brine was extracted in a horizontal plane to minimise mixing through the centre of the diffuser. The brine flowed through a 10mm diameter hose connected to a 12V pump and the outlet was on the salt charger as shown in Figure 3.14.

Figure 3.13 Diffuser used in RMIT solar pond

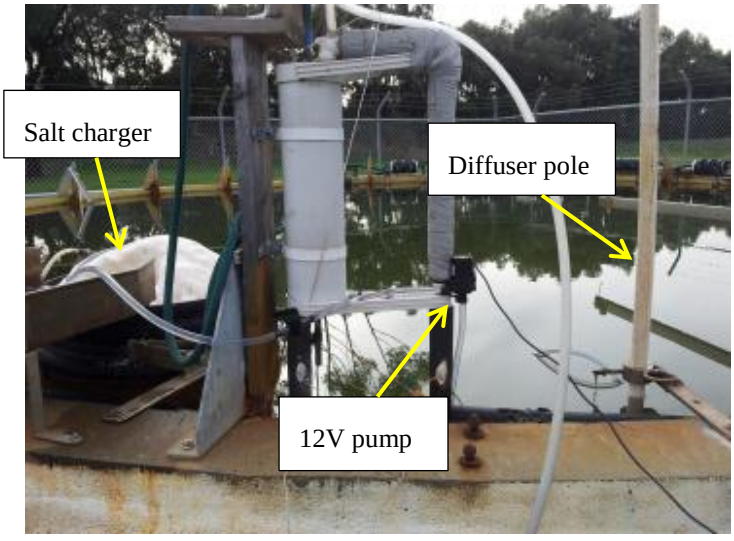

Figure 3.14 Gradient repair arrangement

3.3.4 Salinity gradient establishment

In the middle of December 2012, the RMIT solar pond was emptied to replace the heat exchanger supports and to repair leakage at the observation window. The existing supports which were made of galvanised steel were badly corroded after being exposed to salty and acidic environments for more than a decade. Figure 3.15 shows new supports being installed at the RMIT solar pond. Approximately 63m^3 of highly concentrated brine from the LCZ of was kept in two evaporation ponds and two other portable pools in the RMIT Renewable Energy Park as shown in Figure 3.16. The remaining pond water was discarded after being diluted. Twenty five new supports made of stainless steel were installed by their supplier. Epoxy was applied to the observation window steel frame to overcome the leakage problem. A hydrostatic pressure test was conducted at 500kPa for both internal heat exchangers on the pond floor as well as for the heat exchanger on the vertical wall to ensure that the pipes were in good condition without any leakage. The thermocouples tracking the brine and heat exchanger wall temperatures were recalibrated with hot and cold water measured both by mercury thermometers and by a DataTaker (DT500) unit.

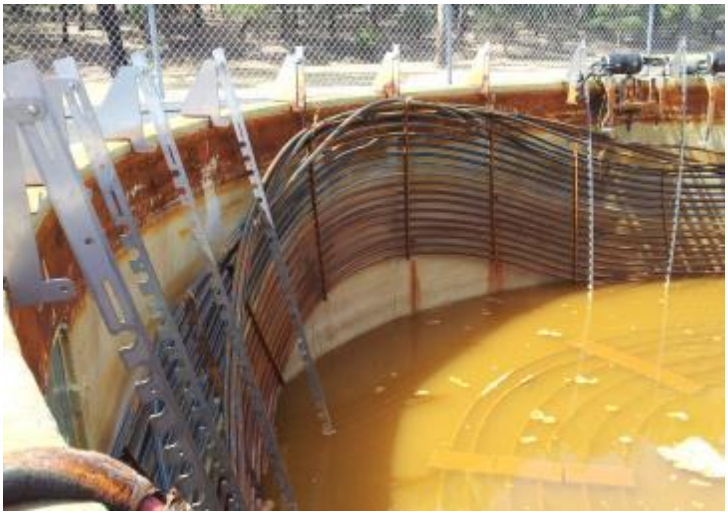

Figure 3.15 Installation of new supports

Figure 3.16 A Circular portable pool used as a storage pond.

3.3.4.1 Refilling

The redistribution technique which was introduced by Zangrando (1980) is used for gradient establishment. The technique requires the pond to be half filled with highly concentrated brine prior to establishing the gradient. Because of a long storage period of nearly three months, the formation of crystal salt was observed at the bottom of the storage pond as shown in Figure 3.17(a). A similar phenomenon occurred with the residual brine in the solar pond as shown in Figure 3.17(b). Before replacing the brine in the pond, the crystal salt in the storage ponds must be dissolved by using a pump to circulate the brine in a loop.

(a) (b)

Figure 3.17 Formation of crystal salt in (a) storage pond and (b) solar pond

The density of each storage pond was measured using the density meter to determine the actual salt levels and the additional salt requirement to achieve a density of 1200kg/m^3 as shown in Table 3.1. In total, 70m^3 of high concentrated salt at 1200kg/m^3 was required to fill half of RMIT solar pond. An additional 7m^3 of fresh water needed to be added to make-up the total requirement in addition to the quantity available in all the storage ponds. Based on the requirements shown in Table 3.1, 3 tons salt was purchased. A 2.5 ton quantity of salt was poured into solar pond before the addition of brine as shown in Figure 3.18.

Table 3.1 Density level at each storage pond and salt requirement

Storage pond	Volume, m^3	Density, kg/m^3	Salt Required, kg
1	7.0	1194	42.00
2	23.3	1187	302.90
3	23.3	1194	139.80
4	9.4	1127	686.20
Fresh water	7.0	1000	1,400.00
Total	70.0		2,570.90

Figure 3.18 Salt being poured into the solar pond before refilling process

The distribution technique can be described with reference to the schematic diagram shown in Figure 3.19. Consider the total depth of the solar pond as $D = L + H$, where L is the designed depth of LCZ with high concentration C_c and H is the designed depth above the LCZ to the surface with an average concentration of ½ C_c. The linear gradient is assumed to reach zero concentration on the surface. Consequently it is required initially that the depth of $L + ½ H$ is filled with highly concentrated brine. Another ½ H is to be filled with fresh water to dilute the brine above the LCZ to obtain the linear gradient.

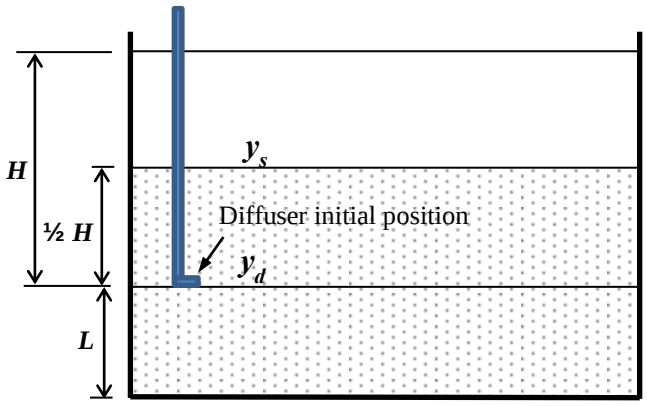

Figure 3.19 Schematic of redistribution technique for gradient establishment

The diffuser is placed in the water at height *L*, just on top of the designed storage zone (LCZ) and needs to be raised at constant rate. Fresh water is injected directly at a constant flow rate through the diffuser to fill the top region of the pond. The lower density injected water will mix with the brine above the diffuser level to create a homogenous layer and simultaneously dilute the brine concentration as the pond is filled to the maximum capacity of *L+H*. The diffuser must be raised at a rate relating to the surface motion so that the diffuser eventually reaches the surface at height *L+H*.

Assuming that the initial position of the diffuser at any time is $y_{d,}$ and that it started from *L*, whereas the initial position of the surface is y_s, and it started at *L +1/2 H*. Then, the equation to solve this problem can be stated as;

$$y_d = c_1 y_s + c_2 \qquad \text{where at } t=0,\ y_d = L \text{ and } y_s = L + 1/2H \tag{3.1}$$

$$\text{at } t=t_f,\ y_d = y_s = L + H$$

Considering the condition at the final position;

$$y_d = 2y_s - (L+H) \quad \text{and} \quad \dot{y}_d = 2\dot{y}_s \tag{3.2}$$

Where $\dot{y}$ represents the time derivative for the diffuser motion rate compared to the surface motion rate. Therefore, at any time the diffuser is raised twice the distance of the surface movement.

Zangrando (1979) has demonstrated that the change in mass and concentration at each point is given by;

$$\frac{dC}{C} = \frac{-dy_s}{L+H-y_s} \tag{3.3}$$

Where, at t=0 $C=C_c$ and $y_s = L + 1/2H$

at $t=t_f$ $C=0$ and $y_s = L + H$

where C is the concentration and C_c is the initial concentration

Hence, the change of concentration in the upward vertical direction becomes;

$$C(x) = 2C_c\left(\frac{L+H-y_s}{H}\right) = 2C_c\left(1 - \frac{x_s}{H}\right) \tag{3.4}$$

where $x_s = y_s - L$

The total time required to complete the gradient establishment is determined by the pump capacity and the size of the pond.

In the RMIT solar pond, fresh water was supplied directly to the diffuser at a constant mass flow rate of 0.33kg/s. The value of the Froude number, Fr, was calculated to be approximately 3 compared to the value of Fr=15 as recommended by Zangrando (1979). A 1.325m part of the 2.05m total depth was filled with highly concentrated brine and the remaining 0.745m was filled using the distribution technique. The remaining depth was distributed into 15 steps each of 5cm thickness. The initial position of the diffuser was at 0.56m above the base and it moved at twice the rate of the water level rise. For each step,

the diffuser was raised 10cm corresponding to twice the motion of water level. The RMIT solar pond was filled using this technique over four consecutive days in March 2013. The evolution of the density gradient during the process of gradient establishment is shown in Figure 3.20. The mixing process to dilute the salt solution, which occurred above the diffuser when fresh water was injected, can be considered to be the major contributor to the success of this technique (Zangrando 1979). Each time the diffuser was raised, the injected fresh water diluted the brine above it and a less dense layer was created. The process was repeated until the diffuser reached the top layer, where the density was close to the fresh water density.

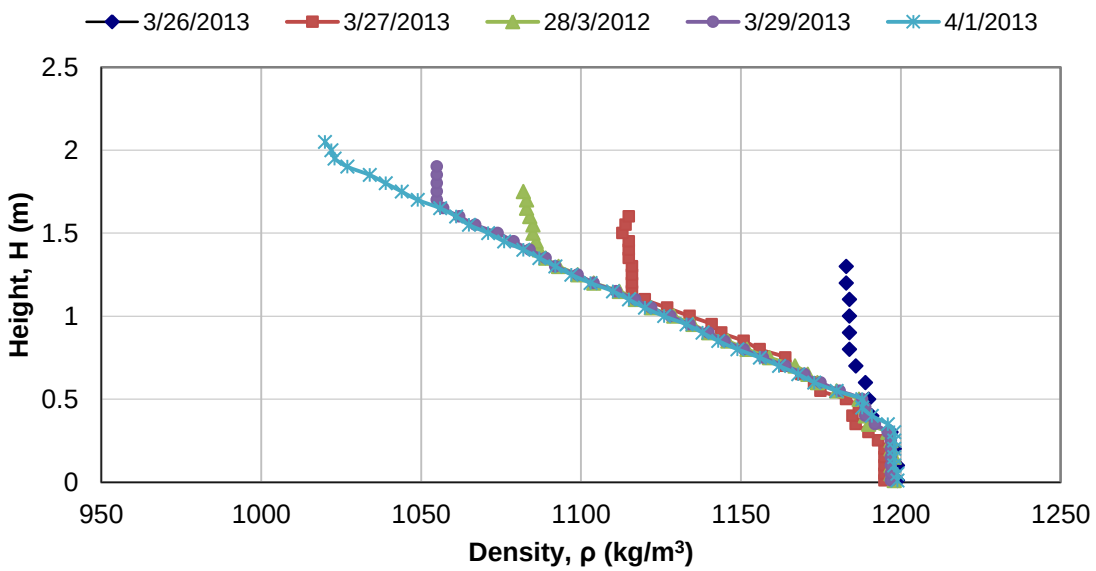

Figure 3.20 The density gradient evolution during gradient establishment

3.3.5 Clarity maintenance

3.3.5.1 Control of turbidity

Brine clarity is one of the key factors in achieving good thermal performance of solar ponds. The turbidity issue may arise because of the presence of suspended particles or populations of algae or bacteria (Hull 1989, Malik, Date et al. 2011). An algae population is common in all brine and therefore represents a problem in relation to maintaining transparent water in solar ponds. Turbidity measurements are based on nepthalometric turbidity units (NTU) or formazin turbidity units (FTU). Typically, the human naked eye notices the effect of turbidity as the NTU reading reaches 5 and above (Myre and Shaw 2006). At El Paso, the NTU was maintained at a maximum level of 3 to allow good penetration of solar radiation into the solar ponds (Xu, Sandoval et al. 1993). One of the most common methods used for controlling algae growth is chemical treatment. This includes chlorination, flocculation, precipitation, algaecide addition and acidification (Hull, Nielsen et al. 1989). In the Alice Springs solar ponds, chlorine was introduced to the surface layer as reported by Sherman and Imberger (1991). Aluminium sulphate was used to treat the 1000m^2 Argonne National Laboratory solar pond in Illinois (Hull 1989). In the Bhuj solar pond, a combination of hydrochloric (HCL) acid and copper sulphate was used to maintain the clarity (Kumar and Kishore 1999). The mixed solution was injected at an appropriate level through a small diffuser with a 2mm slit.

A number of methods of clarity maintenance have been demonstrated in the RMIT solar pond including introduction of brine shrimps as a biological treatment and chemical treatment using HCL acid as reported by Malik (2003). Later, Gasulla, Yaakob et. al (2011) have introduced a copper sulphate in their search for a suitable chemical as an alternative to HCL acid because of the corrosion issue. In their experiments, a new stable copper-based algaecide solution known as cupricide was used. The cupricide must be diluted beforehand at a proportion of 1:10 with brine from the layer to be treated. Algae-

affected brine from the layer between 37cm and 88cm from the pond floor was treated using cupricide. The results indicated that the use of the cupricide improved the brine transparency, as shown in Figure 3.21. The improvement can be seen in the turbidity readings after one week of cupricide treatment. The turbidity reading on the affected layer reduced from a maximum of 8NTU to 4NTU. The remaining layers showed a good reading at approximately 1NTU.

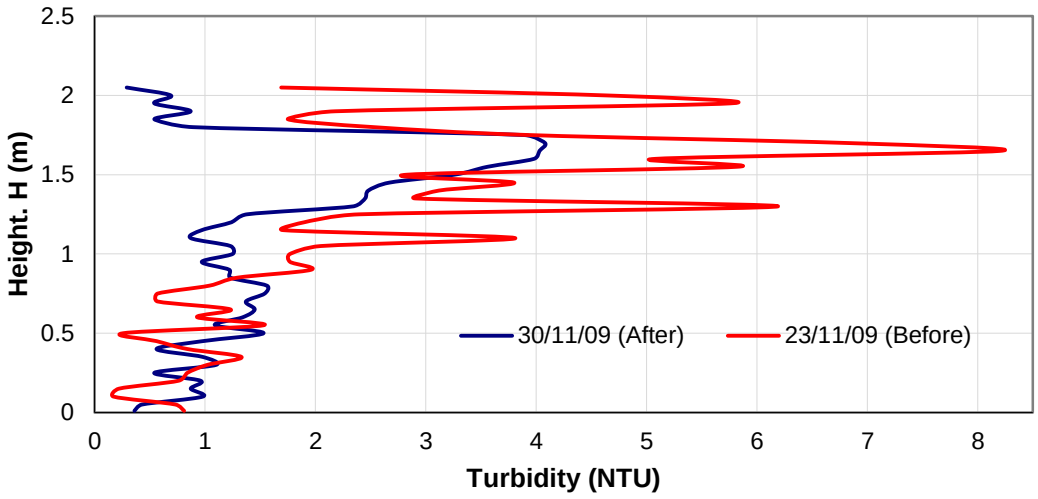

Figure 3.21 Evolution of turbidity profiles before and after Cupricide treatment

An alternative method for quantifying the turbidity of the brine is by using a photovoltaic cell. A calibrated polycrystalline solar cell, which could be immersed in water, was used to measure the solar radiation absorbed by the solar pond brine. By varying the resistance and recording the corresponding currents through and voltages across the cell, the I-V characteristic performance and power curve can be developed (Green, Joyce et al. 1987).

Figure 3.22 shows the schematic and equipment arrangement for the single PV cell current absorption technique. The voltmeter was connected in parallel with a variable resistance and an ammeter was connected in series. The solar cell was placed at the

bottom of a 150mm diameter PVC cylinder. The solar pond water sample was then filled to a fixed depth in the cylinder. A constant light source of 100W was used to supply radiation to the test rig. Brine with different turbidity levels determines the level of absorption of the radiation, thereby resulting in different performance curves for the PV cell. The resulting I-V and power curves are shown in Figure 3.23. It can be seen that after Cupricide treatment the maximum current (I-V) and maximum power increased from 7.5mW to 11.5mW which represented a 35% improvement.

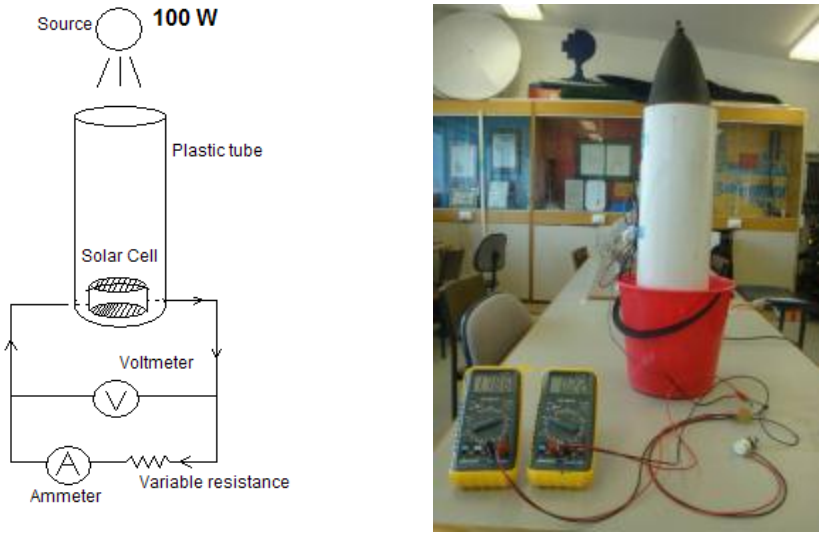

(a) (b)

Figure 3.22 (a) Schematic and (b) solar cell experimental set up

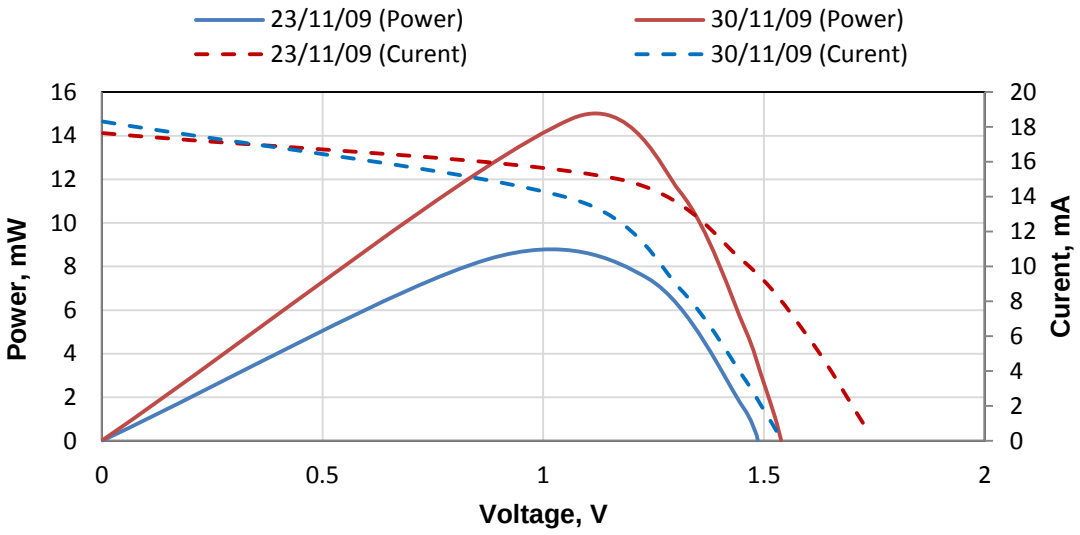

Figure 3.23 Power and current curves before and after Cupricide treatment

Cupricide proved to be less corrosive than hydrochloric acid by comparing the weight losses of metal samples dipped in the two solutions. A downside of the cupricide treatment method is that cupricide costs much more than hydrochloric acid.

3.3.5.2 Control of pH value

Hull (1989) suggested that another practical means of maintaining clarity is to keep the pH of the brine at a value of 4 or less by adding HCL acid. At the RMIT solar pond, the same method has been employed with HCL acid added to maintain the pH value below 4. Figure 3.24 shows the evolution of pH values after adding HCL acid to the pond. HCL acid was added on the 4th October 2011when the pH value was 4 within the NCZ. The pH was constant at approximately 6.2 in the LCZ, but gradually reduced as it passed above the lower interface. The pH values were approximately constant between 1.2m and 1.6m above the floor. From that point, the pH value started to increase until it reached the maximum value at the UCZ. After one week the pH value dropped drastically to 3, and

then slowly increased with time. The HCL was injected into the NCZ at different depths via the acid injection pipes as shown in Figure 3.25 (left).

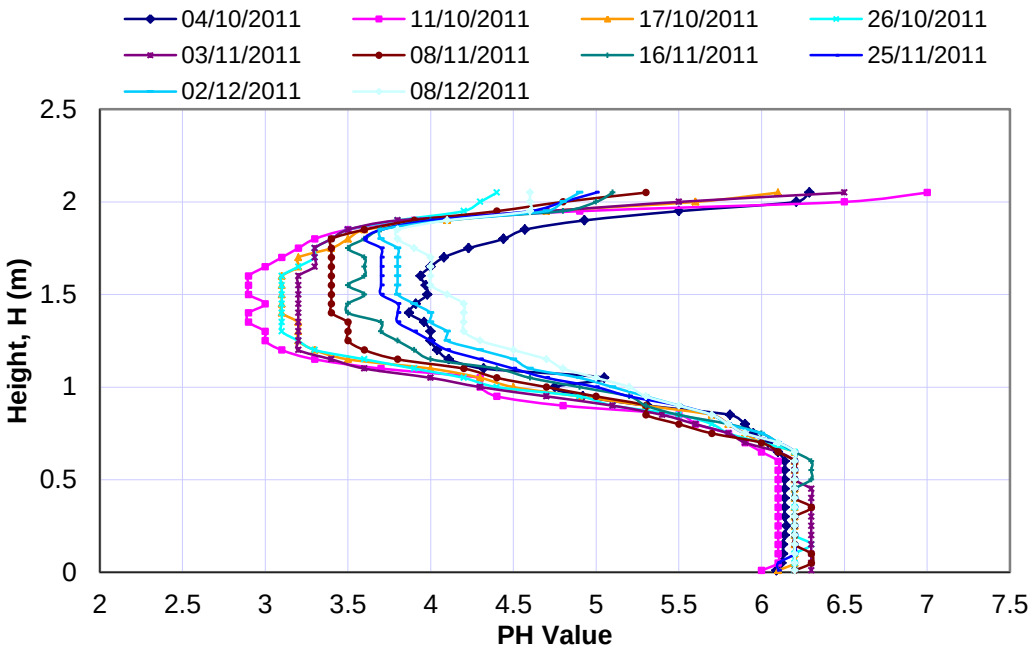

Figure 3.24 pH values evolution after chemical treatment

For the treatment procedure, 5 litres of HCL were used and divided into four portions for four different levels within the NCZ. HCL was diluted at the ratio of 1.25:5 using the brine which was siphoned out from the same level that the acid was to be added to. The solution was normally mixed in a bucket and poured into the pipes fixed to the wall at the top of the surface as shown in Figure 3.25 (right). A disadvantage of this practice is the difficulty of controlling the flow injected into the gradient layer when controlling the bucket manually. A simple method of injecting the HCL with better control of injection flow is by using a diffuser. A 10L container with a flow control valve is connected to the diffuser by using a plastic hose. The container is placed on the highest platform, and the valve is slowly opened to allow the HCL solution to flow down into the diffuser under

gravitates. This simple method provided better injection flow into the gradient layer and represented a safe working practice as shown Figure 3.26.

(a) (b)

Figure 3.25 (a) Acid injection pipes and (b) the injection process using funnel

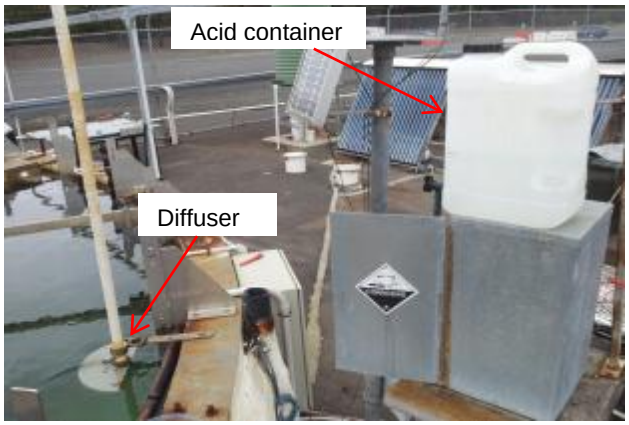

Figure 3.26 Injecting acid through the diffuser

3.4 Heat extraction system

A submerged heat exchanger, also termed an internal heat exchanger system, was installed in the RMIT solar pond. Reinforced polyethylene pipe of 32mm outside

diameter and 3mm wall thickness of conductivity 0.37W/m^{o}C was used as the heat exchanger. There were two sections of the internal heat exchanger. The heat exchanger laid on the pond floor was intended for heat extraction solely from the LCZ, and the heat exchanger fixed onto the side wall was intended for heat extraction from the NCZ as well as the LCZ. There were 22 rows of pipes on the wall giving a total length of 560m for a total surface area of 56.3m^2. For the LCZ heat exchanger, an 83m length of pipe was supported by hollow bricks to form six circular layers with an outer diameter of 5.4m and 0.2m spacing between the loops. The total surface area of the LCZ heat exchanger was 8.34m^2. The arrangements of both heat exchangers are shown in Figure 3.27.

(a) (b)

Figure 3.27 (a) Internal heat exchanger for LCZ and (b) heat exchanger for NCZ-LCZ

A submersible pump with flow rate of 950 litres per hour and maximum head of 1.8 m was used to circulate cold brine from the surface back to the heat exchanger in order to collect the available heat from the pond and return it to the surface at an increased temperature as shown in Figure 3.28. A floating board was introduced in order to avoid mixing in the UCZ layer.

(a) (b)

Figure 3.28 (b) Submersible pump and (b) outlet of the heat exchanger

3.4.1 Performance of LCZ heat exchanger

Theoretical performance of the pan-cake type LCZ heat exchanger can be calculated using the following formulation (Jaefarzadeh 2006);

$$AU\frac{(T_o-T_i)}{Ln\left(\frac{T_p-T_i}{T_p-T_o}\right)} = \dot{m}c_p(T_o - T_i) \tag{3.5}$$

where A is the total heat exchanger surface area (8.34m²) , U is the overall heat transfer coefficient of heat exchanger, $\dot{m}$ and c_p are the mass flow rate and the specific heat of the heat transfer fluid respectively, T_p is solar pond LCZ temperature, while T_o, and T_i are the temperatures of heat transfer fluid at outlet and the inlet of the heat exchanger respectively.

The outlet temperature of heat exchanger can be calculated by rearranging equation 3.5 as follow;

$$T_o = T_p - \frac{(T_p-T_i)}{exp\left(\frac{UA}{\dot{m}c_p}\right)} \tag{3.6}$$

Assuming the overall heat transfer coefficient for natural convection in water as 25 $W/m^2.^oC$, the temperature of LCZ to be 35^oC and the inlet temperature of heat transfer fluid to be 20^oC and mass flow rate of heat transfer fluid is 1 kg/min. The average solar radiation received on the pond surface is assumed to be $200W/m^2$. The total heat exchanger surface area is $8.34m^2$. Based on these input parameters, the instantaneous outlet temperature is predicted to be 34.2^oC, with temperature difference of 14.2^oC. From here the instantaneous thermal efficiency of the LCZ heat exchanger is predicted to be around 10%.

The performance of LCZ heat exchanger was performed in October 2013. The performance was monitored for twenty four hours as shown in

Figure 3.29. The average of outlet temperature was 29^oC which was close to LCZ average pond temperature of around 31^oC. The inlet temperature is always maintained close to ambient temperature which is around 17^oC. The temperature difference obtained from this observation was around 12^oC.

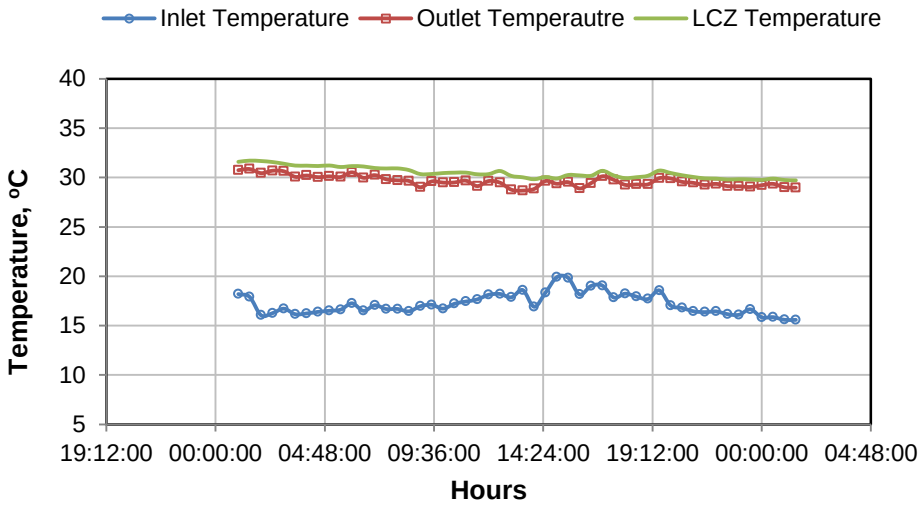

Figure 3.29 The inlet and outlet temperature of LCZ heat exchanger in 24 hours monitoring on 11th to 12th October 2013

Figure 3.30 shows the amount of heat extracted compared to the average of solar radiation received in the earlier week. The dotted line shows the calculated thermal efficiency of the LCZ heat exchanger with an average of 9%. The experimental results show a good agreement with the predicted instantaneous thermal efficiency of 10%.

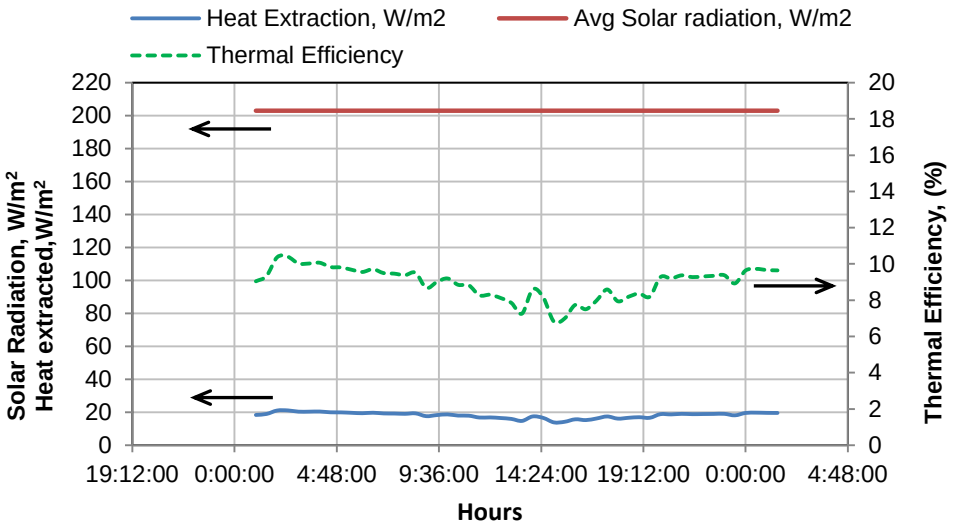

Figure 3.30 The performance of LCZ heat exchanger in RMIT solar pond

3.4.2 Performance of NCZ-LCZ heat exchanger

Heat extraction using the NCZ-LCZ heat exchanger was performed for one week from 15th of Mar 2010 to 22nd of Mar 2010 to observe the performance of the RMIT solar pond. The pump flow rate was set at 0.04 litres per second (L/s approximately equivalent to Kg/s). Figure 3.31 below shows the daily average temperature of the UCZ, LCZ, heat exchanger inlet and heat exchanger outlet during the heat extraction period. It can be seen that the temperature of the heat exchanger fluid at the inlet was close to the UCZ temperature. This is because the UCZ brine was used as a heat exchanger fluid

circulating through the whole length of the heat exchanger pipe. The variation of temperature of the heat exchanger fluid at the outlet parallels that of the LCZ with 3.6^{o}C temperature difference. This conition could be attributed to the frictional losses as well as to heat loss from the pipe wall to the surrounding fluid. Figure 3.32 shows the amount of heat extracted from the RMIT solar pond from both the NCZ & LCZ over a typical week. The efficiency of solar pond was calculated using equation (2.10). The result shows, the efficiency of the RMIT solar pond was approximately 23% within this period of time. The performance was expected to be higher, but poor brine clarity due to algae bloom had limit the penetration of sunlight.

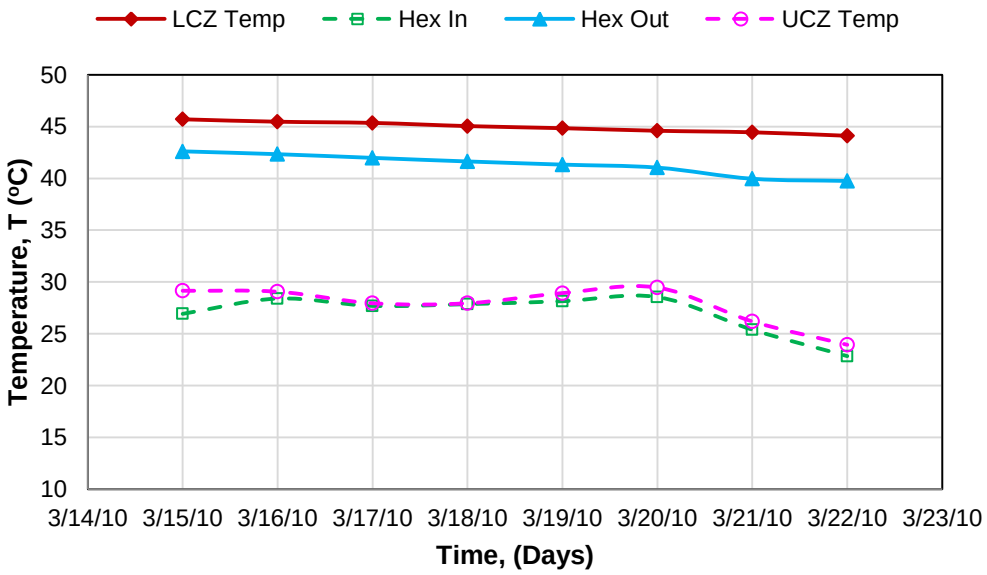

Figure 3.31 Average daily temperature of UCZ, LCZ, inlet and outlet of heat exchanger

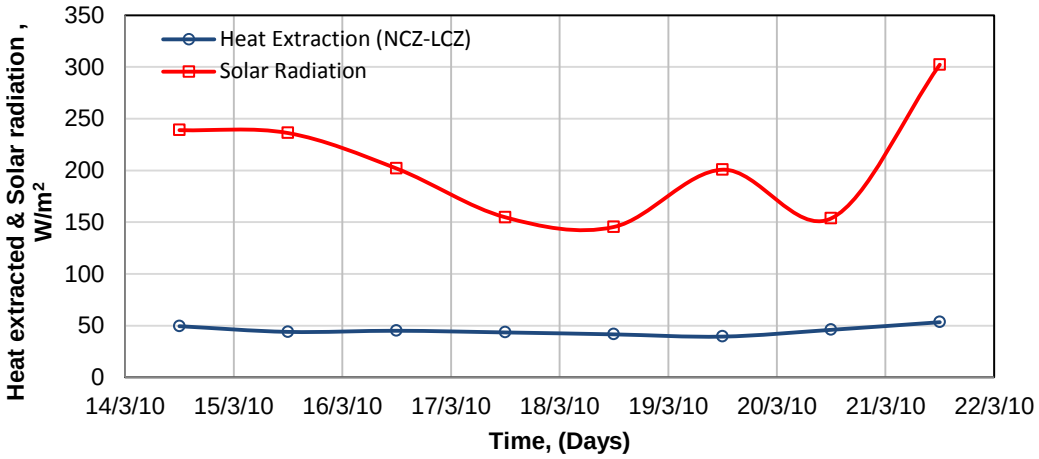

Figure 3.32 Sample heat extraction data for RMIT solar pond

3.5 Instrumentation and monitoring system

3.5.1 Temperature tracking

A DataTaker (DT500) was used as a data acquisition system to track the temperatures in the pond and solar irradiance throughout a 24 hour day. The DataTaker was connected to a computer inside the Renewable Energy building which was situated approximately 50m from the pond. The monitoring system was programmed to record temperature readings at 30 minute intervals and to track the solar irradiance at 5 minute intervals. Temperature monitoring was accomplished by using 57 thermocouples. The thermocouple arrangement is shown in Figure 3.33. Forty four thermocouples were arranged vertically starting from a height of 0.2m above the pond floor. They were placed at intervals of 80mm up to a height of 1.88m above the floor. At each position the thermocouple was fixed to a polyethylene tube and covered with Armaflex insulation in order to measure the heat exchanger wall temperature. A thermocouple was located 20mm from the pond floor to measure the lower region temperature of the LCZ. Two thermocouples was placed about 2mm below surface and out of surface to track the UCZ and ambient

temperatures respectively. One thermocouple was placed on top of the concrete floor 2m from the side wall and another nine thermocouples were installed below the concrete floor to measure the heat losses to the ground. Three thermocouples were placed 5mm below the concrete floor at distances of 20mm, 2m and 4m from the side wall. There are three thermocouples in between the concrete slab and the insulation at the same distances. Three more thermocouples were placed at the same manner below the insulation. The arrangements of the thermocouples below the concrete floor are shown in Figure 3.2.

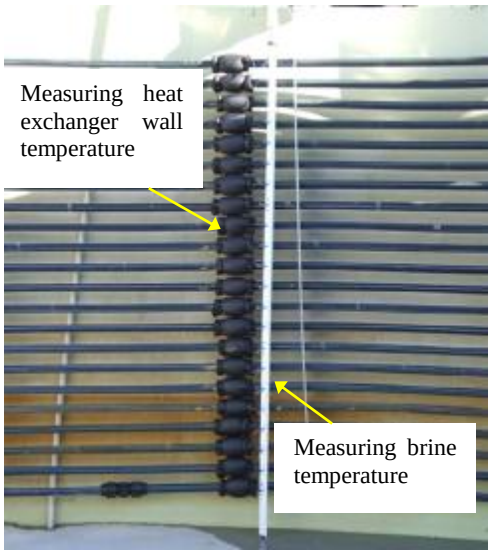

Figure 3.33 Arrangement of thermocouples in RMIT solar pond

Figure 3.34 shows the monthly average of LCZ and ambient temperatures for a period of twenty four months from October 2010 to September 2012. The LCZ temperature reached its peak of 61^{o}C during summer of January 2012. The lowest temperature of the LCZ was 24^{o}C recorded during winter of July 2012. The ambient temperature showed a similar pattern with a maximum temperature of 27^{o}C in summer and a minimum

temperature of 13^{o}C in winter. There was a temperature difference between the LCZ and the surroundings of approximately 34^{o}C in summer which reduced to 11^{o}C in winter.

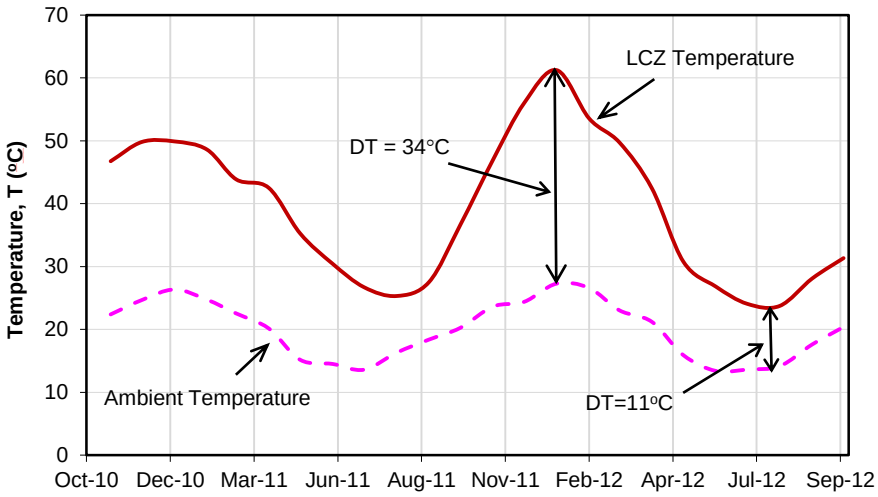

Figure 3.34 Monthly averages of LCZ and ambient temperatures from October 2010 to September 2012

Considering that the thickness of the LCZ is 0.6m, that the cross sectional area of the pond is 50m^2 and that the density of the brine in LCZ is uniform at 1200kg/m^3, the pond thermal capacity is calculated as follows;

$$Q = m_{LCZ} C_p DT \tag{3.7}$$

Where, m_{LCZ} is the mass of the brine in the LCZ in kg, C_p is the specific heat in J/kg.^{o}C and *DT* is the temperature difference in ^{o}C.

Hence, the maximum heat storage capacity of the RMIT solar pond in summer is estimated to be 151MJ and is calculated as follows,

Q = 1200 kg/m^3 x 0.6 m x 50 m^2 x 4.2 kJ/kg. ^{o}C x 34^{o}C

$= 1.51 \times 10^5$ kJ

3.5.2 Solar radiation tracking

Solar radiation was measured by the SolData 80SPC pyranometer in a horizontal plane, positioned next to the solar pond and connected to a DataTaker. The pyranometer employs a photovoltaic solar cell to absorb the solar irradiance and provides a voltage output mV. A typical calibration factor, *K* provided by the manufacturer was 160mV/(kW/m^2). This calibration implies that when the solar irradiance, *S* is 1kW/ m^2 at noon of a sunny day with a clear sky, the pyranometer will provide an output voltage of 160mV. Hence the obtained output value in mV at any time needs to be divided by 160 and multiplied by 1000 to calculate the solar irradiance to W/m^2. The pyranometer at the RMIT solar pond has been used for approximately a decade. In February 2012, it was calibrated at the Vipac Engineers & Scientist facility in Melbourne as shown in Figure 3.35. The results showed that, the calibration factor subsequently reduced to 143mV/(kW/m^2). Details of the calibration data can be found in Appendix A.

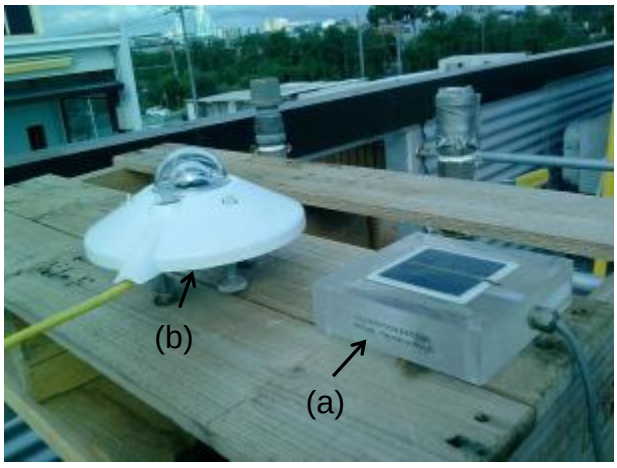

Figure 3.35 Calibrating (a) a single cell pyranometer with (b) global diffuse pyranometer

Figure 3.36 shows the monthly average solar radiation levels and ambient temperatures for the six years starting from January 2007 until December 2012. These data were obtained from Bureau of Meteorology website, where the nearest weather station is located at La Trobe University, about 5.3km away from the RMIT solar pond site. In January 2009 the highest level of solar radiation recorded was at an average of 360W/m^2. The lowest solar radiation level recorded was in June 2012 at an average of 60 W/m^2. The two readings represent the amount of solar radiation in summer and winter respectively. On average, 196.4W/m^2 of solar radiation was received in Bundoora over the past six years and the average ambient temperature for the same time period was 20.6^{o}C.

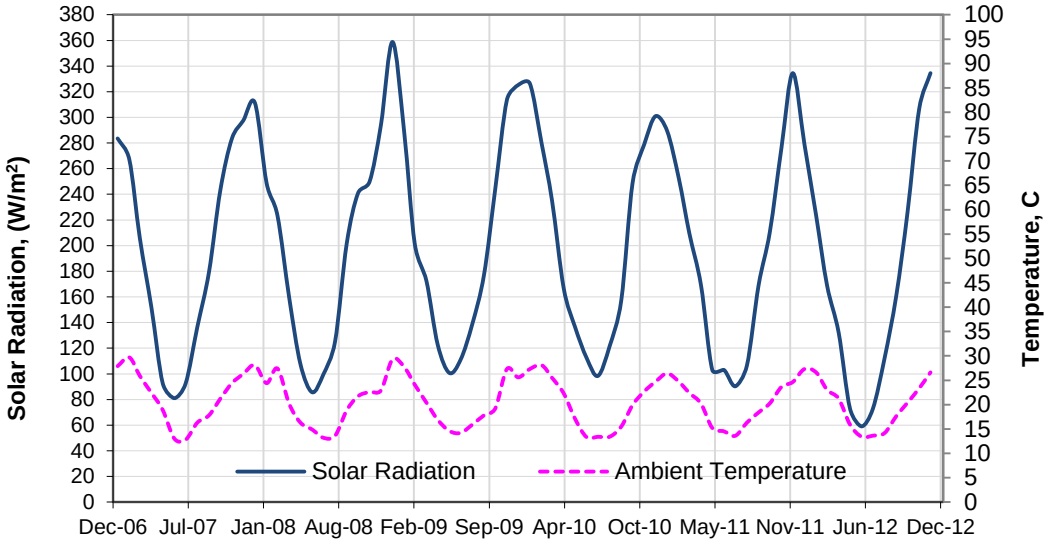

Figure 3.36 Monthly average solar radiation and ambient temperatures from January 2007 to December 2012 (www.bom.gov.au 2013)

3.5.3 Density, pH level and clarity measurement

Manual measurement of temperature, density, pH and turbidity profiles was carried out fortnightly as a monitoring routine. A small hose of 9mm diameter inserted into a 20mm diameter PVC pipe was used as a probe to draw out water samples at each 5cm height increment descending from the upper surface. A supporting post was fixed to the top of the pond wall with an adjustable holder as shown in Figure 3.37. A portable digital thermometer was connected to the k-type thermocouple sensor and a hand-held Anton Par density meter, the hand-held Hanna Instruments pH meter and a turbidity meter were used for measurements as shown in Figure 3.37, Figure 3.38 and Figure 3.39 below. All of these instruments were regularly calibrated to ensure their accuracy.

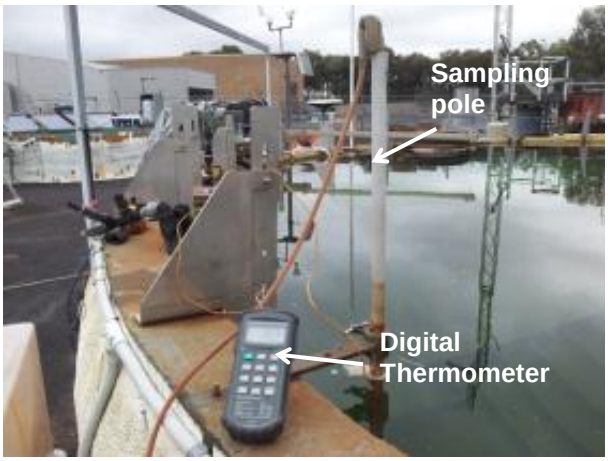

Figure 3.37 The sampling pole and hand-held digital thermometer

pH meter

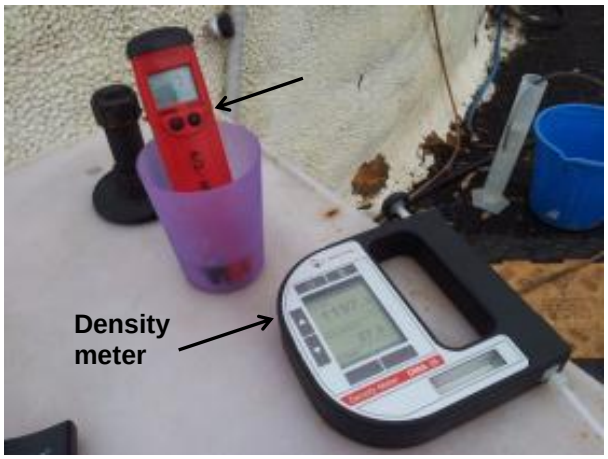

Figure 3.38 Hand-held pH meter and density meter

Figure 3.39 Portable turbidity meter (www.hannainst.com)

Chapter 4 - Theoretical performance of solar pond

4.1 Introduction

This chapter presents a theoretical analysis of solar pond thermal performance with and without heat removal. The analysis is divided into steady state and transient conditions. The steady state analysis investigates the development of temperature profiles in the NCZ and temperature in the LCZ based on the amount of radiation received at the surface. The development of the LCZ temperature is predicted for a period of three years for different thicknesses of NCZ layer. Finally the efficiency of a solar pond with heat extraction from the NCZ and the LCZ is determined. This chapter further explains in detail the design and steady state theoretical analysis of the proposed heat extraction system with external shell and tube heat exchangers for the RMIT solar pond.

4.2 Solar radiation and transmission

4.2.1 Solar radiation

The sun emits radiation in a wide spectrum at an average temperature of 6000K (McVeigh 1977) in the form of electromagnetic radiation with the wavelength ranging from approximately 0.3μm to over 3μm, and clustered into three parts as follows;

i. Ultraviolet (wavelength less than 0.38μm)

ii. Visible (wavelength between 0.38 to 0.78μm)

iii. Infrared (wavelength more than 0.78μm)

Solar radiation takes eight minutes to reach the earth's atmosphere with an approximate velocity of 3×10^8m/s. The solar radiation energy received on the earth's surface is called insolation and is measured in unit power per square meter, W/m^2.

The rate of incoming solar radiation received outside the earth's atmosphere perpendicular to the solar beam at the mean distance between earth and sun is called the solar constant. The present accepted value is 1360.8 ±0.5W/m^2 (Kopp and Lean 2011).

As solar radiation passes through the atmosphere, some portion of the radiation is absorbed by the air and water vapour while the rest is scattered by molecules of air, water vapour and dust particles. The portion that reaches the earth with unchanged direction from the sun is called direct radiation and the radiation scattered by the atmosphere that reaches the earth is called diffuse radiation. The global solar radiation is the sum of total direct and diffuse radiation falling on a horizontal surface depending on the solar direction to the zenith and the daily total of solar time (Goswami and Kreith 2008).

When solar radiation strikes the surface of an object some will be absorbed and the remainder will be reflected. The absorbed solar radiation is converted to thermal energy causing increase of the object's temperature. The proportion of radiation reflected or absorbed depends on the object's reflectivity ranging from one (1) to zero (0). The proportion for fresh snow is 0.9 and for charcoal is 0.04 which is close to a blackbody, which is a perfect absorber (Goode, Qiu et al. 2001).

Water is relatively transparent to visible sun light and absorbs most of the short wavelength solar radiation but is opaque to long wavelengths. The waviness of the water surface also contributes to reducing reflectivity compared to that of a flat surface. With these characteristics, water acts as a good thermal absorber.

The concept of a salinity gradient solar pond is to use salt water as a medium to collect solar radiation and keep it as thermal storage. As an estimate, 20m^2 of solar pond surface area is required in order to produce 1kW of thermal output (Hull and Nielsen 1989).

4.2.2 Transmission of solar radiation in water

As mentioned previously, part of the incident solar radiation is reflected to the atmosphere when the sunlight hits a water surface. The amount of reflection loss depends on the angle of incidence as detailed by Rabl and Nielsen (1975). Table 4.1 shows approximate reflection loss adjustment factors relevant to the range of the latitudes presented by Fynn and Short (1983) in their practical solar pond manual. These values are in good agreement with the values estimated by Tabor and Weinberger (1981) when considering the transmission coefficient as a function of latitude for equinox and solstice conditions.

Table 4.1 Reflection loss adjustment factor for various values of latitude

Latitude Range (degrees)	Reflection Loss Adjustment Factor, *f*
0 - 29	0.98
30 – 43	0.97
44 – 49	0.96
50 – 53	0.95
54 – 56	0.94
57 – 58	0.93
59 – 60	0.92
61 – 62	0.91

Absorbed solar radiation penetrating the interface between air and water must pass through the body of water to reach the storage zone. As the solar radiation moves downwards it suffers further attenuation partly because of the natural absorptivity of the

solution and from the suspended particles, resulting in only a fraction reaching the bottom as thermal energy (Weinberger 1964).

Another factor which affects the transmission of solar radiation in a solar pond is the transparency. Maintaining good clarity of the solar pond water is essential for maximising the penetration of solar radiation to the LCZ (Hull 1989). Pure distilled water is the best indicator for reference when analysing the level of transparency. Weinberger (1964) indicates that the absorption of light by saturated salt solutions when mixed with distilled water is as good as distilled water alone. There were numerous previous studies modelling the absorption of solar radiation into a solar pond as compiled by Hull et al. (1989).

Rabl and Neilsen (1975) have suggested a transmission function *H* of depth *x* in clean seawater for four difference wavelength ranges as:

$$\tau(d) = \tau_s \sum_{i=1}^{4} S_i \, exp\left(-\frac{d}{\delta_i}\right) \tag{4.1}$$

Where;

$\tau(d)$ is the total transmission of a beam of solar radiation incident on a water surface through a distance *d*

τ_s is the fraction of solar radiation that penetrates the air/water interface

S_i is a normalised spectrum distribution function of the incident solar radiation for wavelength band *i*.

δ_i is the characteristic attenuation length for wavelength band *i*.

Table 4.2 Parameters for the four-term series of sunlight transmission in water

i	Wave length	Pure water	Clean Seawater

		S_i	$\delta_i(m)$	S_i	$\delta_i(m)$
1	0.2 – 0.6 µm	0.156	34.7	0.237	31.2
2	0.6 – 0.75 µm	0.249	13.3	0.193	2.22
3	0.75 – 0.9 µm	0.259	0.781	0.167	0.333
4	0.9 – 1.2 µm	0.156	0.0509	0.179	0.0286

Hull et al. (1989) have tabulated the values of S_i and δ_i for pure water to compare with the values for clean seawater by Rabl and Nielsen (1975) as shown in Table 4.2. Bryant and Colbeck (1977) have simplified that function for salt water in order to acceptably fit the Rabl-Nielsen model for vertical depth of 0.1 < z < 3.0 m. The simplified function was;

$$\tau(d) = a - bln(cz) \tag{4.2}$$

Where, a = 0.36, b = 0.08 and c = 1.0 are constants valid at depth, *z* greater than 0.1 m.

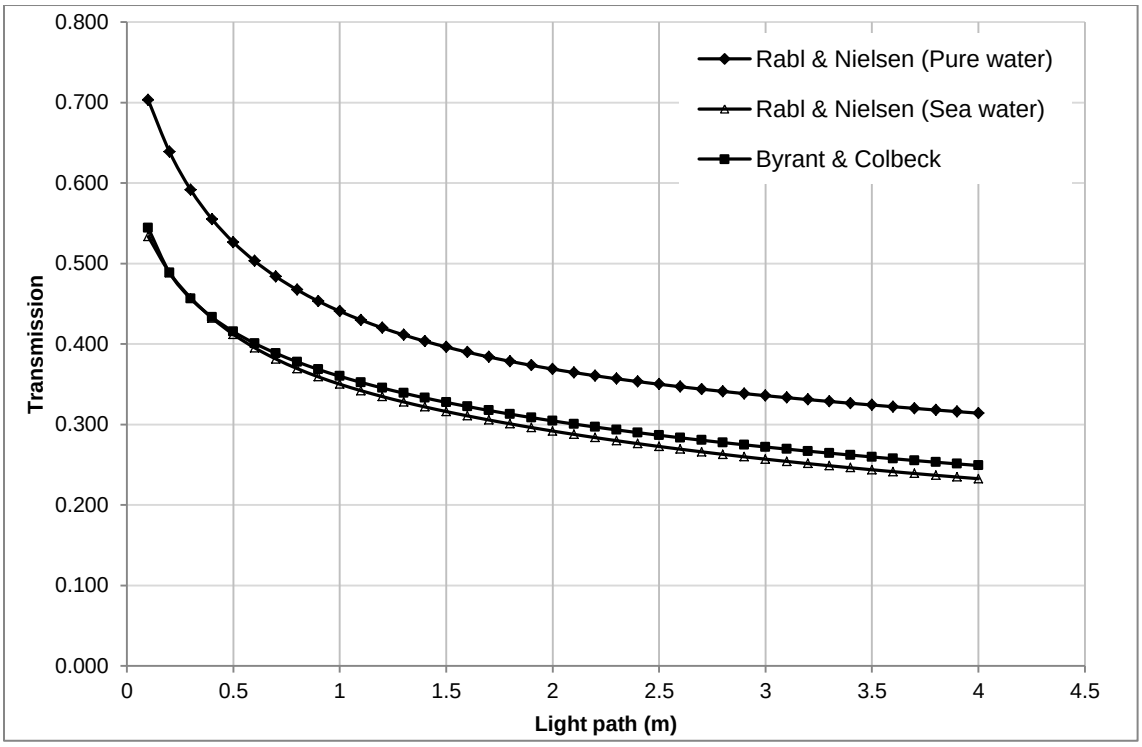

Figure 4.1 Comparison of the clean seawater transmission function of Rabl and Nielsen (1975) with the four series fit for pure water and Byrant and Colbeck (1977)

From Figure 4.1, the Bryant and Colbeck transmission function shows good agreement with the function suggested by Rabl and Nielsen for clean seawater. Though the function is without physical meaning, but has less complexity, it has attracted many researchers to use it as an approximation for solar radiation transmission through solar ponds.

4.3 Steady state temperature profile

Steady state analysis provides an approximation to the solar pond thermal performance. The analysis is extremely useful in designing a solar pond based on location and energy demand for particular applications. The mean local climate data of ambient temperature and solar radiation are used for predictions based on the energy balance over a horizontal fluid layer as shown in Figure 4.2.

In the UCZ, very little absorbed radiation is retained because of convection phenomena. In such a thin layer, heat is released to atmosphere naturally. The absorbed radiation through the non-convective layers and the heat conducted upward contribute to the formation of the temperature gradient in the NCZ. The steady state analysis within the NCZ by Kooi (1979) and Hull et. al (1989) showed that the temperature gradient at any level is higher than the temperature gradient below it. The temperature gradient reduces towards the lower boundary layer, and the maximum temperature is reached when the gradient is equal to zero. At this point, the pond has accumulated the maximum working temperature at the optimum depth z. At this depth, the extraction of useful heat is feasible and heat loss to the ground from the LCZ is assumed to occur.

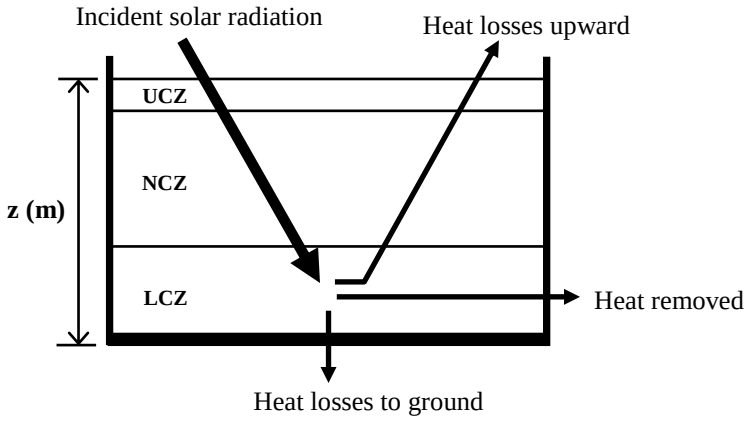

Figure 4.2 Schematic diagram of solar pond energy balance

4.3.1 Surface temperature

The surface of a solar pond in the UCZ is exposed to the environment and creates a mixed layer caused by the wind and by complex mass and heat transfer losses as described by (Hull and Nielsen 1989) and (Hawlader and Brinkworth 1981). An experiment by Zangrando (1979) has supported the claim where the surface temperature is not exactly identical to ambient temperature. Akbarzadeh and Ahmadi (1979) have

mentioned that, the surface temperature is mainly higher than the ambient temperature, although in some cases it could be lower.

However, to avoid the complexity of the calculations for the surface, most models of solar pond performance have considered the temperature of the surface to equal the ambient temperature. This temperature is assumed constant in the thin convective layer of low and uniform salt content (Kooi 1979). The surface temperature varies by 1.3^{o}C during sunny days and varies by 1.1^{o}C during cloudy days (Zangrando 1979). These findings are reasonable as the effect of surface temperature is minimal.

4.3.2 Temperature profile development in the NCZ

In the NCZ layer, the vertical temperature distribution can be calculated from the following one dimensional heat conduction equation as shown by Hull et. al (1989);

$$k\frac{\partial^2 T}{\partial z^2} - I\frac{\partial \tau(z)}{\partial z} = c\frac{\partial T}{\partial t} \tag{4.3}$$

where k is thermal conductivity of the water , I is the radiation received at the surface, $\tau(z)$ is the fraction of absorbed radiation at the depth z which is measured positive downward, C is heat capacity per unit volume and t is time. Equation (4.3) has been used by Kooi (1979) and Hull et. al (1989) to solve the steady state equations applying the Bryant-Colbeck and Rabl-Nielsen transmission functions respectively.

For the steady state condition, the time derivative is zero and the integration of equation (4.3) is simplified to;

$$k\frac{dT}{dz} - I\tau(z) = const \tag{4.4}$$

At the lower interface, with $z = z_2$ the constant integration becomes;

$$\frac{dT}{dz} = \left(\frac{I}{k}\right)[\tau(z) - \tau(z_2)] + \left(\frac{dT}{dz}\right)_{z_2} \quad (4.5)$$

As radiation flux enters the LCZ, part of the heat is conducted upward to the above layer and part of the heat may be removed as useful heat and some is lost to ground. Hence;

$$I\tau(z_2) = k\left(\frac{dT}{dz}\right)_{z_2} + I\eta \quad (4.6)$$

Where, ŋ represent the fraction of the radiation *I* as heat removed during heat extraction and heat lost to the ground. Combining equation (4.6) with equation (4.5) yields;

$$\frac{dT}{dz} = \left(\frac{I}{k}\right)[\tau(z) - \eta] \quad (4.7)$$

Integrating equation (4.7), where the function of transmission of (4.1) or (4.2) can be used to obtain the temperature from *z* to z_2.

$$\left(T_z - T_{z_2}\right) = \left(\frac{I}{k}\right)[(\tau(z) - \tau(z)_2) + (\tau(z)_2 - \eta)](z - z_2) \quad (4.8)$$

Figure 4.3 shows the temperature profile obtained from equation (3.8) and the temperature gradient obtained from equation (3.7) with values of ŋ (0.4, 0.35, 0.3, 0.25, 0.3 and 0.1). The calculation assumed the value of insolation, I = 200 W/m^2, and applied the Bryant and Colbeck transmission function with the thickness of the UCZ equal to 0.1 m. It was shown that, when the value of temperature gradient, ΔT is equal to zero at a certain depth, the temperature of the solar pond has reached the maximum value. Different values of ŋ give difference depths to achieve the maximum temperature.

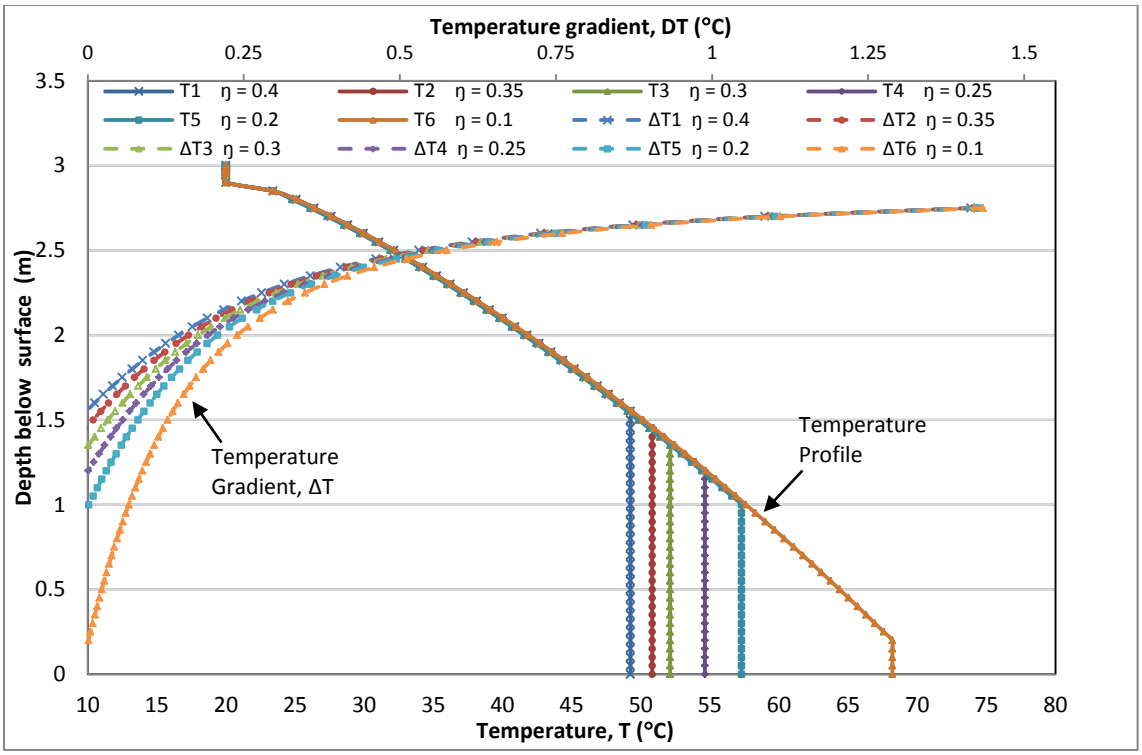

Figure 4.3 Temperature profiles and temperature gradients with solar pond depth for different values of ŋ, combined with the Bryant & Colbeck transmission function.

4.4 Solar energy absorbed by the NCZ

The penetration of light decreases abruptly as it enters the surface of water based on the formulation by Bryant and Colbeck (1977) as shown in Figure 4.4. Assuming a solar pond of depth 2.5 m with a 0.3 m thick UCZ, 1.5 m thick NCZ and 0.7 m thick LCZ, the amount of solar radiation is reduced to 42% as it reaches the upper interface of the UCZ-NCZ and only 28% of the remaining solar radiation reaches the lower interface NCZ-LCZ.

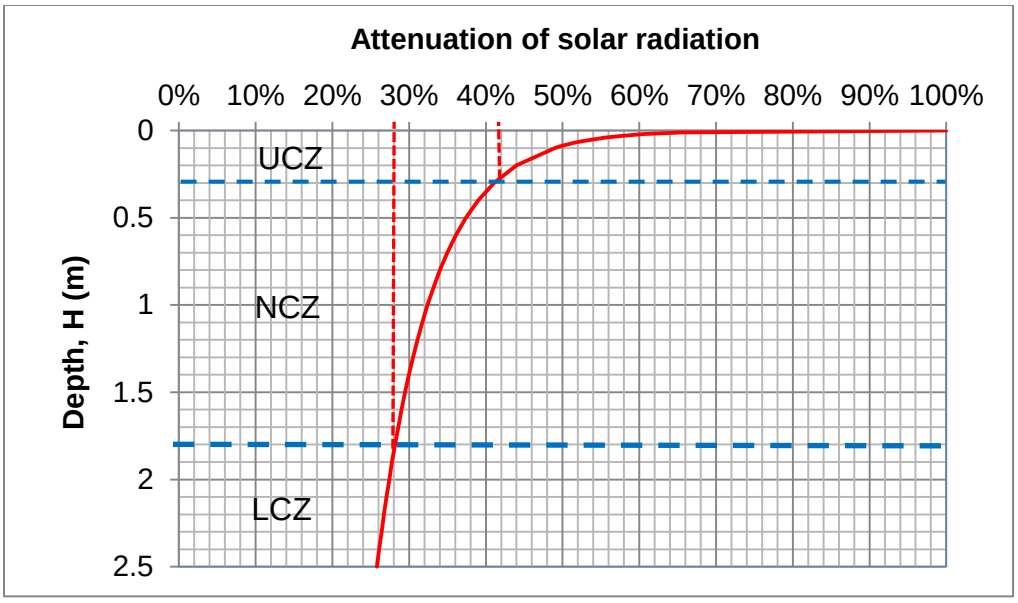

Figure 4.4 Penetration of sun light into clear water (Bryant and Colbeck 1977)

By extracting heat solely from the LCZ, the efficiency of a solar pond is limited to between 11%and 15% (Weinberger 1964, Tabor 1981). However, the overall efficiency of a solar pond could be improved further if some portion of the available heat in the larger thickness of the NCZ could be extracted.

4.4.1 Advanced solar pond (ASP)

The concept of an advanced solar pond (ASP) was introduced by Osdor (1984) where the prime objective was to improve the thermal performance of a conventional solar pond (CSP). There are two main features that characterise the ASP against the CSP, which are increasing the overall salinity of the pond and introducing a stratified thermal layer (STL) at the lower part of the gradient layer (NCZ) (Keren, Rubin et al. 1993). Increasing overall salinity is proposed to reduce the evaporation rate at the surface and heat loss to surrounding. The stratified thermal layer (STL) comprises several sub layers and is

introduced to allow multi selective injection and withdrawal procedure (Rubin and Bemporad 1989) as shown in Figure 4.5 .

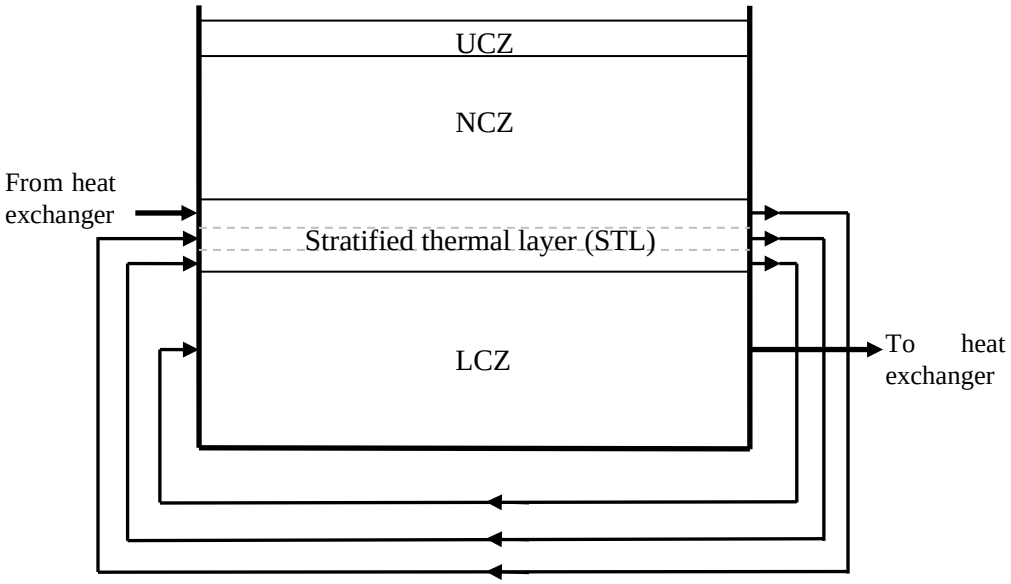

Figure 4.5: Schematic of an advanced solar pond (ASP) with multi selective injection and withdrawal procedure (Rubin and Bemporad 1989)

A flowing layer is created between the LCZ and NCZ to remove heat hence reducing the temperature at that particular layer. This results in reduced heat and diffusion loss upward and the trapped heat is confined to provide better heat extraction from the stratified layer as well as LCZ. The stratified thermal layer (SFL) is subjected to horizontal flow and the salinity gradient avoids the thermohaline circulating currents. It is carried out by injection and withdrawal ports creating numbers of sub-layers. The fluid withdrawn from the first sub-layer is injected into the second sub-layer and so on as shown in Figure 4.5. The flow from the last sub-layer is injected into the LCZ. The process takes place simultaneously with heat extraction, where the flow from the LCZ passes through the heat exchanger to be returned to the first sub-layer to complete the loop.

Keren et. al (1993) have carried out an experimental investigation to evaluate further the performance of an ASP compared to a CSP based on previous studies by Keren et. al (1991). A laboratory scale solar pond of 4.2 m^2 diameter was constructed to demonstrate a working ASP. The overall depth filled was 1.3 m and a 0.5 m LCZ was established. The prototype was equipped with injection and withdrawal ports. The 0.36m depth of the STL was created consisting of nine sub-layers of 0.04 m each. The necessary piping, heat exchanger, cooling unit, mixing unit and a pump were installed to circulate the brine. The results showed that heat energy trapped in the LCZ increased by approximately 14% and an additional 11% of heat energy can be collected from the SFL. This experimental ASP produced up to 50% overall efficiency.

The main concern with the ASP concept is the occurrence of instabilities caused by the injection and withdrawal of the fluid layers with different temperatures, salinities and velocities (Bemporad and Rubin 1994). Theoretical study by Rubin and Bemporad (1989) show that the flow must have a smooth and continuous laminar profile, $Re \leq 1000$ to avoid instability of circulating currents and prevent mixing between the sub-layers. Increased flow rates in the STL require excessive thermal energy which may lead to turbulent flow and create instability. This phenomena can be controlled by designing a sufficiently large NCZ with special attention to appropriate adjustment of multi injection and withdrawal procedures (Rubin and Bemporad 1989). Further studies by Bemporad and Rubin (1991) analysed the hydrodynamics aspects related to formation of internal Kelvin Hemholtz waves in the fluid layers due to the mixing of densities. Their recent study determined that the aspect ratio of the pond size should not be larger than 5 to prevents the development of thermohaline convection in horizontal planes parallel to the flow which will create over-stability (Bemporad and Rubin 1992). Atkinson et al. (1993) have proposed for each sub-layer to have a separate withdrawal port and pumping system to prevent the vertical deviation jet due to buoyancy from density difference between sub-layers.

The concepts of an ASP proved that better performance of solar ponds could be achieved. However, practicality should be taken into account where complex arrangements such as piping systems, pumping requirements, mixing of solutions and proper injection and withdrawn ports are involved. Cost effectiveness is the key factor in determining feasibility of advanced solar ponds. In another issue, it is difficult to maintain the stability of stratified fluid layers (SFL). This disadvantage has made the ASP concept less attractive to users.

4.4.2 Heat extraction from non-convective zone (NCZ)

4.4.2.1 Theoretical study

An alternative method of extracting heat from solar ponds was investigated theoretically by Andrews and Akbarzadeh (2005) with the aim of increasing the overall energy efficiency of delivering heat to applications compared with conventional heat extraction solely from the LCZ. This concept has the potential benefits of utilising available heat in the NCZ and reducing upward heat loss by conduction. One-dimensional heat transfer in the vertical direction for the steady state condition has been examined based on the following assumptions;

i. The side and bottom wall is well insulated, so that heat losses are negligible as suggested by Kooi (1979) and Wang and Akbarzadeh (1983).

ii. The heat transfer fluid is in thermal equilibrium with the surroundings before entering the heat exchanger.

iii. The working temperature of the fluid in the heat exchanger is the same as the pond temperature at the same depth.

iv. The entire thickness of the NCZ is covered by an internal heat exchanger, where heat transfer by conduction is in the vertical direction only.

Cold heat transfer fluid close to ambient temperature enters the heat exchanger near the upper interface and leaves near the lower interface with a higher temperature close to the LCZ temperature. In addition another heat exchanger is used to extract heat conventionally from the LCZ. The effects of heat extraction solely from the NCZ, heat extraction solely from the NCZ and heat extraction from both NCZ and LCZ have been simultaneously examined.

A formulation by Bryant and Colbeck (1977) was employed to estimate the attenuation of solar radiation in clear water of the pond. Thermal efficiency, η of the pond is defined by;

$$\eta = \frac{C[T_p(d) - T_a] + \dot{q}}{\bar{H}} \tag{4.9}$$

where $\bar{H}$ is the average of solar radiation in (W/m^2), $C[T_p(d) - T_a]$ is the rate of heat transfer per unit area from the NCZ and $\dot{q}$ is the rate of heat transfer per unit area extracted from the LCZ. $T_p(d)$ is the temperature at the lower part of the NCZ and T_a is the ambient temperature. *C* is the heat capacity rate per unit area of the pond in the NCZ in W/^{o}C/m^2.

The following assumption had been made;

i. The thickness of the UCZ was 0.5m.

ii. The daily average solar radiation was 200 W/m^2.

iii. The thermal conductivity of the solar pond brine was 0.6 W/m.^{o}C

iv. The ambient temperature was 20^{o}C.

Heat extraction from the NCZ was expressed in terms of heat capacity rate *C* and unit area of pond, where *C* varied between 0.0042 W/^{o}C/m^2, referring to a mass flow rate in

heat exchanger of NCZ of 0.000001 kg/s/m^2 (close to zero) and 2.1 W/$^oC/m^2$ and $\dot{m} =$ 0.0005 kg/s/m^2.

The results show that, by extracting heat only from the LCZ. It has delivered heat of 45 W/m2 with temperature of 70 ^oC constituting 22% efficiency. Heat extraction from NCZ as well as from the LCZ delivered heat at 56 W/m^2, increasing the overall efficiency to 28%. Heat extraction from both the LCZ and NCZ, it would reduce the amount of heat removed from LCZ while additional heat can be simultaneously extracted from the NCZ. Finally, heat extraction from NCZ only has increased the efficiency to 33% as it delivered heat at 65 W/m^2. The scientific basis was that the solar radiation penetrates to the LCZ is counterbalanced the upwards heat flow out of LCZ into the NCZ to provide heat for continuous heat extraction. Hence, heat extraction from NCZ has substantially increased efficiency up to 50% compared to heat extraction only from LCZ. At the same time, the proposed system significantly reduces heat losses to the surface. The hydrodynamic stability of the pond remains unaffected with additional heat extraction from the NCZ.

4.4.2.2 Experimental study

Further related study has been carried out experimentally on a 50m^2 solar pond by Leblanc et al. (2011) at RMIT University, Melbourne. The experiment used an internal heat exchanger made of 30mm OD and 3 mm thick polyethylene pipe with a total length of 560 m. The pipe was fixed at the circumference of the vertical wall from the UCZ and NCZ interface to the bottom of the pond as shown in Figure 4.6. Cold water from the surface at close to ambient temperature was used as heat transfer fluid to collect heat from the top of the NCZ down to the LCZ. Hot water close to LCZ temperature was returned to the surface of the pond.

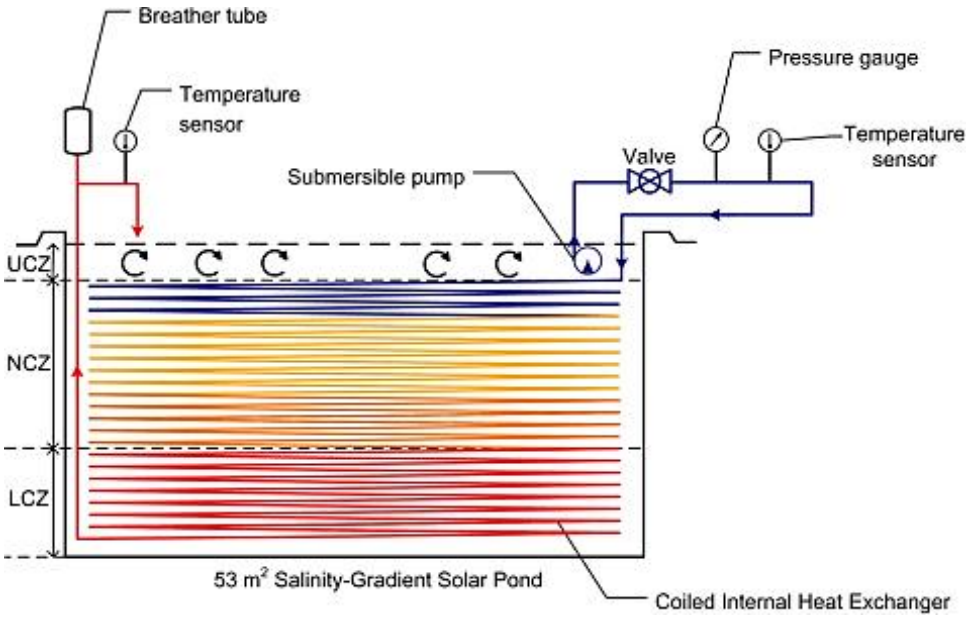

Figure 4.6 Schematic of the heat extraction system in the RMIT solar pond (Leblanc, Akbarzadeh et al. 2011)

The rate of thermal energy extracted is given by;

$$\dot{Q} = \dot{m}C_p(T_o - T_i) \tag{4.10}$$

Where $\dot{m}$ is the mass flow rate in kg/s, C_p is the specific heat of the heat transfer fluid in J/kg.^{o}C and T_o and T_i are the outlet and inlet temperatures of the heat transfer fluids entering and leaving the heat exchanger.

The pond thermal efficiency is defined as;

$$\eta = \frac{\dot{m}C_p(T_o - T_i)}{HA_{sp}} \tag{4.11}$$

Where *H* is the average solar radiation received at the pond surface and A_{sp} is the surface area of the solar pond.

Heat was extracted in winter 2008 from early May to early July with a mass flow rate of 4.3 LPM. The flow rate was adjusted to be higher to prevent development of air bubles in the heat exchanger pipe. Two steady state conditions were identified, both over a period of one week. Within these periods, temperatures gained were recorded at 5.3 ^{o}C and 4.9 ^{o}C respectively. These correspond to heat gains of approximately 1.5 kW, where 63% and 37% of the heat has been extracted from the NCZ and the LCZ respectively. Overall heat delivery efficiency from these two steady states was 33% and 36% respectively.

The results indicated that heat extraction from the gradient layer increased the overall efficiency of the solar pond by up to 55% compared with the solar pond in which heat was extracted only from the LCZ. Previous simulation studies by Zhang and Wang (1990) revealed that the ground thermal storage of solar ponds is more efficient when heat is removed from the pond during the cold season. No instabilities were recorded in temperature or salinity gradient.

A similar study has been conducted numerically for a 0.64 m^2 mini solar pond in Tunisia by Ould Dah et al (2010). The thicknesses of the UCZ, NCZ and LCZ were 0.08 m, 0.42 m and 0.4 m respectively and the total depth was 1m. A control-volume formulation has been adopted in order to solve numerically for simultaneous continuous heat extraction using internal heat exchangers from the NCZ and LCZ with different mass flow rates. Heat extraction solely from the LCZ provides minimum efficiency of 14.5% with an average mass flow rate of 0.00055 kg/m^2. In the case of heat extraction solely from the NCZ, higher maximum efficiency of 19.2% was recorded with a mass flow rate of 0.00076 kg/m^2. The result is likely to be due to less upward heat loss in the NCZ. The results showed that the efficiency of the solar pond was considerably improved. However, heat extraction solely from the NCZ reduced stability at the lower interface.

4.5 Proposed heat extraction system

Efforts have been made to enhance the efficiency of solar ponds by utilising heat available in the NCZ. The concept of an advanced solar pond appeared ideal, but the implementation was never achieved because of instability issues in the NCZ and the complexity of the system required to support multi-injection. Work on heat extraction from the NCZ using an internal heat exchanger shows promising results both theoretically and in experimental ponds. However, installation of an internal heat exchanger as demonstrated at the RMIT experimental solar pond is not practical for larger scale working solar ponds from an economic point of view.

4.5.1 Heat extraction system

This study is to investigate the possibility of using an external heat exchanger to extract available heat from the NCZ to enhance overall efficiency of a solar pond. The proposal is to carry out a multi-layer heat extraction from the NCZ using a number of external heat exchangers and using a mechanical pump to withdraw hot brine from the NCZ into a series of external heat exchangers and return cooled brine to the same level in the NCZ as schematic diagram shown in Figure 4.7 below.

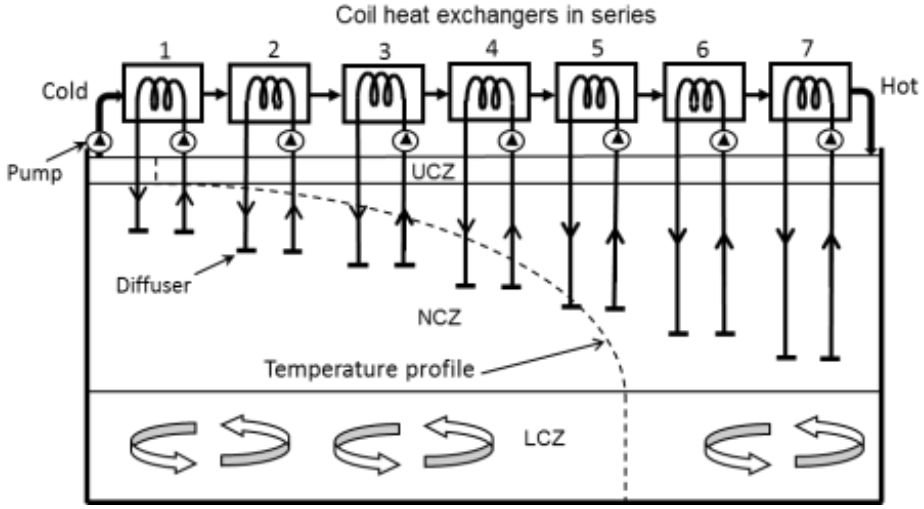

Figure 4.7 Proposed multi-layer heat extraction system from the NCZ of the RMIT solar pond

The active multi-layer heat extraction system shown in Figure 4.7 is mainly performing two tasks;

i. Extracting heat from the NCZ by withdrawing hot brine throught the tube heat exchanger and returning it to the same level.

ii. Collecting the extracted heat at each layer by circulating cold brine from the pond surface to pass through the shell of heat exchangers Number 1 to Number 7.

The exact locations of the diffusers from heat exchangers 1 to 7 from upper to lower parts of the NCZ are shown in Figure 4.8 with three different temperature profiles during summer of January 2012, autumn of April 2012 and winter of June 2012. The inlet and outlet of heat exchanger number 1 were located 20 cm below the upper boundary and inlet and outlet of heat exchanger number 7 were located 15 cm above the lower boundary. The vertical gap between the diffusers was 15 cm covering 0.9 m of of the total 1.2 m NCZ layer thickness.

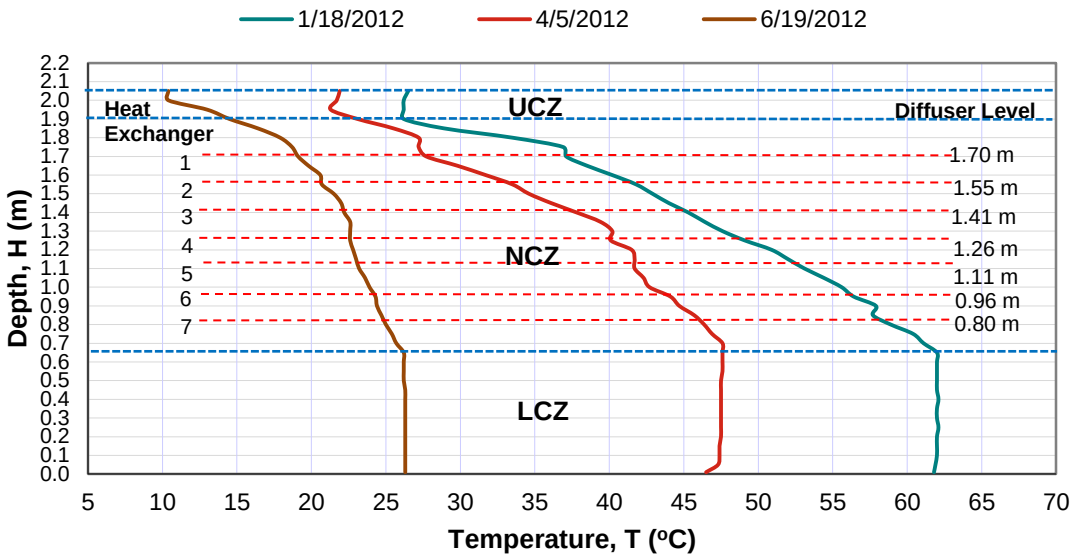

Figure 4.8 Location of diffusers in NCZ

4.5.2 Heat exchanger (HEX)

The shell and tube heat exchanger using copper tube was designed to handle a single phase of counter flow operation. The cold brine flowed through the shell and the hot brine circulated through the tube. A shell and tube heat exchanger was chosen because it could be manufactured rapidly and economically in the RMIT workshops, and copper tube has relatively low cost with good thermal conductivity of 400 W/m^2.^{o}C.

4.5.2.1 Design of heat exchanger coil

The following equations are used to determine the heat transfer rate of the heat exchanger;

$$\dot{Q} = UA\Delta T_{LM} \tag{4.12}$$

where $\dot{Q}$ is heat transfer rate in W, U is the overall heat transfer coefficient in W/m^2.^{o}C, A is the heat transfer surface area in m^2 and ΔT_{LM} is the log mean temperature difference in ^{o}C.

By neglecting the fouling factor, the following case has been considered in designing the required heat exchanger for this experiment;

i. Heat Transfer rate , $\dot{Q}$ = 1000 W

ii. Overall heat transfer coefficient for water, U = 1000 W/m^2. ^{o}C

iii. The inlet and outlet temperature difference, ΔT = 4 ^{o}C

iv. Heat transfer area, A= πdl, where d = 9.52 mm of copper tube diameter, and l is the length of copper tube in meter.

Therefore, using equation (4.3), the total length of copper tube required was estimated to be 8.35 m for each heat exchanger. Based on this calculation, the coil heat exchanger was designed as shown in Figure 4.9.

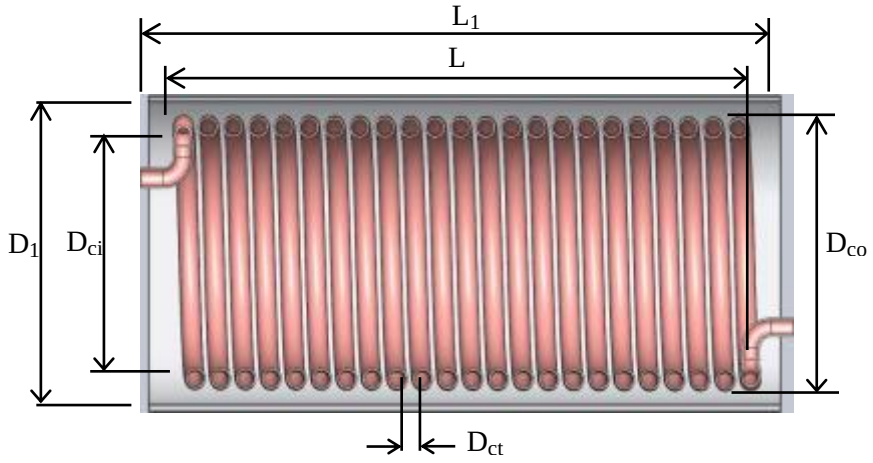

Figure 4.9 Cross sectional drawing of heat exchanger coil

The physical geometry of the coil heat exchanger is shown in Table 4.3. The shell was made from 150 mm diameter PVC pipe cut to 300 mm length.

Table 4.3: Physical geometry of heat exchanger coil

L_1	L	L_{ct}	D_1	D_{co}	D_{ci}	D_{ct}
300 mm	288 mm	8.35 m	150 mm	130 mm	111 mm	9.52 mm

4.5.2.2 Heat exchanger theoretical performance analysis

The following governing equations were used to analyse the performance of the coil heat exchanger based on an energy flow diagram as shown in Figure 4.10.

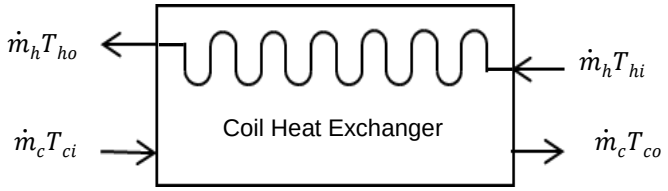

Figure 4.10 Schematic of energy flow through a coil heat exchanger

Considering heat transfer from the coil and the heat absorbed by the cold water with a constant mass flow rate of each stream, the energy balance is;

$$\dot{m}_c C_p (T_{co} - T_{ci}) = \pi D_{ct} L_{ct} h_o \left[\left(\frac{T_{hi} + T_{ho}}{2} \right) - T_s \right] \quad (4.13)$$

where, $\dot{m}_c$ is the cold water mass flow rate in kg/s, C_p is specific heat in J/kg. ^{o}C, T_{co} and T_{ci} are the outlet and inlet cold temperatures in ^{o}C, T_{ho} and T_{hi} are the outlet and inlet hot temperatures in ^{o}C, D_{ct} is the diameter of the copper tube, L_{ct} is the length of the

copper tube, h_o is the convective heat transfer coefficient outside the copper tube in W/m^2.^{o}C. and T_s is the coil surface temperature.

The heat transfer rate, associated with temperature difference between the flowing fluids and the surfaces inside and outside the coils, is dominated by convection effects derived as;

$$\left[T_s\left(\frac{T_{ci}+T_{co}}{2}\right)\right]h_i=\left[\left(\frac{T_{hi}+T_{ho}}{2}\right)-T_s\right]h_o \tag{4.14}$$

where h_i and h_o are the convective heat transfer coefficients inside and outside the coil respectively.

The Reynolds numbers for steady incompressible flow with a uniform cross sectional area and with constant mass flow rates through the circular coil and in the copper tube, are given by;

$$\mathrm{Re}_1=\frac{4\dot{m}_h}{\pi D_H\mu} \tag{4.15}$$

$$\mathrm{Re}_2=\frac{4\dot{m}_c}{\pi D_{ct}\mu} \tag{4.16}$$

where $\dot{m}_h$ is the hot brine mass flow rate in kg/s, D_H is the hydraulic diameter of the heat exchanger coil and μ is the dynamic viscosity in N.s/m^2.

The outside Nusselt number, Nu_o of the coil heat exchanger was evaluated using the length of the tube as the characteristic length correlated to the Rayleigh number for $9\text{x}10^9 \leq \mathrm{Ra} \leq 4\text{x}10^{11}$, as described by Prabhanjan, Rennie et al. (2004).

$$Nu_o=0.0749Ra^{0.3421} \tag{4.17}$$

Rayleigh number is defined as;

$$Ra = \frac{g\beta(T_{hi} - T_{ci})L_{ct}^3}{\nu\alpha} \tag{4.18}$$

For fully developed turbulent flow in a smooth circular tube, the local Nusselt number Nu_i equation was employed as explained by Rogers and Mayhew (1964) related to curvature ratio;

$$Nu_i = 0.023\,\mathrm{Re}_2^{0.85}\left(\frac{D_{ct}}{D_{co}}\right)^{0.1}\mathrm{Pr}^{0.4} \tag{4.19}$$

where *Pr* is the Prandtl number.

The convective heat transfer coefficients inside and outside the copper tube are expressed as follows;

$$Nu_i = \frac{h_i D_{ct}}{k} \tag{4.20}$$

$$Nu_o = \frac{h_o D_H}{k} \tag{4.21}$$

Microsoft Excel was used to solve the nine unknowns from equations 5.4 to equation 5.12 simultaneously. Table 4.4 shows the known values consist of input parameters, constant physical geometry and constant fluid properties. The effect of different input parameters is observed to obtain the output of the modelling.

Table 4.4 Known values for the mathematical modelling

KNOWN	Symbol	Value	Unit
Input parameters			
Hot water inlet temperature	T_{hi}		^oC
Cold water inlet temperature	T_{ci}		^oC
Hot water mass flow rate	$\dot{m}_h$		kg/s
Cold mass flow rate	$\dot{m}_c$		kg/s
Physical geometry			
Diameter of shell heat exchanger		0.15	m
Cross sectional of shell heat exchanger		0.02	m^2
Length of the copper tube	L_{Ct}	8	m
Diameter of copper tube	D_{ct}	0.00952	m
Outer Diameter of coil	D_{co}	0.13	m
Inner Diameter of coil, (D_{co}-2D_{ct})	D_{ci}	0.11096	m
Cross Section Area of coil normal to flow, (π/4 x (D_{co}^2-D_{ci}^2)	Ac	0.00360331	m^2
Wetted Perimeter normal to flow, π(D+D_{co}+D_{ci})	P_w	1.22823706	m
Hydraulic diameter of heat exchanger coil, 4(A_{Ther} -Ac)/P_w	D_H	0.04581574	m
Fluid properties			
Prandtl number, (C_p.μ)/K	Pr	6.941	
Density of water	ρ	998	kg/m^3
Thermal conductivity of water	K	0.598	W/m.K
Thermal expansion	β	0.000652	K^{-1}
Gravitational force	g	9.81	m/s^2
Water specific heat	C_p	4180	J/kg.K
Water Kinematic Viscosity	μ	9.93E-04	$N.s/m.s^2$
Thermal Diffusivity	α	1.4335E-07	m^2/s

The outputs of the modelling are Re_1, Re_2, Ra, Nu_o, Nu_i, h_i, h_o, T_{ho}, T_{co} and T_s. The specific interest is on the obtained values of T_{ho} and T_{co}. These values are used to determine the temperature difference, which is one of the dominant factors determining the heat transfer rates from both hot and cold areas.

The heat transfer rate from the hot side is given by;

$$\dot{Q}_h = \dot{m}_h C_p (T_{hi} - T_{ho}) \tag{4.22}$$

The heat transfer rate absorbed by cold side is given by;

$$\dot{Q}_c = \dot{m}_c C_p (T_{co} - T_{ci}) \tag{4.23}$$

The effectiveness of the heat exchanger is calculated as :

$$\varepsilon = \frac{T_{co} - T_{ci}}{T_{hi} - T_{ci}} \tag{4.24}$$

where $0 \leq \varepsilon \leq 1$ is converted into percentage.

For validation purposes, a balance energy of $\dot{Q}_c = \dot{Q}_h$ must be achieved to satisfy the conservation of energy requirement. Input values of inlet hot brine temperature and ambient temperature are based on temperature profiles from 5th April 2012 and 18/01/2012 as shown in Figure 4.8. The input values used for modelling validation are shown in Table 4.5 below. The hot brine mass flow rate is kept constant at of 0.03 Kg/s for all heat exchangers with cold brine mass flow rates of 0.015 Kg/s and 0.03 Kg/s.

Table 4.5 Input cold temperature and hot temperature for each heat exchanger

	05/04/2012		18/01/2012	
Heat Exchanger	Inlet Hot Temp, ^{o}C	Inlet cold Temp, ^{o}C	Inlet Hot Temp, ^{o}C	Inlet cold Temp, ^{o}C
1	27.7	21.7	37.1	26.2
2	33.5		41.8	
3	37.8		45.3	
4	40.1		49.1	
5	41.7		53.1	
6	44.1		56.4	
7	46.4		58.9	

Figure 4.11 and Figure 4.12 show theoretical performance of the shell and tube heat exchanger with different cold brine mass flow rates of 0.015 Kg/s and 0.03 Kg/s passing through the shell side. The results show that each of heat exchanger heat transfer quantities produce a balanced energy condition, where the amount of heat transferred by the hot side is equal to the amount of heat absorbed by the cold side. The results indicate the validity of the developed model, which will be applied for further analysis.

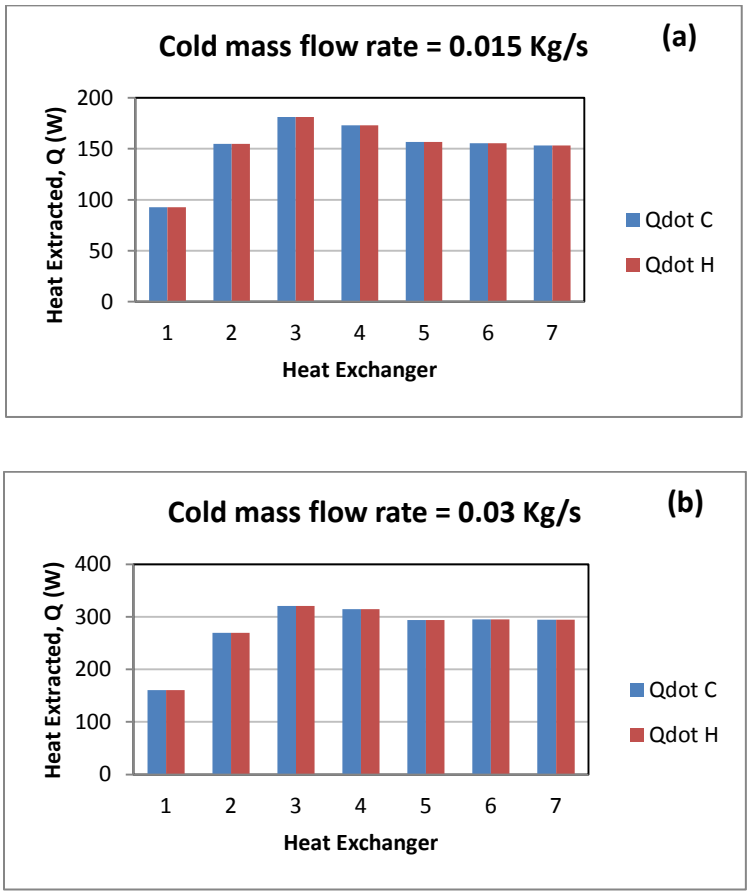

Figure 4.11 Performance of the coil heat exchanger on 5/4/2012 with cold brine mass flow rates; (a) 0.015 Kg/s and (b) 0.02 Kg/s, at constant hot brine mass flow rate 0.03 Kg/s

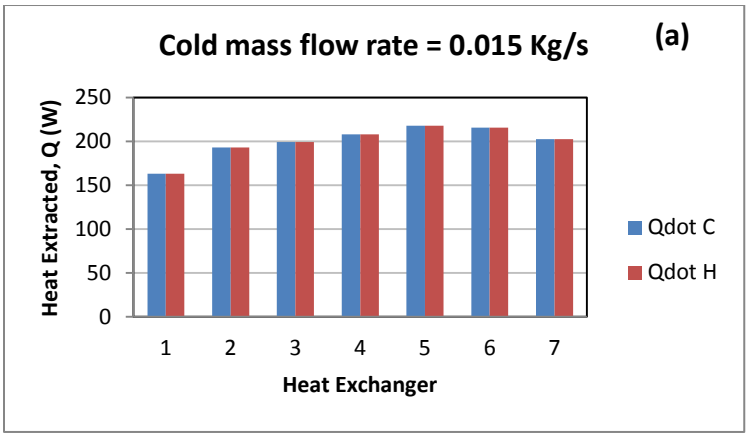

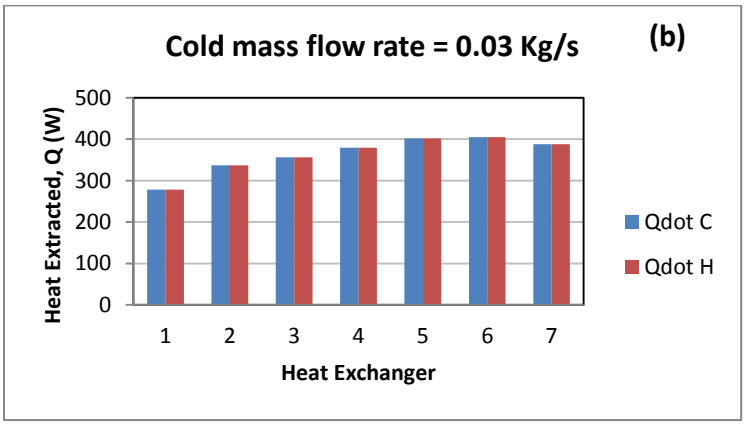

Figure 4.12 Performance of coil heat exchanger on 18/1/2012 with cold brine mass flow rates; (a) 0.015 Kg/s and (b) 0.02 Kg/s, at constant hot brine mass flow rate 0.03 Kg/s

The maximum amount of heat was extracted at heat exchanger 3 on 5/4/2012 for both cold brine mass flow rates. However on 18/1/2012, heat exchangers 5 and 6 showed the highest heat extraction rate. This phenomenon showed that, the temperature gradient affects the rate of heat flow from the NCZ into the heat exchanger. Based on the modelling outcomes, it is observed that the temperature profiles of the NCZ and the heat extraction capacity of the heat exchanger are interdependent and very sensitive to each other. Consequently, heat extraction affects the temperature profile of the NCZ, which in turn changes the heat extraction rate. Hence, to achieve optimum NCZ heat extraction,

the system must be actively controlled, i.e. by controlling the mass flow rate of hot fluid using a temperature sensor in the NCZ.

Two cold brine mass flow rates were added to the prediction model as shown in Figure 4.13 to determine the total capability of the heat extraction system. The results show that the performance of the heat extraction system is increased with the increased cold mass flow rate, but, the effectiveness of the system is decreased from 58% to 52% as the cold brine mass flow rate is increased. Therefore, the appropriate cold mass flow rate must be determined in order to obtain a stable heat extraction system which can minimise the effect of instability resulting from intensive heat extraction from the NCZ.

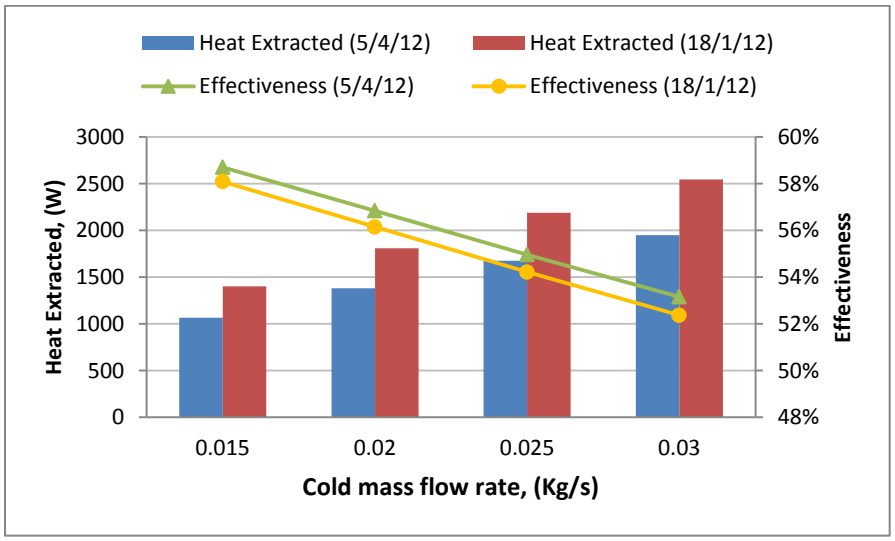

Figure 4.13 Theoretical prediction of instantaneous heat extracted from the NCZ and the effectiveness of the heat extraction system

4.5.2.3 Manufacture and installation of the heat exchanger

In total, 58.5 m copper tube of diameter 9.52 mm were required to build seven units of shell and tube heat exchanger. Four rolls of copper tube were purchased, each roll of 18m length. Each roll was cut into half to become two 9m rolls, so that each heat exchanger

coil had a 0.5 m extra length to be used as inlet and outlet connectors as shown in Figure 4.14(b). A special jig made from 110 mm OD steel pipe was used to coil the copper tube so that the coil could be put into the shell. A lathe was used for the coiling process. Figure 4.14 shows the coiling process using a lathe in the RMIT workshop and the finished coil heat exchanger.

(a) (b)

Figure 4.14 (a) Coiling process and (b) finish coil heat exchanger

The coil was assembled with the shell and installed at top of the RMIT solar pond wall as shown in Figure 4.15 below. A timber support was installed to hold the pump and both the inlet and oulet plastic pipes to the diffuser. Flow control valves were connected to each heat exchanger to measure fluid flow. The inlet and outlet lines of hot brine, the connector between the heat exchanger and the heat exchanger shell were insulated with Armaflex material. Figure 4.16 shows the fully insulated heat exchanger.

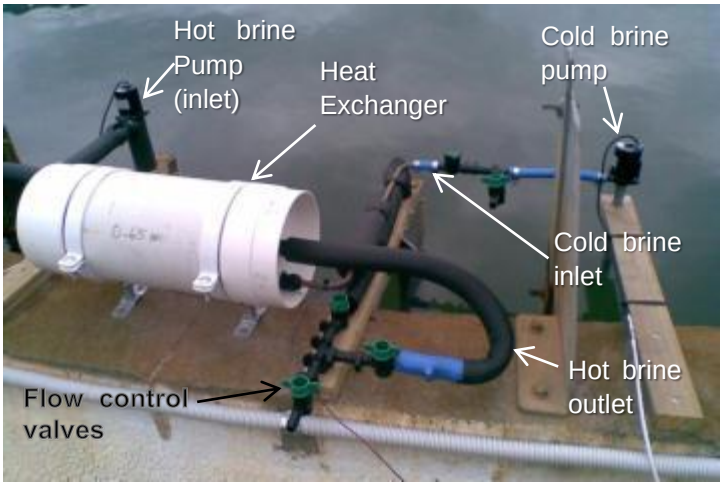

Figure 4.15 Installed heat exchanger (HEX) at RMIT solar pond

Figure 4.16 Insulated heat exchangers (HEX)

Figure 4.17 shows the arrangement of heat exchangers 1 to 7 with increasing diffuser levels from the pond surface. . Red arrows pointing upward show the inlet flows of hot brine into the heat exchanger (HEX) tubes and yellow arrows show the outlet flows of cooled brine return to the same level. Light blue arrows represent flow of cold brine from the surface through the heat exchanger shell to collect the heat in stages. Using equation

4.24, the performance of the heat extraction system can be determined by comparing the outlet heated-up surface-brine temperature from HEX 7 and the inlet temperature to the HEX 1, and divided by the temperature difference between inlet hot brine to HEX 7 and inlet cold brine to HEX 1.

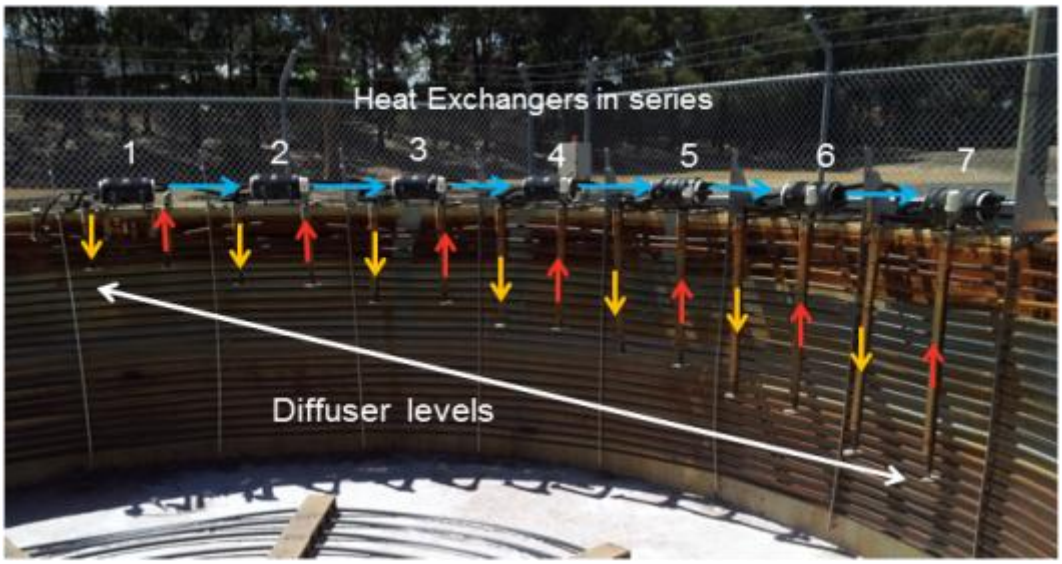

Figure 4.17 Arrangement of heat exchangers (HEX) and diffuser levels

4.5.3 Pump and diffuser

4.5.3.1 Pump

A 12 Volt pump as shown in Figure 4.18 (left) was used to withdraw the hot brine to pass through the heat exchanger coil and return to the same level. Another 12 volt pump was used to inject the cold brine from the surface through the shell of each heat exchanger to collect the heat in stages and return it to the surface of the pond. This was to avoid unnecessary waste of water when conducting the experiment and thereby keep a sustainable work practice. A simple pump head test was carried out in the thermodynamics laboratory to measure the actual pump output power and its effectiveness. The test outcomes and the pump technical data are attached as Appendix B.

Total power consumed during the operation was approximately 43W at any time, coming from seven pumps of 450mA each. The pumps were connected in series with 5Amp fuses and a 12V output power supply.

Figure 4.18 The 12 Volt pump model DC40

4.5.3.2 Diffuser

Figure 4.19 shows the inlet and outlet of the hot brine which were attached to diffusers to minimise the mixing effect of re-injected brine to the gradient layer. The concept of using a diffuser was introduced by Zangrando (1991) as explained in section 2.4.1.4, where the value of the Froude number need to be maintained at close to 15.

Figure 4.19 Semi-circular diffuser attached to inlet and outlet of hot brine

4.5.4 Temperature sensor and data acquisition

A type T thermocouple with range of (-50 to 200 ^{o}C) was used as a temperature sensor in the heat extraction system. Figure 4.20 shows the location of the temperature sensors for two heat exchangers, as for each heat exchanger in the system. In total, twenty two thermocouple sensors were employed in the system. The arrangement enables separate measurement of individual heat exchanger and heat extraction system performances. The thermocouple wires were connected to the DataTaker 500 data acquisition system for data tracking.

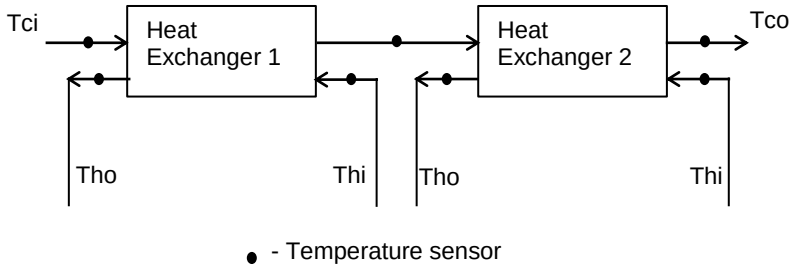

Figure 4.20 Location of temperature sensor

The Datalogger program was set to capture temperature readings at 15 minute intervals. The system was connected to the desktop computer in the Renewable Energy Laboratory for monitoring. The temperature readings from the heat extraction system during the whole period of experiments could later be downloaded and transferred into an Excel spread sheet, for use in measuring the performance of the heat extraction system.

4.5.5 Uncertainty Analysis

The total uncertainty in every measurement was obtained by combining the sensor accuracy and measuring instruments accuracy using the root sum of square method (Leblanc, Andrews et al. 2010) as follows;

$$\delta_{total} = \sqrt{(\delta_{Sensor})^2 + (\delta_{Instruments})^2} \tag{4.25}$$

Where, δ is the uncertainty of the measured value.

The detail of uncertainty analysis can be found in Appendix E.

Chapter 5 - Heat extraction from a solar pond using a thermosiphon heat exchanger

5.1 Introduction

One of the issues in heat extraction from a solar pond is the consumption of electricity for pumping. A larger pump is required for a larger pond. In this chapter, the concept of extracting heat from a solar pond using a thermosiphon heat exchanger is described. This concept is proposed as an alternative to the conventional method of using a mechanical pump to withdraw hot brine from the NCZ and the LCZ to an external heat exchanger. A theoretical model governed by the relevant basic equations has been developed and is explained in detail in the first section of this chapter. Subsequently, an experimental arrangement and experimental procedure including a flow visualisation technique are explained.

5.2 Thermosiphon heat exchanger

The concept of a thermosiphon has been widely used in applications including solar water heating (Harding and Zhiqiang 1985, Mulaweh 2006, Koffi, Andoh et al. 2008), geothermal development (Tago, Morita et al. 2006), heat recovery systems (Dube, Akbarzadeh et al. 2004, Mulaweh 2006) and many others. Application of the thermosiphon effect to extract heat from a solar pond was done by Tundee et al. (2010). They installed a heat pipe heat exchanger made of 60 copper tubes of outside diameter 22mm and thickness 3mm, using R134a as a heat transfer medium. Each tube consisted of an 80cm evaporator and a 20cm condenser and was inclined at 60^{o} to horizontal to enhance the thermal performance. The heat extraction process required forced ambient air to be blown over the condenser at a specific velocity. The results show that, the effectiveness of heat extraction can be increased to 43% when a heat pipe is used with an

appropriate air velocity (Tundee, Terdtoon et al. 2010). Singh et al. (2011) have investigated the possibility of generating electrical power from a solar pond by combining heat pipes and thermal electric cells (TEC). They fabricated a single evacuated copper tube experimental heat pipe so that it could be held vertically from the bottom (LCZ) to the top (UCZ) of the pond. Sixteen TECs of size 40mm x 40mm x 3.9m were attached to the upper parts of the heat pipe. The hot side of the evacuated tube and the cooled side at close to ambient temperature in the UCZ created sufficient temperature difference to generate power from the TEC. The module was able to produce a maximum power of 3.2W with conversion efficiency of 1%.

Unlike a heat pipe, the closed coil thermosiphon heat exchanger employs external gravity, buoyancy and centrifugal forces to return the condensate fluid to the evaporator. The system has the advantage of continuous large rates of heat transfer in the one direction loop as the condensate fluid is returned in the direction of the driving force (Lee and Mital 1971).

The present study investigates the performance and potential for passive heat extraction from the LCZ. In order to achieve this aim, the concept of a thermosiphon heat exchanger was studied theoretically and laboratory experiments on thermosiphon heat exchanger prototypes were carried out for validation.

5.3 Theoretical Analysis

Governing equations for the system model have been derived using conservation of mass, momentum and energy principles to determine the performance of a U-shaped thermosiphon heat exchanger as shown in Figure 5.1(a). When the tank water is heated, the temperature difference and buoyancy effects initiate natural convection in the system. Less dense hot water rises in the thermosiphon pipe because of natural convection and buoyancy effects. As the hot water covers the cold surface of the coil, the temperature is

reduced and the water density is increased. Due to gravitational effect, the cool water in the system falls back into the tank. Eventually, the process is repeated as more water in the tank is heated. This phenomenon shows that cold water inside heat exchanger coil is extracting heat from the hot water.

Figure 5.1(b) shows a cross section of the heat exchanger coil. It illustrates important dimensional information for the coil, which are input parameters to the mathematical model.

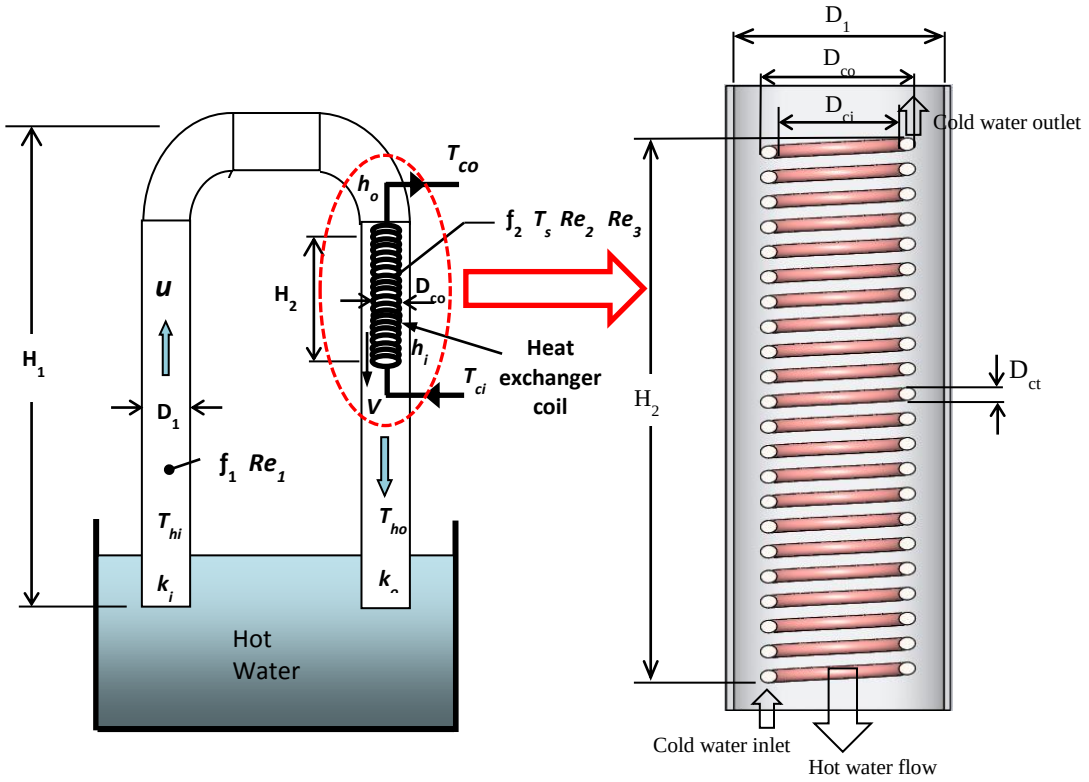

Figure 5.1 (a) Schematic diagram of the proposed U-shaped thermosiphon, (b) Cross section of the heat exchanger coil

Input parameters for the theoretical model are mass flow rate of cold water $\dot{m}_c$, cold water inlet temperature T_{ci}, and physical geometry of the thermosiphon heat exchanger as shown in Table 5.1.

Table 5.1: Physical geometry of the thermosiphon and heat exchanger coil

H_1	H_2	L_{ct}	D_1	D_{co}	D_{ci}	D_{ct}
1.1 m	0.35 m	5.75 m	0.1 m	80 mm	60.96 mm	9.52 mm

The following theoretical modelling was carried out using a Basic Excel worksheet to solve for sixteen of the following unknowns;

$$\left(u, V, h_i, h_o, T_{co}, T_{ho}, T_s, \Delta P, f_1, f_2, \mathrm{Re}_1, \mathrm{Re}_2, \mathrm{Re}_{ct}, Ra_{Dhx}, Nu_o, Nu_i\right)$$

The physical properties of cold water inside the coil and hot water passing along the coil are assumed constant. The energy balance between hot water and cold water in the system is given by;

$$\dot{m}_c C_p\left(T_{co} - T_{ci}\right) = u\frac{\pi}{4} D_1^{\,2} C_p\left(T_{hi} - T_{ho}\right) \tag{5.1}$$

The energy balance in form of heat transfer rate absorbed by the cold water inside the coil from the hot water surrounding the coil is defined by;

$$\dot{m}_c C_p\left(T_{co} - T_{ci}\right) = \pi D_{ct} L_{ct} h_o \left[\left(\frac{T_{hi} + T_{ho}}{2}\right) - T_s\right] \tag{5.2}$$

The heat transfer rate from forced convection between the hot water outside the coil wall and inside the coil is defined by;

$$\left[T_s\left(\frac{T_{ci}+T_{co}}{2}\right)\right]h_i=\left[\left(\frac{T_{hi}+T_{ho}}{2}\right)-T_s\right]h_o \tag{5.3}$$

The difference of hot water velocity caused by the restriction by the coil in the system is given by;

$$uA_1=VA_2 \tag{5.4}$$

Available pressure in the system allowing for buoyancy and pressure losses using Darcy's pressure drop correlation is expressed by;

$$\begin{aligned}\Delta P=&\left[\rho.g.\beta(H_1-H_2)(T_{hi}-T_{ho})\right]\\&+\left[\rho.g.\beta.H_2\left(T_{hi}-\left(\frac{T_{ho}+T_{hi}}{2}\right)\right)\right]\end{aligned} \tag{5.5}$$

$$\begin{aligned}\Delta P=&\left[f_1\left(\frac{2H_1-H_2}{D_1}\right)\frac{1}{2}\rho u^2\right]+\left[f_2\left(\frac{H_2}{D_{hx}}\right)\frac{1}{2}\rho V^2\right]\\&+\left[k_i\frac{1}{2}\rho u^2\right]+\left[k_o\frac{1}{2}\rho u^2\right]\end{aligned} \tag{5.6}$$

where the friction factors in fully developed flow in the thermosiphon and coil are given by;

$$\begin{aligned}&f_1=(0.79\ln \mathrm{Re}_1-1.64)^{-2}\\&3000<\mathrm{Re}_1<5x10^6\end{aligned} \tag{5.7}$$

$$\begin{aligned}&f_2=(0.79\ln \mathrm{Re}_2-1.64)^{-2}\\&3000<\mathrm{Re}_2<5x10^6\end{aligned} \tag{5.8}$$

The critical Reynolds number for flow in the helical coil which was suggested by Srinivasan et al. (Srinivasan, Nandapukar et al. 1970) and was employed by Ghorbani et al. (2010) is adopted;

$$\mathrm{Re}_{crit} = 2100\left[1+12\left(\frac{D_{ct}}{D_{co}}\right)^{0.5}\right] \tag{5.9}$$

The Reynolds numbers for the flow in the thermosiphon pipe and through the circular coil are given by;

$$\mathrm{Re}_1 = \frac{\rho u D_1}{\mu} \tag{5.10}$$

$$\mathrm{Re}_2 = \frac{\rho V D_{hx}}{\mu} \tag{5.11}$$

The outside Nusselt number, Nu_o of the coil heat exchanger was evaluated using the length of the tube, as the characteristic length as described by Prabhanjan, Rennie et al. (2004).

$$Nu_o = 0.0749 Ra^{0.3421} \tag{5.12}$$

for $9\text{x}10^9 < \mathrm{Ra} < 4\text{x}10^{11}$

where Ra is the Rayleigh number using characteristic length outside the coil and is given by;

$$Ra_{Dhx} = \frac{\rho\beta(T_{hi}-T_{ci})L^3}{\nu\alpha} \tag{5.13}$$

The heat transfer coefficient inside the copper tube as introduced by Rogers and Mayhew (1964) related to curvature ratio is given by;

$$Nu_i = 0.023\,\mathrm{Re}^{0.85}\left(\frac{D_{ct}}{D_{co}}\right)^{0.1}\mathrm{Pr}^{0.4} \tag{5.14}$$

where, the Reynolds number inside the copper tube is given by;

$$\mathrm{Re}_{ct} = \frac{4\dot{m}_c}{\pi L_{ct}\mu} \tag{5.15}$$

The convection coefficients for heat transfer inside and outside of the copper tube are given by;

$$Nu_i = \frac{h_i D_{ct}}{k} \tag{5.16}$$

$$Nu_o = \frac{h_o D_{hx}}{k} \tag{5.17}$$

Assuming the specific heats C_p for both hot and cold brine are equal and constant, the effectiveness, ε of the coil heat exchanger of the counter flow is calculated as follows;

$$\varepsilon = \frac{T_{co} - T_{ci}}{T_{hi} - T_{ci}} \tag{5.18}$$

5.4 Experimental study

5.4.1 Thermosiphon heat exchanger rig

An experimental U-shaped thermosiphon heat exchanger rig has been fabricated and installed at RMIT Bundoora East thermal laboratory as shown in Figure 5.2. The main objective was to measure the performance of a thermosiphon heat exchanger and compare the measured results to the theoretical results. The U-shaped thermosiphon heat exchanger was made from polyvinyl chloride (PVC) pipe, of mean inside diameter (ID)

and wall thickness 103 mm x 3.5 mm with appropriate fittings. The heat exchanger coil made from copper tube was inserted vertically at one side. The other side of the thermosiphon was constructed from clear polycarbonate tube for flow visualisation purposes. A vacuum pump was connected to the thermosiphon to completely fill the system with water.

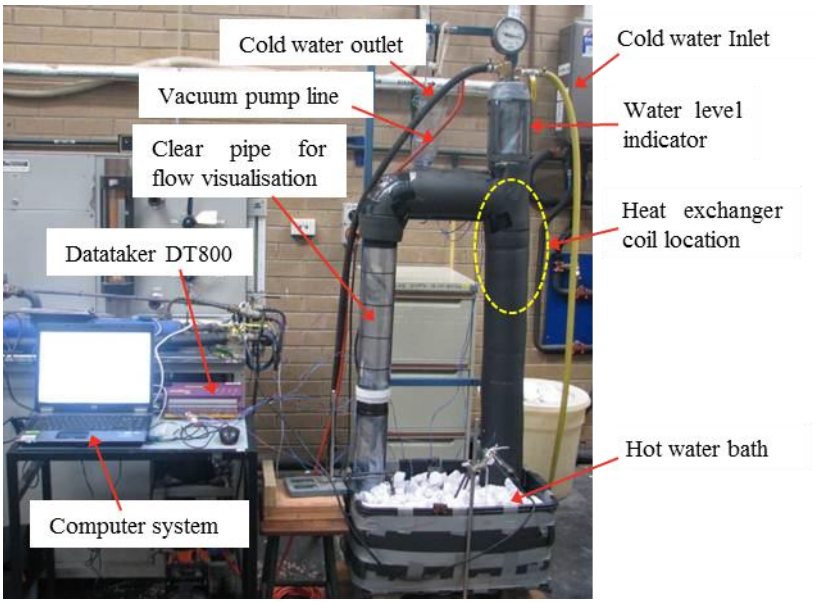

Figure 5.2 Thermosiphon heat exchanger experimental set-up

A DataTaker (DT800) data acquisition system with accuracy of ±0.02% of DC voltage measurement was used for continuous temperature measurements at six different locations. T type thermocouples with an accuracy of ±0.4% were used to measure temperatures at locations at the inlet and outlet of the cold water; inlet and outlet of the hot water on the thermosiphon; in the tank; and the ambient temperature. The thermocouple accuracies were validated using boiling water and melting ice, where temperatures shown were 99^{o}C and 0^{o}C respectively. A mercury thermometer was used to confirm the readings. Details on arrangement of the thermocouple validation can be found in Appendix C.

Data from the system were captured by a DataTaker at 15-second intervals. Average measured values within the experimental period were used for further calculations. A liquid laundry brightener with specific gravity close to 1, as used by Lim (2000) for his experiment, was used as a dye tracer to measure velocity of hot water in the U-shaped thermosiphon. The temperature sensors locations and dye injection location are shown in Figure 5.3.

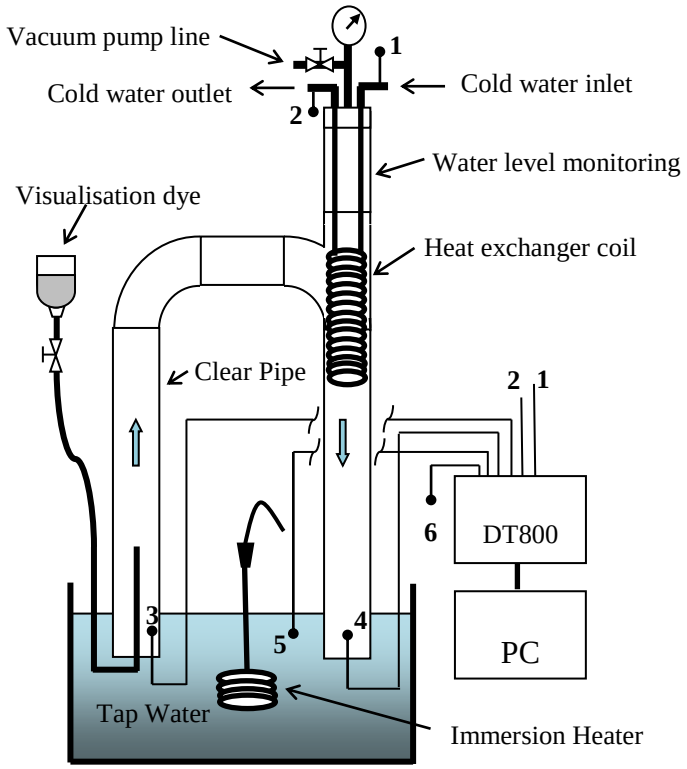

Figure 5.3 A schematic of the thermosiphon heat exchanger rig

The heat exchanger coil as shown in Figure 5.4 was made of a copper tube of 9.52mm OD and 0.91mm wall thickness and was carefully formed in-house using a lathe. A 60mm straight metal pipe was used as a jig to obtain a uniform 80mm OD of the coil. The end of the coil was bent through 90^{o} to become a straight inlet pipe passing through

the coil centre. Rubber O-rings were used for tight-fit between the copper tube and the PVC cap to prevent leakage in the system.

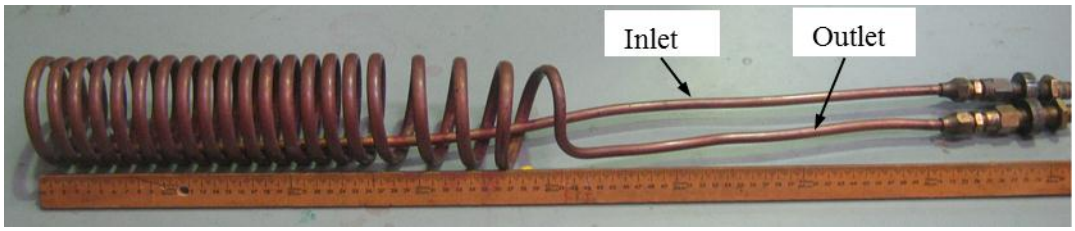

Figure 5.4 Heat exchanger coil

5.4.2 Experimental procedure

Vacuum pump was used to lift the water in both the arms such that the thermosiphon is filled with water. This was to ensure that the cooling coil was completely immersed in water. The data acquisition system was switched on for approximately five minutes to ensure system stability prior to the heating process. The 3kW-immersed coil heater was used to heat the tank water. When the temperature reached 70^{o}C, the cold water inlet valve was opened to the designated flow rate to enable the correct cold water circulation in the heat exchanger coil which was extracting the heat in cross flow. The purpose of setting a maximum temperature of 70^{o}C was to match the RMIT solar pond LCZ temperature which reaches approximately 60^{o}C to 65^{o}C during summer. For safety reason, the heating process temperature was required to not exceed 70^{o}C to avoid overheating.

Using a method similar to that used by Ghorbani et al.(2010) for their experiment, the volume flow rate in litres per second, was measured manually by using a stopwatch to measure the time taken by the water to fill up a measuring cylinder. The stopwatch had an accuracy of ±1%. A short length of wool was patched inside the clear pipe to monitor the flow. It was observed that the thermosiphon was seen to be operating when the tank water temperature reached 30^{o}C.

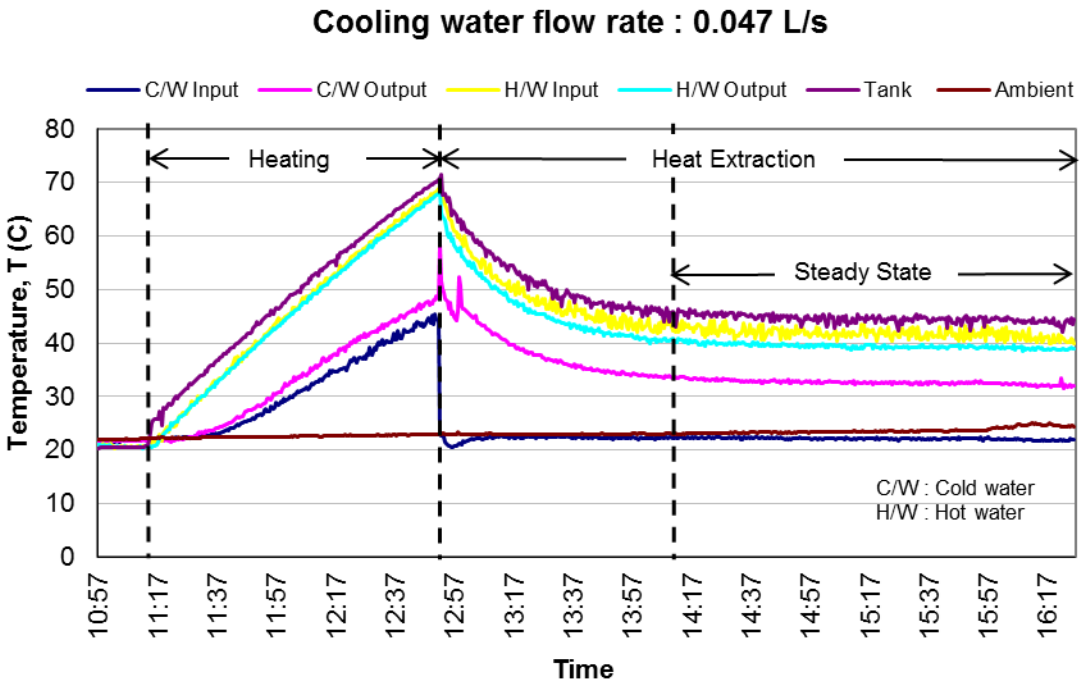

Figure 5.5 Sample data from thermosiphon heat extraction experiment

Figure 5.5 shows the experimental data for the case of 0.047 L/s cold water mass flow rate. It took one hour and 40 minutes to heat the tank water from 20^{o}C to 70^{o}C. The temperature in the system dropped abruptly when cold water flowed through the heat exchanger coil. This indicated that heat was being extracted by the cold water. After approximately two hours and 15 minutes, the system reached a steady state condition. At that time, the flow could be visualised by injecting dye into the transparent pipe. This was done for five different cold water mass flow rates which were at 0.033, 0.038, 0.047, 0.067, 0.102 and 0.125 L/s. During the process, data were captured every 15 seconds by the DT800.

5.4.2.1 Flow visualisation

For flow visualisation purposes, the dye was injected into the transparent pipe section when hot water was circulating in the system at a steady state condition, as explained in the previous section. Figure 5.6 shows the arrangements for flow visualisation. An additional light source was required to provide sufficient illumination to obtain good visualisation. A Canon digital camera in video mode was used to capture the movement of the dye. A stopwatch with accuracy of ±1 % was used to record the time for the dye flow to pass the marked scale with 0.1 m intervals in the transparent pipe section.

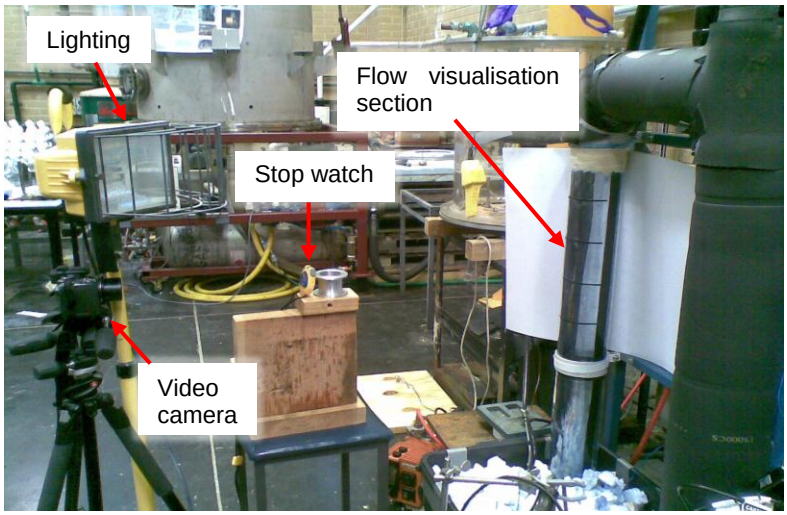

Figure 5.6 Flow visualisation set-up

By analysing the video obtained, distance travelled by dye during a particular time was calculated to determine the flow velocity of hot water in the thermosiphon. Figure 5.7 shows the time taken by the dye as it travelled pass the scale on the transparent pipe. The velocities obtained from this procedure were used to calculate the mass flow and to compute heat loss from the hot water.

(a) (b) (c)

Figure 5.7 Flow visualisation using dye; (a) Start, (b) Midway, (c) Finish

The flow visualisation could only be repeated once for each cold mass flow rate because the injected dye transformed the water into dark blue and prevented proper visualisation. The coloured water was replaced with clear water for the next experiment. For this reason, only one experiment with one cold mass flow rates could be run at any one time.

5.4.3 Implementation of thermosiphon heat exchanger in solar ponds

The semi-passive of thermosiphon heat exchanger system may be installed in working solar pond in series as shown in Figure 5.8. The thermosiphon pipe should be well insulated to minimise heat loss. The diffusers should be attached to the inlet and outlet so that the hot brine is withdrawn and returned with minimum mixing effect. Cold heat transfer fluid is pumped through thermosiphon 1 to thermosiphon n that are connected in series. The heat transfer fluid received heat from the hot water withdrawn from different levels of NCZ. Conventionally heat has been extracted from LCZ, using the new proposed system heat transfer fluid could be gradually pre-heated and helps improve overall system efficiency.

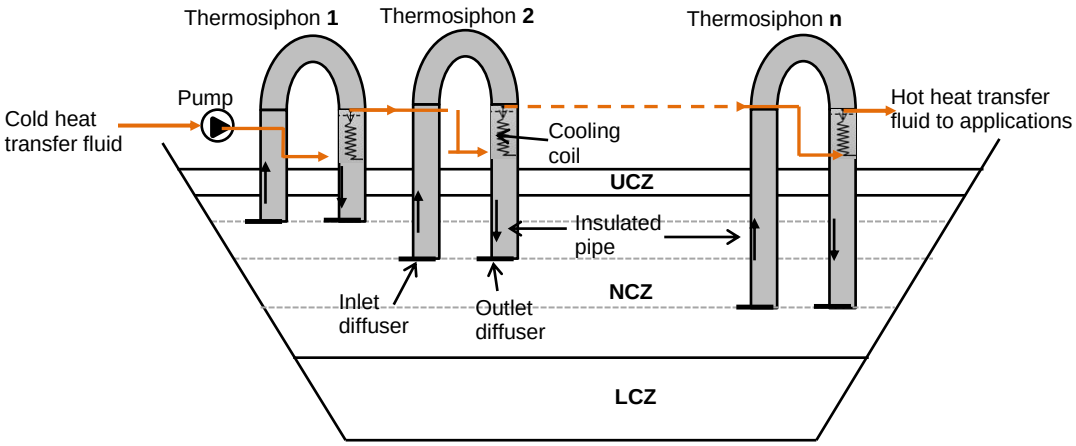

Figure 5.8 Proposed arrangement of thermosiphon heat exchanger in solar ponds

5.4.4 Summary

This chapter describes laboratory experimentation with a thermosiphon test rig. A theoretical model was developed for optimization of the thermosiphon heat exchanger. A coil heat exchanger made using a 9.52mm diameter copper tube was incorporated into a U-shaped thermosiphon heat exchanger prototype. Cold mains water at various mass flow rates was used as heat exchanger fluid to extract heat from the hot water. The theoretical model was validated using the experimental data and was used to predict performance of the thermosiphon heat exchanger, as described in the next chapter.

Chapter 6 - Experimental Results and Discussions

6.1 Introduction

This chapter describes experimental results obtained for heat extraction from the NCZ of a solar pond and describes a thermsosiphon HEX laboratory set-up. The performance of the heat extraction system, installed to extract heat from the NCZ, is analysed and discussed. Also the effect of brine withdrawal and re-injection into the salinity gradient layer is discussed in detail. The performance of a thermosiphon HEX prototype is measured and discussed to assess its feasibility for extracting heat from the LCZ of a solar pond without requiring a mechanical pump.

6.2 Heat extraction from NCZ using external HEXs

Experimental investigation of multi-layer heat extraction from the NCZ has been conducted to measure the performance of the system for different seasons as shown in Table 6.1.

Table 6.1 Climate data and LCZ temperature during experiment

Months	Monthly average of ambient temperature, ^{o}C	Monthly average of solar radiation, W/m^2	Monthly average of LCZ temperature, ^{o}C
Jan-12	27.3	278.9	61.2
Feb-12	26.6	223.4	53.6
Apr-12	21.2	132	42.4
Oct-12	20.4	226	31.4

Figure 6.1 shows the monthly averages of ambient temperature, solar radiation and RMIT solar pond LCZ temperature over eighteen months, from May 2011 to October 2012. The experiments were carried out from mid-summer in January followed by a second

experiment in February. The third and the forth experiments were carried out in autumn 2012 and spring 2012 respectively. The ambient temperature and specific global insolation (Ig) data from Bureau of Meteorology (BOM) can be found in Appendix E.

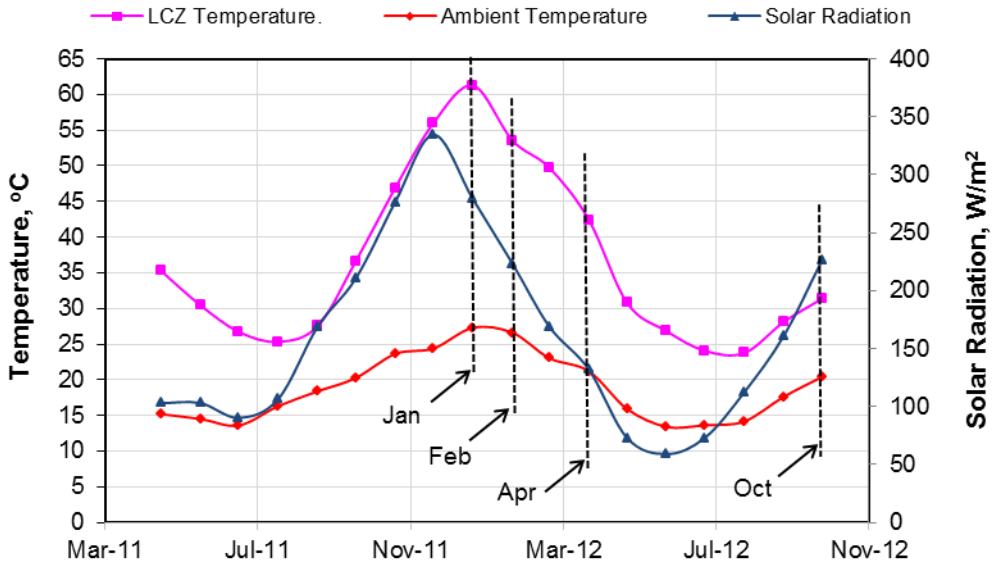

Figure 6.1 The monthly averages of climate data and the LCZ temperature of the RMIT solar pond from May 2011 to October 2012

6.2.1 Experiment in January 2012

This experiment was carried out over one week from the 24th to the 30th January 2012 with heat extracted from multiple locations within the NCZ using an external HEX. The flow rate of cold brine to collect heat from the HEX system in series was set at 0.025 L/s. The flow rate of hot brine for individual HEX was set initially at 0.03 L/s. However, the flow rates of some pumps were reduced or stopped completely after running for a few days. The problems arose from floating objects such as dried leaves or dead insects blocking the diffuser intake. Another issue relating to pump stoppage was accumulated

salt inside the pump spool. Pump stoppage affects the overall performance of the heat extraction system.

Figure 6.2 shows the outlet temperature from the heat extraction system compared to the LCZ temperature over the period of one week at the end of January 2012. The outlet temperature from the heat extraction system was approximately 5^{o}C less than the temperature in the LCZ. This finding shows the validity of the result from the case where the last diffuser level was located 0.15cm above the NCZ-LCZ boundary with a temperature difference of approximately 5^{o}C. The other curve shows the temperature of the UCZ which was used as the temperature at the inlet to the HEX system. The results show that the heat transfer fluid was pre-heated from ambient to the NCZ-LCZ interface temperature and in turn reduced the entropy as compared with that of the conventional LCZ only heat extraction system.

The effectiveness of the heat extraction system as shown in Figure 6.2 is calculated using Equation (4.24) by considering conditions at reference points 1 and 2 with maximum and minimum UCZ temperatures respectively. The temperature outcomes and effectiveness of the heat extraction system at references 1 and 2 are shown in Table 6.2. The effectiveness of the system varies from 81% to 84% relating to fluctuation of the UCZ temperature.

Table 6.2 Temperature outcome and effectiveness of heat extraction system

	T_{co}, ^{o}C	T_{UCZ}, ^{o}C	T_{LCZ}, ^{o}C	ϵ
Reference 1	56.35	32.67	61.82	81.2%
Reference 2	55	23.71	60.83	84.3%

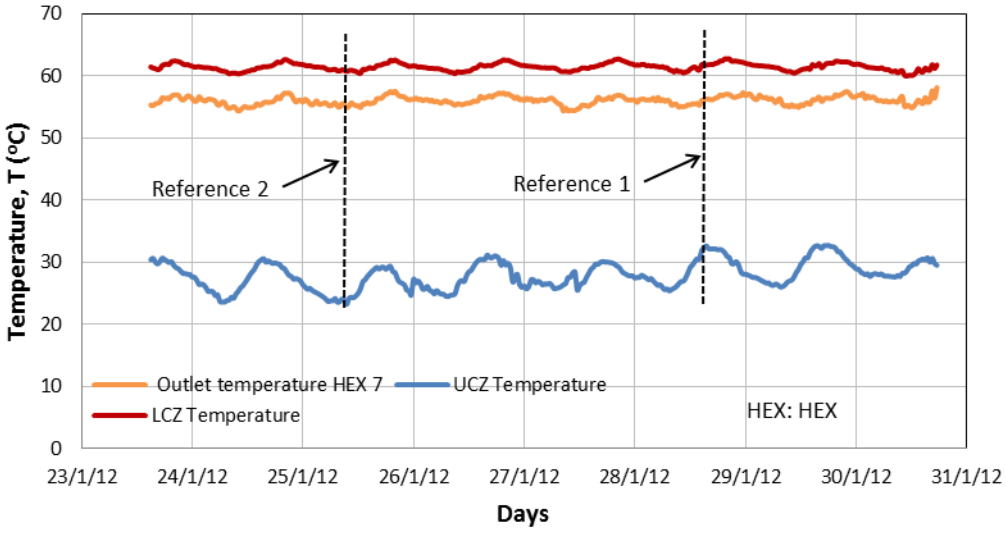

Figure 6.2 The outlet temperature of the heat extraction system

Figure 6.3 shows the temperature difference across the heat extraction system measured at the inlet of HEX 1 and outlet of HEX 7 compared to the temperature difference between the top of the NCZ and the bottom of the NCZ. The effectiveness of the HEX system can be verified by comparing both temperature differences from the heat extraction system and the solar pond. Referring to Table 6.3, the HEX system effectiveness ranged from 83% to 85% taking the reference at maximum and minimum values of temperature difference. Basically, the supply mass flow rate (kg/s) was constant, but the temperature difference varied because of change in ambient temperature. At night time, the temperature difference was seen to be higher because of the drop in ambient temperature. At day time, the temperature difference was lower because of higher ambient temperature. This caused fluctuation in the heat extraction rates during a 24hr cycle although the mass flow rate of heat transfer fluid was maintained constant. For an actual industrial process-heat application, the heat transfer fluid would be expected to be at a constant temperature at the inlet of HEX 1.

Consequently, the rate of heat extraction in that case would be expected to remain constant.

Equation (4.23) was employed to calculate the amount of heat extracted from the NCZ in W/m^2 as shown in Figure 6.3. The main parameters considered are the measured mass flow rate in kg/s, the measured temperature difference of the system and the assumption of constant water specific heat at 25^oC of $4.18kJ/kg^oC$. The calculated heat extracted is in the range of $35W/m^2$ to $56W/m^2$ depending on fluctuation of ambient temperature. The average amount of heat calculated from these measurements is $47.5W/m^2$.

Table 6.3 Effectiveness of the system based on temperature difference

	DT_{HEX}, ^oC	DT_{SP}, ^oC	ϵ
Reference 1	30.34	35.72	84.9%
Reference 2	26.83	32.40	82.8%

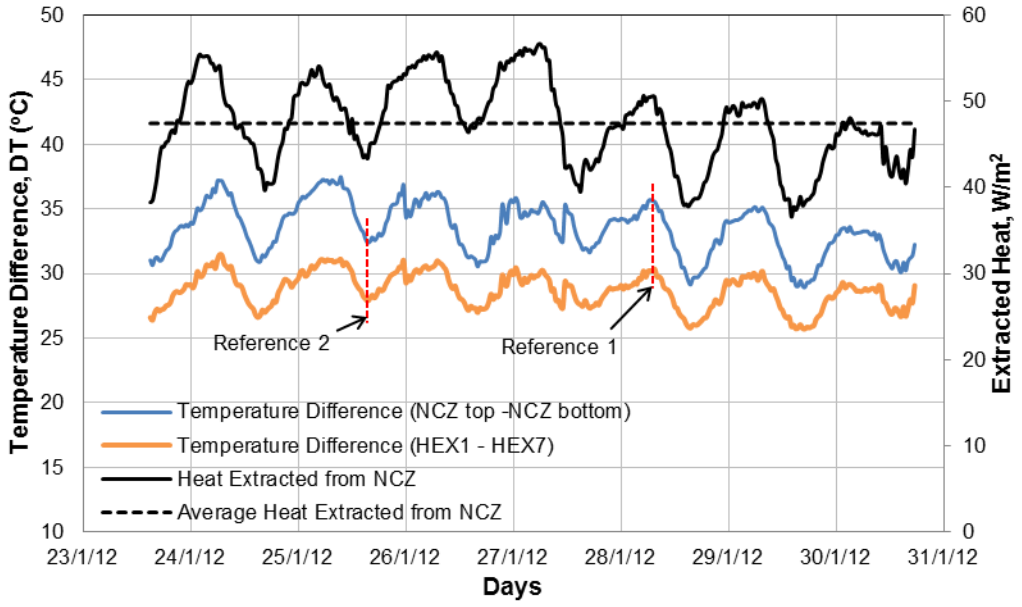

Figure 6.3 Temperature difference of heat extraction system and amount of heat extracted from the NCZ

Figure 6.4 shows the potential for overall efficiency improvement of the solar pond of up to 50% by extracting heat from the NCZ as well as the LCZ. The efficiency of heat extraction from the NCZ only ranges from 13% to 19%. Equation (4.11) was employed for the efficiency calculation. The calculation compared the amount of heat extraction from the NCZ with the average solar radiation received on the surface of the solar pond. The monthly average solar radiation for the month of January 2012 was 278.89 W/m^2 as shown in Figure 6.1. The overall efficiency of the solar pond for heat extraction from the LCZ only is estimated at approximately 15%. This is based on previous studies including the El Paso, Texas and Dead Sea solar ponds where the size of the pond was large. For a small pond as in RMIT, heat will be easily lost through the walls and to the ground. However, in large solar ponds this amount of heat is remains available for heat extraction, providing a potential overall efficiency improvement for the solar pond when heat is extracted from the NCZ as well as the LCZ. As explained from previous results,

fluctuations can be eliminated when constant temperature fluid is supplied to the inlet of the heat extraction system with the extracted heat quantity constant as shown by the dotted line.

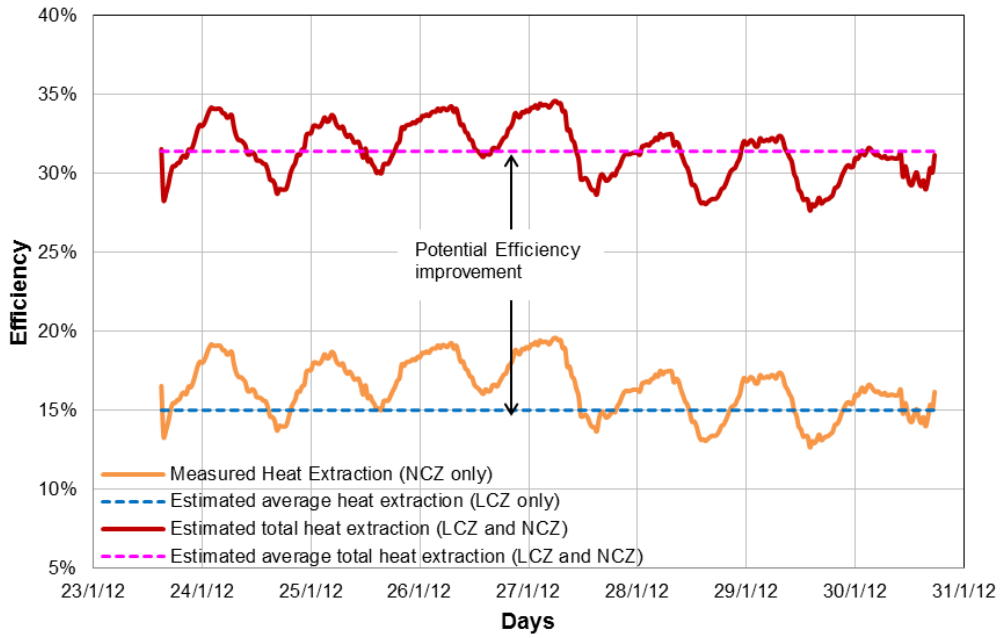

Figure 6.4 Potential for solar pond overall efficiency improvement

6.2.2 Experiment in February 2012

Figure 6.5 shows the temperature at the outlet of the heat extraction system for the period of two weeks from 8th to 24th of February 2012. The mass flow rate of the cold brine was set at 0.025 kg/s. Two set of data at reference 1 and reference 2 representing maximum and minimum temperatures of the UCZ were selected. As mentioned in relation to Figure 6.2, the temperature of the UCZ is used as the HEX inlet temperature. Table 6.4 shows the output temperature from the system compared to the LCZ temperature and the effectiveness at reference1 and reference 2. The temperature difference between the

system outlet and the LCZ temperature fluctuates between 7°C and 7.5°C. The calculated effectiveness's at reference 1 and reference 2 are 70.5% and 71.5% respectively.

Table 6.4 Temperature output, temperature difference, and effectiveness at reference 1 and reference 2

	T_{LCZ}, °C	T_{co}_HEX 7, °C	T_{UCZ}, °C	DT, °C	Є
Reference 1	49.75	42.21	23.27	7.54	71.5%
Reference 2	53.04	46.06	29.37	6.98	70.5%

Temperature in the LCZ decreased with time, while UCZ temperature remained more nearly constant. This is mainly ascribed to heat extraction from the NCZ which enhanced the heat flow from the LCZ to the NCZ and therefore caused the LCZ temperature to drop. On 17th February the ambient temperature was lower than usual which caused the UCZ temperature to be lower on that day and on the following day (18th February).

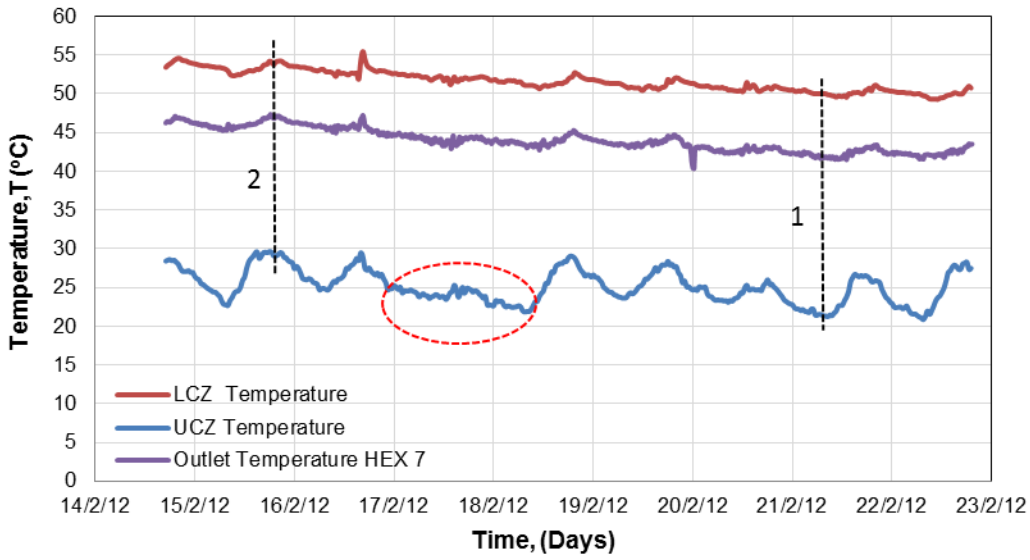

Figure 6.5 The outlet temperature of the heat extraction system for February 2012

Figure 6.6 shows the temperature difference of the heat extraction system compared to the temperature difference in the solar pond. The effectiveness of the system can be verified by comparing temperature differences of the HEX system and the temperature difference of the solar pond. The HEX system temperature difference is the difference between cold inlet temperature to HEX 1 and hot outlet temperature from HEX 7. The solar pond temperature difference is the difference between the UCZ-NCZ interface temperature and the NCZ_LCZ interface temperature. The average temperature difference was used to estimate the effectiveness of the HEX system. Table 6.5 shows the average temperature differences of the HEX system and the solar pond. The results show that the effectiveness of the HEX system could reach up to 80%.

Table 6.5 Effectiveness based on average value of temperature difference

Average DT_{HEX}, ^{o}C	Average DT_{SP}, ^{o}C	Effectiveness, ϵ
20.33	25.43	79.9%

The top curve in Figure 6.6 shows the amount of extracted heat in W/m^2. The calculated extracted heat is in the range of $32W/m^2$ to $47W/m^2$. The average temperature calculated from these measurements is $40W/m^2$.

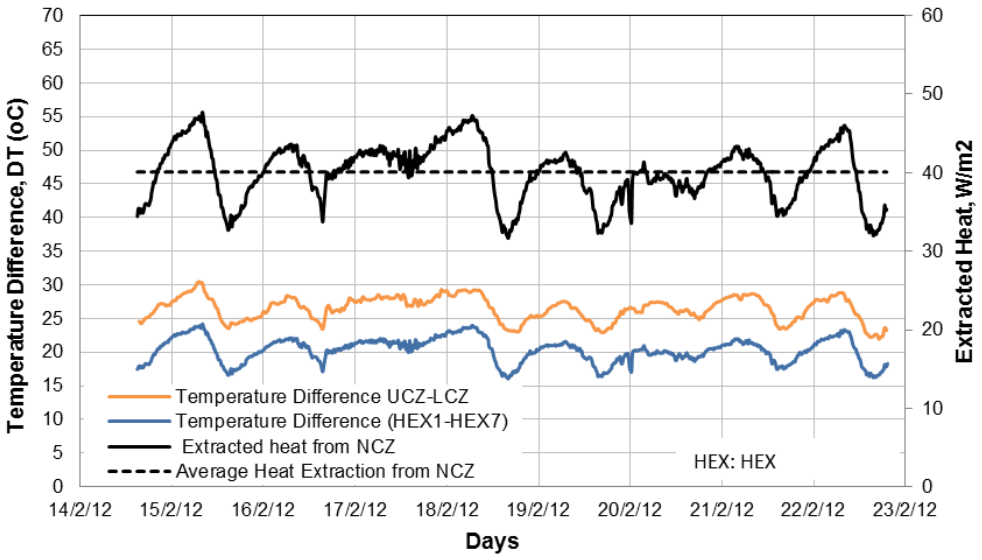

Figure 6.6 Temperature difference of the heat extraction system and the amount of extracted heat from the NCZ for February 2012

Figure 6.7 shows the potential for overall solar pond efficiency improvement of up to 50% by extracting heat from the NCZ as well as the LCZ compared to heat extraction solely from the LCZ. The efficiency of heat extraction from the NCZ only ranges from 21% to 15%. The overall efficiency of the solar pond for heat extraction from the LCZ only is estimated at approximately 15%. The estimated average overall efficiency of the solar pond when heat is extracted from the NCZ as well as the LCZ is 33%. This is a potential increment of 18% over conventional heat extraction solely from the LCZ.

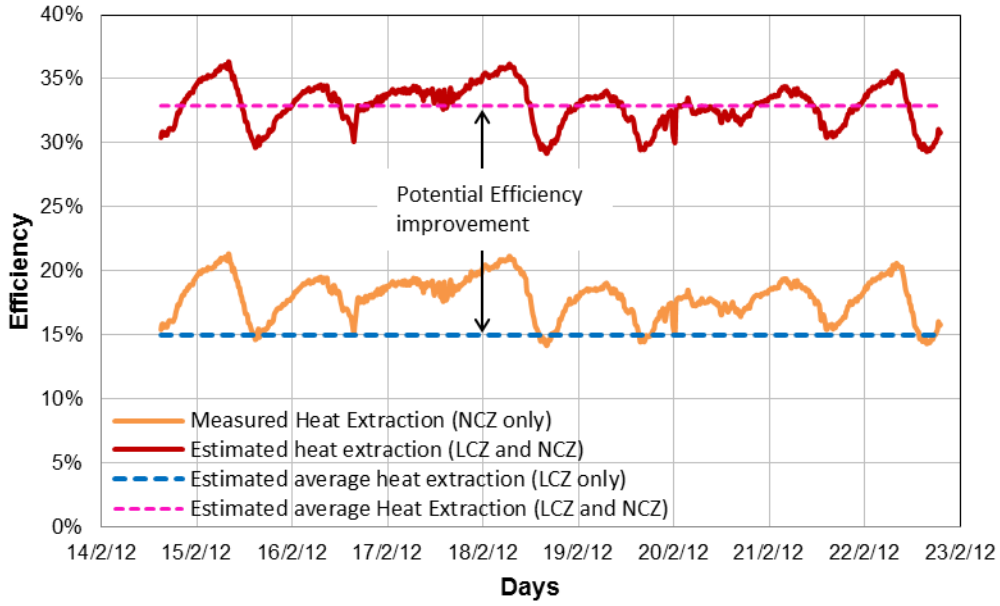

Figure 6.7 Potential for solar pond overall efficiency improvement for February 2012

6.2.3 Experiment in April 2012

A planned experiment was omitted during March. Many of the pumps were not working properly after the February experiment. Therefore, another ten pumps were ordered and delivered in March. The experiment was resumed between 10th and 20th of April 2012. The month of April falls in mid-autumn in the Southern Hemisphere, where the average monthly ambient temperature is approximately 21^{o}C as shown in Figure 6.1.

Figure 6.8 shows the measured outlet temperature of the heat extraction system compared to the measured LCZ temperature during the experimental period. The blue curve is the measured cold brine inlet temperature at HEX 1 which is close to the UCZ temperature. The average values of these temperatures have been used to determine the effectiveness, ϵ of the heat extraction system as shown in Table 6.6 below. The average LCZ temperature within the experimental period was 40.5^{o}C. The average temperatures of the HEX system

inlet and outlet are 15.4°C and 35.1°C respectively. The calculated HEX system effectiveness is 78.3%. Equation (4.24) was used to calculate the HEX system effectiveness.

Table 6.6 The average (Avg) temperature of the LCZ, HEX inlet and outlet and the effectiveness of heat extraction system.

Avg. T_{LCZ}, °C	Avg. T_{HEX_OUT}, °C	Avg. T_{HEX_IN}, °C	Є
40.5	35.1	15.4	78.3%

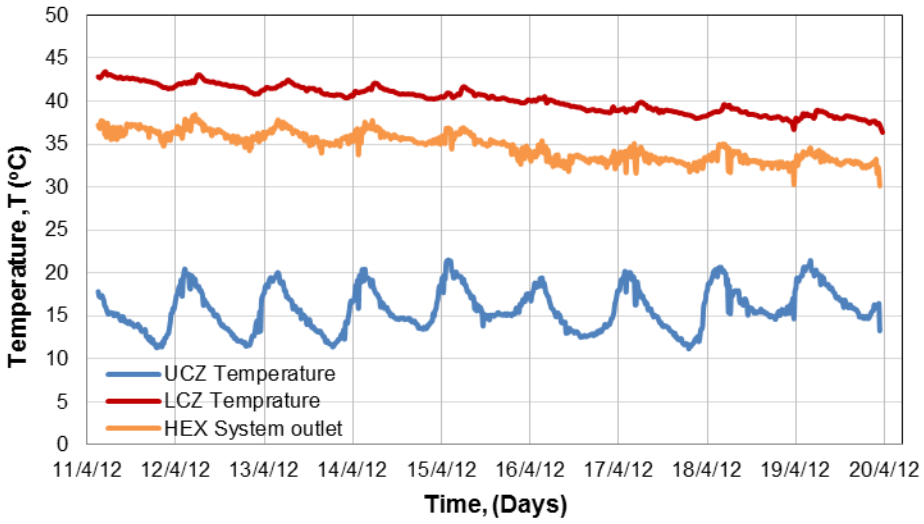

Figure 6.8 The outlet temperature of the heat extraction system for April 2012

Figure 6.9 shows the temperature difference of the HEX system in the blue curve compared to the solar pond temperature difference in the red curve. The temperature difference of the HEX system was taken as the difference between the cold inlet temperature to HEX 1 and the hot outlet temperature from HEX 7. The solar pond temperature difference is taken as the difference between the UCZ-NCZ interface

temperature and the NCZ-LCZ interface temperature. The UCZ temperature is close to the inlet temperature to the HEX system. By comparing the temperature difference from the HEX system with the solar pond temperature difference, the effectiveness of the system can be estimated. The average values for these temperature differences and the effectiveness of the system are shown in Table 6.7. The results show that the effectiveness of the heat extraction system could be as high as 79.2%.

Table 6.7 The estimated HEX system effectiveness based on temperature difference

Avg. DT_{HEX}, ^{o}C	Avg. $DT_{SP,}$ ^{o}C	ϵ
19.68	24.8	79.2%

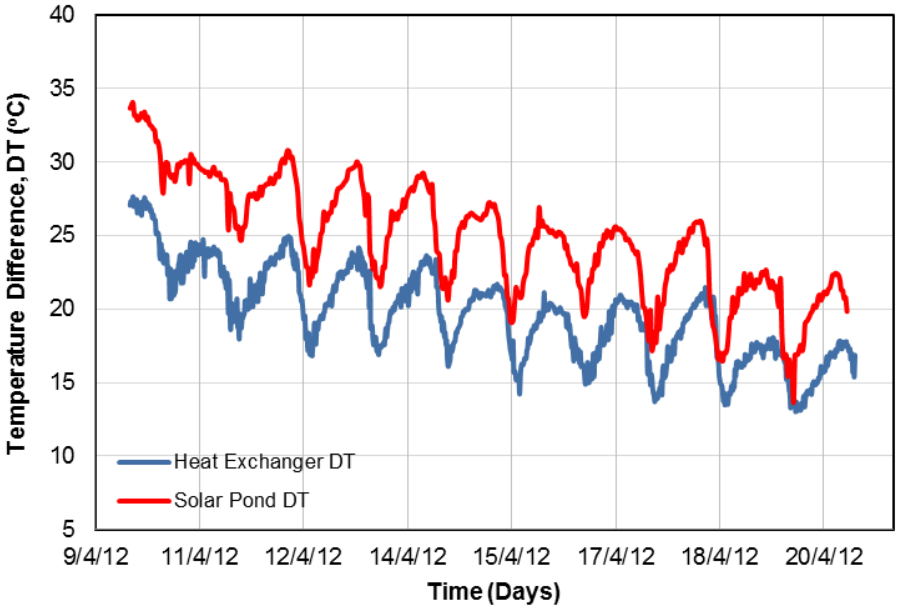

Figure 6.9 Temperature difference of HEX system compared to solar pond temperature difference

Table 6.8 shows the net heat extraction in W/m^2 by cold brine compared to the total heat extraction by hot brine from the NCZ of the solar pond. On average 21.9 W/m^2 of heat was extracted compared to 54.5 W/m^2 heat that was extracted by hot brine from the NCZ. This indicated that the effectiveness of the heat exchanger system is 0.45. On average, at any instant, 1.1kW net heat was extracted from the NCZ of the RMIT solar pond in the month of April 2012. The results shows 50% reduction compared to the heat extraction in January and February during summer. The effectiveness of the heat exchanger system could be improved by increasing the surface area and reducing the hot brine flow rate.

Table 6.8 The performance of the heat extraction system in April 2012

Avg. Heat Extracted by Hot Brine, W/m^2	Avg. Heat Extracted by Cold Brine, W/m^2	Heat Exchanger Effectiveness	Net heat extraction, at any instant, kW
49	22	0.45	1.1

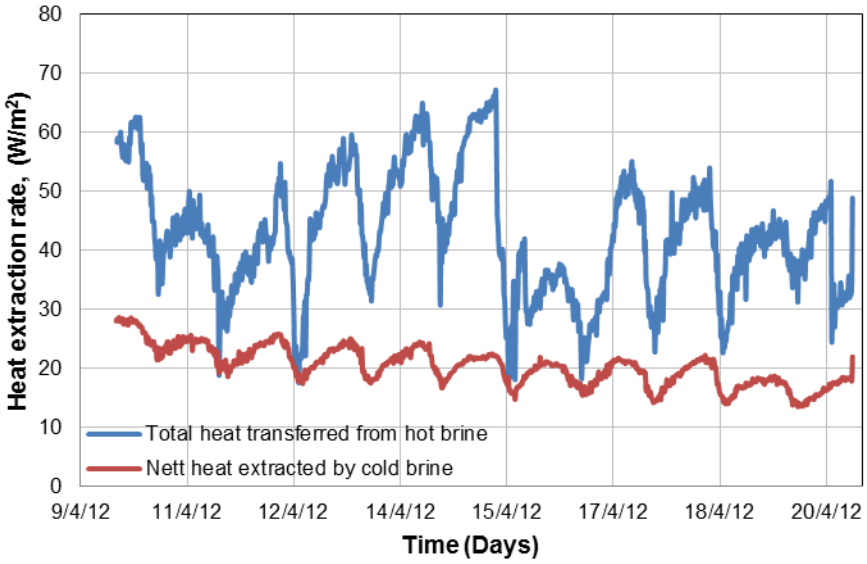

Figure 6.10 Net heat extraction from the NCZ

Figure 6.11 shows the potential for overall solar pond efficiency improvement by up to 50% by extracting heat from the NCZ as well as the LCZ compared to heat extraction solely from LCZ. On average, the efficiency of heat extraction from the NCZ was 17.8%. The estimated overall efficiency of the solar pond for heat extraction from the LCZ only is 15%. Hence, the estimated average overall efficiency of the solar pond when heat is extracted from the NCZ as well as from the LCZ is 32%. This is a potential improvement of 17% over conventional heat extraction solely from the LCZ. Therefore, the efficiency of a solar pond can potentially be increased by up to 50% compared to conventional heat extraction solely from the LCZ.

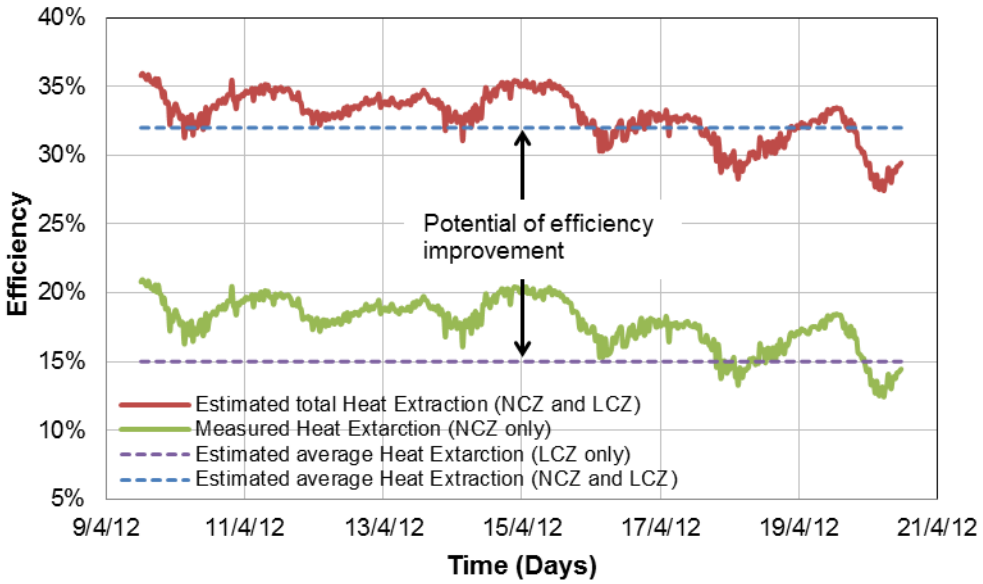

Figure 6.11 Potential of solar pond overall efficiency improvement for April 2012

6.2.4 Effect in salinity gradient layer

One of the concerns in withdrawal and reinjection of brine in the NCZ is the disturbance to the salinity gradient. The disturbed salinity gradient affects overall performance of a

solar pond. It creates a convective layer in the NCZ and weakens the ability of the NCZ to be a thermal insulator. Figure 6.12 shows the evolution of the density gradient from 9 March to 19 April 2013. It clearly shows the disturbed salinity gradient because of heat extraction using an external HEX with withdrawal and reinjection of hot brine from the NCZ. The most affected zone was located between the diffuser of HEX 3 and the diffuser of HEX 6. Development of a 0.4m thick convective layer was observed. Another smaller convective layer was seen on top of the NCZ. This clearly shows the effect of reinjection of brine from the diffuser of HEX 1. The earlier profiles in March have also shown the effects of disturbance of the salinity gradient. They show that the heat extraction activity in February created the convective layer which developed in the NCZ. Similarly, the temperature profile was badly disturbed at the same location as shown in Figure 6.13. The repair of the gradient layer was carried out as explained in Section 3.2.3 in order to restore a stable salinity gradient.

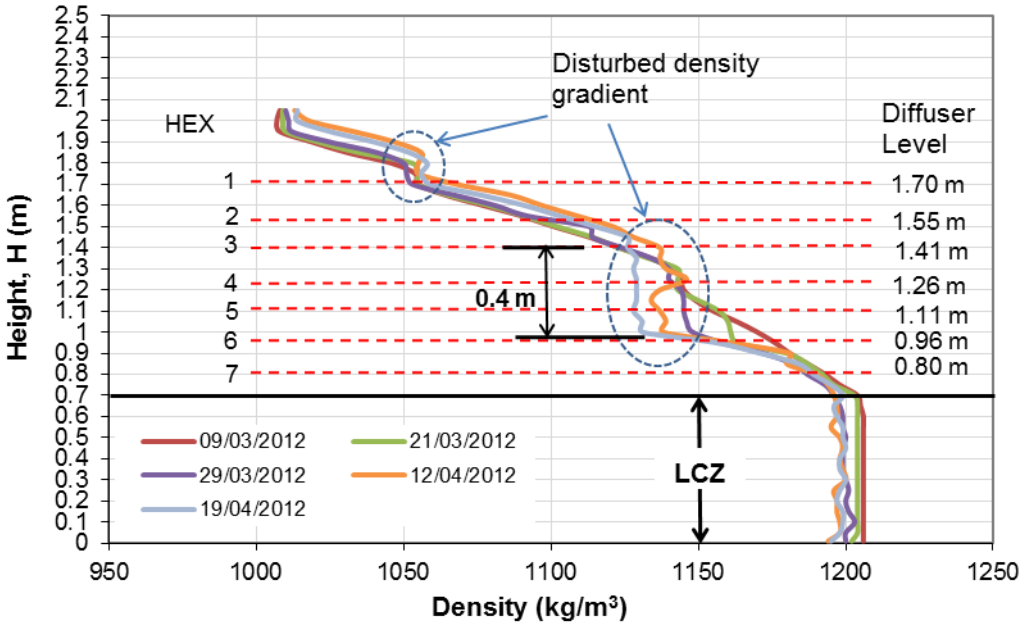

Figure 6.12 The affected density gradient after heat extraction from the NCZ

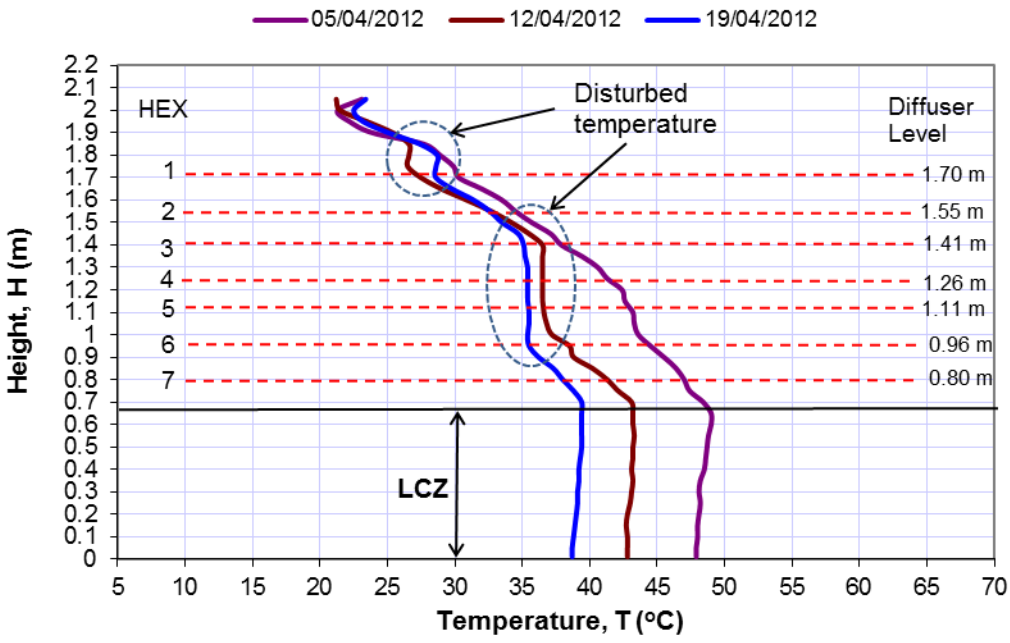

Figure 6.13 Effects on temperature gradient after heat extraction from the NCZ

6.2.4.1 Observation in October 2012

The salinity gradient was restored at the end of July 2012. In October 2012, another experiment using heat extraction from the NCZ was carried out. The main purpose was to demonstrate different modes of heat extraction and to observe their effects on the LCZ temperature. The details of the observations are explained in the next section of this chapter. In this experimental period, the density of re-injected brine into NCZ was measured manually. The sample was collected through flow control valve and the measurement was done using hands held density meter. Table 6.9 shows the calculated Froude number for each diffuser level of the re-injected brine. The shape of the diffuser helps to reduce the velocity at both inlet and outlet. The mass flow rates were reduced to

the minimum level to avoid jet entrance effects. Relatively small Froude numbers were obtained at each diffuser level.

A small density difference was observed at each diffuser level. This is predictable as the returned brine is colder than the withdrawn brine. The detail of the diffusers is shown in Appendix D.

Table 6.9 The Froude number of re-injected brine into NCZ and stability ratio, Rρ

HEX No	T_{layer}, ^{o}C	T_{inlet}, ^{o}C	ρ_{layer}, kg/m^3	ρ_{inlet}, kg/m^3	mdot, kg/s	V_{inlet}, (m/s)	Fr_{inlet}	dS, %	dT, ^{o}C	Rρ
1	26.70	23.60	1061	1064	0.01496	0.01403	1.5	3.0	3.1	0.97
2	28.30	25.20	1092	1096	0.00874	0.0116	1.1	4.0	3.1	1.29
3	29.80	26.80	1116	1119	0.01329	0.01543	1.7	3.0	3.0	1.00
4	31.00	29.30	1139	1141	0.01546	0.01526	2.1	2.0	1.7	1.18
5	31.30	31.10	1149	1150	0.01484	0.01363	2.7	1.0	0.2	5.00
6	31.90	31.50	1167	1168	0.01515	0.01657	3.3	1.0	0.4	2.50
7	32.30	30.70	1193	1195	0.01463	0.01659	2.4	2.0	1.6	1.25

In Table 6.9, T_{layer} is temperature of surrounding fluid, T_{inlet} is the temperature of re-injected fluid, ρ_{layer} is the density of surrounding fluid, ρ_{inlet} is the density of re-injected fluid, mdot and V_{inlet} is the mass flow rate and velocity of reinjected fluid, Fr_{inlet} is the Froude number of the re-injected fluid, dS and dT is the salinity difference and temperature difference between surrounding fluid and the re-injected fluid and Rρ is the stability ratio.

The effect of fluid injection into double diffusive stratified fluids has been discussed by many researchers previously. Most of the outcomes shows the effect of instabilities when fluid with different temperature and salinity is introduced into the thermal stratified layers (Manins 1976, Manins 1976, Turner 1979). In Table 6.9, the stability ratio, Rρ due to re-injected cooled brine into NCZ layer was estimated based on equation (2.5) assuming the

value of α and β are constants. As mentioned earlier in section 2.4.2, to maintain the static stability at any depth in NCZ of solar pond the effect of salinity must be equal or greater than the effect of temperature, or $R\rho \geq 1$. The same criteria was used by Xu, Golding et al. (1991) when introducing stability margin number (SMN) in equation (2.8), Sherman and Imberger (1991) have concluded that, $R\rho_{crit}=1.14$. If $Rp<R\rho_{crit}$ the stability would be disturbed. In El Paso, it was observed that the instability was occurred at SMN=1.6 (Xu, Swift et al. 1992). Result in Table 6.9 shows that, except for diffuser of HEX 5 and HEX 6 the remaining diffusers exhibit the occurrence of instability and risk of instabilities to occur. The small temperature difference compared to salinity difference in HEX 5 and HEX 6 diffuser layer made it stability undisturbed.

Figure 6.14 shows the effects of different densities of returned cooled brine at each diffuser level. The figure shows that a small density difference has created some instability in the salinity gradient. As the cooled brine is re-injected into the same layer in NCZ, it sinks due the effect of its initial buoyancy and mixes with the surrounding fluids. A continues re-injection cooled brine into the layer would cause further mixing. This would effects the fluid to sinks further and reduces the density in that layer and the layer below it. It was suggested that the level of return diffuser need to be lift higher than the withdrawal level. But, the similar phenomenon would expected to happened for continues re-injection of cooled brine into difference surrounding fluid density. The similar phenomenon have been reported by Atkinson, Priven et al. (1993) after conducting an experiments of laboratory scale of advance solar pond (ASP) involving injecting and withdrawing fluid into and from thermal stratified layer.

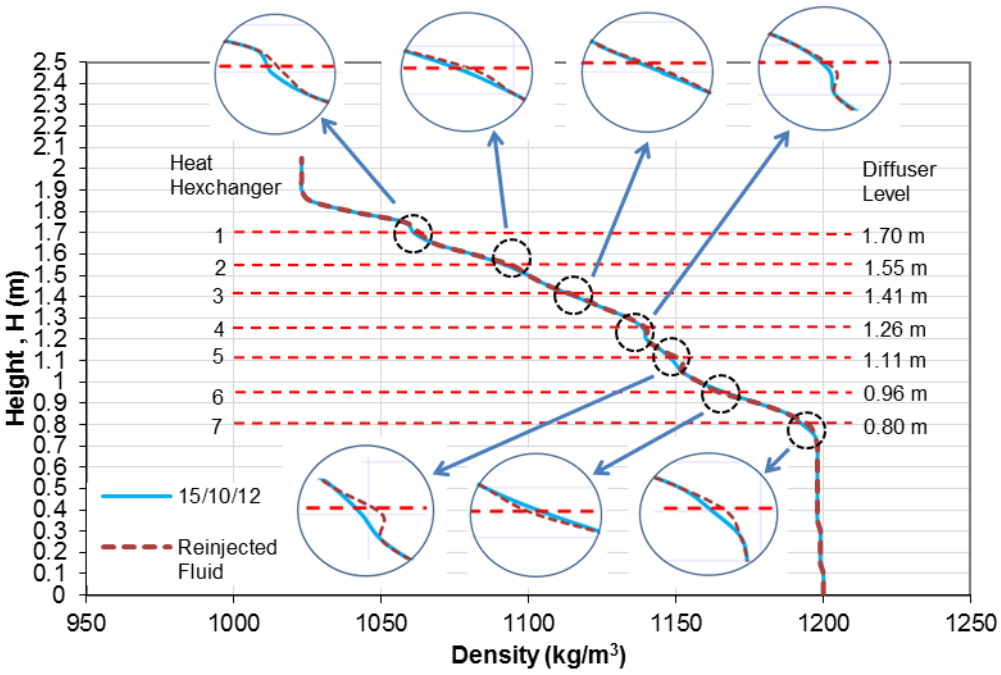

Figure 6.14 The effect of re-injected fluid on the density gradient in the NCZ

This issue is apparently due to double diffusive behaviour in stratified thermal layer. It needs further investigation to better understanding of this phenomenon. A possible solution to this issue is to control a slow mass flow rate by spreading it horizontally using multiple diffusers while maintaining higher velocities. This is to force the velocity of jet travel as maximum horizontally. Another possibility is to preheat the return cooled brine by laying long return line immersed to the same depth of the particular layer before injects it back to the same level.

6.2.5 Effect on LCZ temperature

An experiment to observe the effect of different heat extraction modes on the LCZ temperature has been carried out over one month from 23rd of September to 23rd of October 2012. The heat extraction was achieved in the following modes;

i. Heat extraction from the NCZ and LCZ connected in series

In this method, the outlet of the external HEX system from the NCZ was connected to the internal HEX in the LCZ as shown in Figure 6.15. The heated brine from the NCZ HEX extracts heat from the LCZ to increase the total amount of heat extraction from the pond.

ii. Heat extraction from the NCZ only

The heat is extracted solely from the NCZ using a multi-layer external HEX system as shown in Figure 6.16.

iii. Heat extraction from the LCZ only

Heat has been extracted using a built-in internal HEX by pumping cold brine from the surface in order to extract the heat and returning it to the surface as shown in Figure 6.16.

iv. Simultaneous heat extraction from the LCZ and NCZ in separate systems

Both heat extraction systems from the NCZ and the heat extraction system from the LCZ were run separately to extract heat at the same time as shown in Figure 6.17.

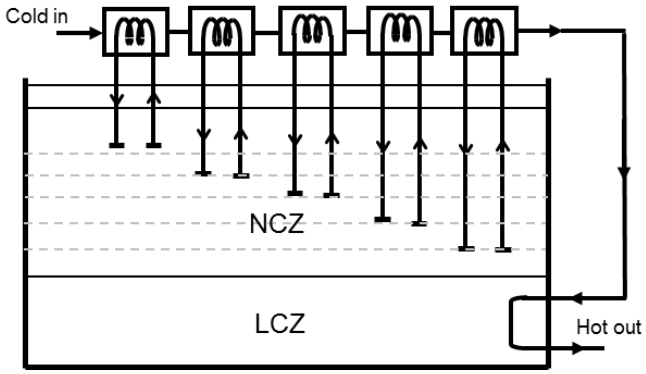

Figure 6.15 Heat extraction from the NCZ and LCZ connected in series

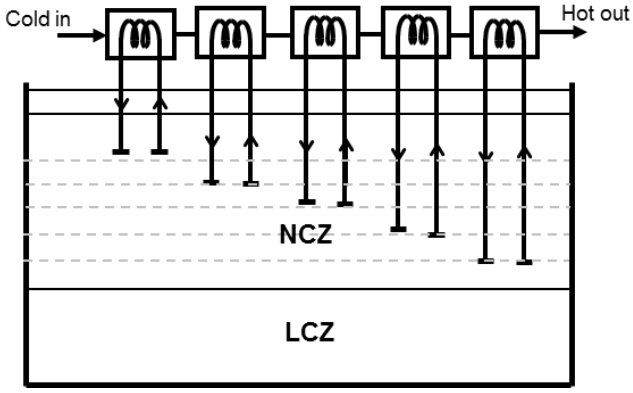

Figure 6.16 Heat extraction from NCZ only

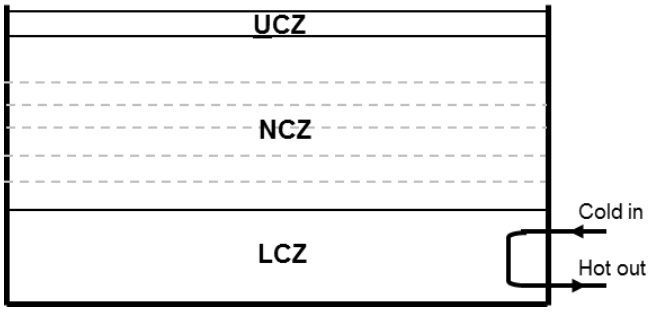

Figure 6.17 Heat extraction from LCZ only

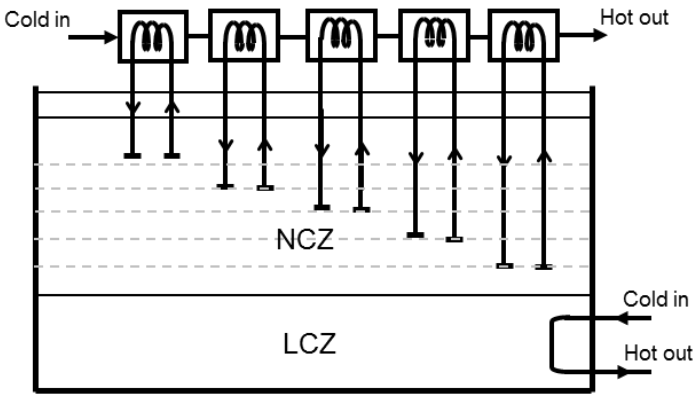

Figure 6.18 Simultaneous heat extraction from the LCZ and NCZ in separate systems

In Figure 6.19, it is observed that heat extraction from the NCZ only, and heat extraction from the NCZ and LCZ connected in series, does not affect the LCZ temperature. However, the LCZ temperature is decreased drastically when heat is extracted from the LCZ only or heat is extracted from the NCZ and LCZ simultaneously by separate systems. The results shows that, by extracting heat from the NCZ with the HEX connected in series to the LCZ as shown in Figure 6.15, the effect of sensible heat addition to heat transfer a fluid from the UCZ-NCZ interface to the NCZ-LCZ interface tends to reduce the upward heat losses in the NCZ. As a result, the heated heat transfer fluids would have small temperature different compare to the LCZ temperature and would avoid the risk of cooling the LCZ layer as experience by the El Paso, Dead Sea and Pyramid Hill solar ponds (Tabor and Doron 1990, Lu, Swift et al. 2004, Leblanc, Akbarzadeh et al. 2011) when heat was extracted only from the LCZ.

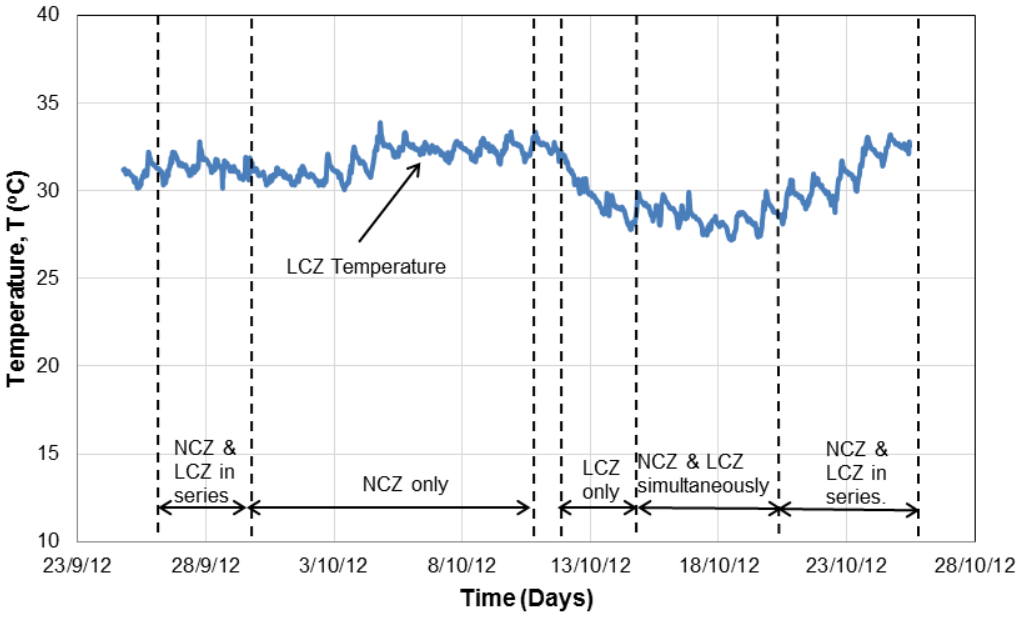

Figure 6.19 The LCZ temperature corresponding to different heat extraction methods

6.2.6 Summary

The results of heat extraction from the NCZ using external HEX are explained in detail. It was shown that, by extracting heat from the NCZ, the efficiency of a solar pond could be potentially improved by up to 50% compared to heat extraction solely from the LCZ. The HEX system has shown good effectiveness of approximately 80%. The amount of heat that can be extracted from the NCZ at approximately 40W/m^2 would be the same as the heat extraction capacity from the LCZ only. The mode of heat extraction from the NCZ connected in series with the HEX in the LCZ has shown the smallest effect on lowering the LCZ temperature. However withdrawing hot brine from the NCZ and re-injecting the cooled brine at the same level has caused the development of a convective layer and weakened the stability of the salinity gradient. This encourages need for further study to optimize the design of the diffuser to avoid the instability issue in the NCZ.

6.3 Performance of thermosiphon HEX

6.3.1 Input parameters to theoretical modelling

The actual experimental data of hot water inlet, T_{hi} and cold water inlet, T_{ci} were used as input values for theoretical modelling at the corresponding cold water mass flow rate, $\dot{m}_c$ as shown in Table 6.10.

Table 6.10 Input parameters based on experimental data

$\dot{m}_c$ (L/s)	T_{hi}, ^{o}C	T_{ci}, ^{o}C
0.033	39.6	16.9
0.038	38.2	17.6
0.047	36.7	17.5
0.067	34.1	17.5
0.102	32.3	17.5
0.125	31.1	16.6

As explained in Section 5.4.2.1, it is possible to carry out only one experiment for each mass flow rate in any particular day. That was the main cause of inconsistency of the inlet temperature for hot and cold water for each experiment. The results of the theoretical modelling are shown in Table 6.11 and the experimental results are shown in

Table 6.12. The water density and heat capacity are assumed constant for both cases as shown in Table 5.2.

Table 6.11 Thermosiphon theoretical results

Theoretical Result

mdotC, (Kg/s)	u hot, (m/s)	Thi, (^oT)	Tci, (^oT)	Tho, (^oT)	Tco, (^oT)	DTh, (^oT)	DTc, (^oT)	mdotH, (Kg/s)	Qc, (W)	Qh, (W)
0.033	0.0446	39.6	16.9	38.6	27.2	1.0	10.3	0.348	1426.5	1426.5
0.038	0.0433	38.2	17.6	37.3	25.9	0.9	8.3	0.338	1317.7	1317.7
0.047	0.0428	36.7	17.5	35.8	24.0	0.9	6.5	0.334	1272.9	1272.9
0.067	0.0411	34.1	17.5	33.3	21.6	0.8	4.1	0.321	1135.2	1135.2
0.102	0.0399	32.3	17.5	31.5	19.9	0.8	2.4	0.311	1038.8	1038.8
0.125	0.0398	31.1	16.6	30.3	18.6	0.8	2.0	0.310	1033.7	1033.7

Table 6.12 Thermosiphon experimental results

Experimental Result

mdotC, (Kg/s)	u hot, (m/s)	Thi, (^oT)	Tci, (^oT)	Tho, (^oT)	Tco, (^oT)	DTh, (^oT)	DTc, (^oT)	mdotH, (Kg/s)	Qc, (W)	Qh, (W)
0.033	0.0588	39.6	17	38.4	33.3	1.2	16.4	0.4586	2262.2	2300.2
0.038	0.0588	38.2	17.6	37	31.3	1.2	13.7	0.4586	2176.1	2300.2
0.047	0.0595	36.7	17.5	35.5	26.8	1.2	9.3	0.4640	1827.1	2327.6
0.067	0.0602	34.1	17.5	32.9	25	1.2	7.5	0.4698	2100.5	2356.6
0.102	0.0578	32.3	17.5	31.1	22	1.2	4.5	0.4508	1918.6	2261.1
0.125	0.0557	31.1	16.6	30	20.2	1.1	3.6	0.4344	1881.0	1997.4

Figure 6.20 shows the variation of hot water velocities with different cold water flow rates based on flow visualisation measurements. Theoretically, the velocity of hot water is decreased with increasing of cold water flow rates. Similar phenomena were observed in experimental results. The effect of buoyancy has dominantly driven the velocity of the hot water because of the temperature difference. Higher cold water mass flow rates tend to reduce heat transfer rates as well as the temperature difference. Lower cold water mass flow rates tend to create a larger temperature difference. They would cause more heat to

be transferred from the hot water and make the water less dense and flow at higher velocity.

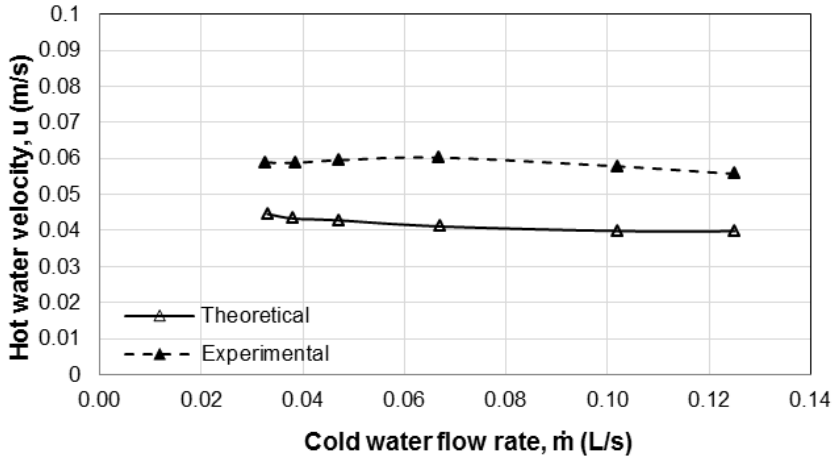

Figure 6.20 The variations of hot water velocity with different cold water flow rates

Figure 6.21 shows the effects of varying cold mass flow rates, $\dot{m}_c$ on hot water outlet temperature in the thermosiphon, T_{ho} and cold water outlet temperature of the cooling coil, T_{co}. The increase of $\dot{m}_c$ has immediate effect of reducing T_{ho} and T_{co} respectively. T_{ho} has shown less temperature drop of approximately 8^{o}C compared to T_{co} which showed experimentally approximately 13^{o}C temperature drop. The reason for this observation was that the hot water flowing in the thermosiphon has larger mass with lesser velocity than the cold water in the cooling coil which is flowing with higher velocity.

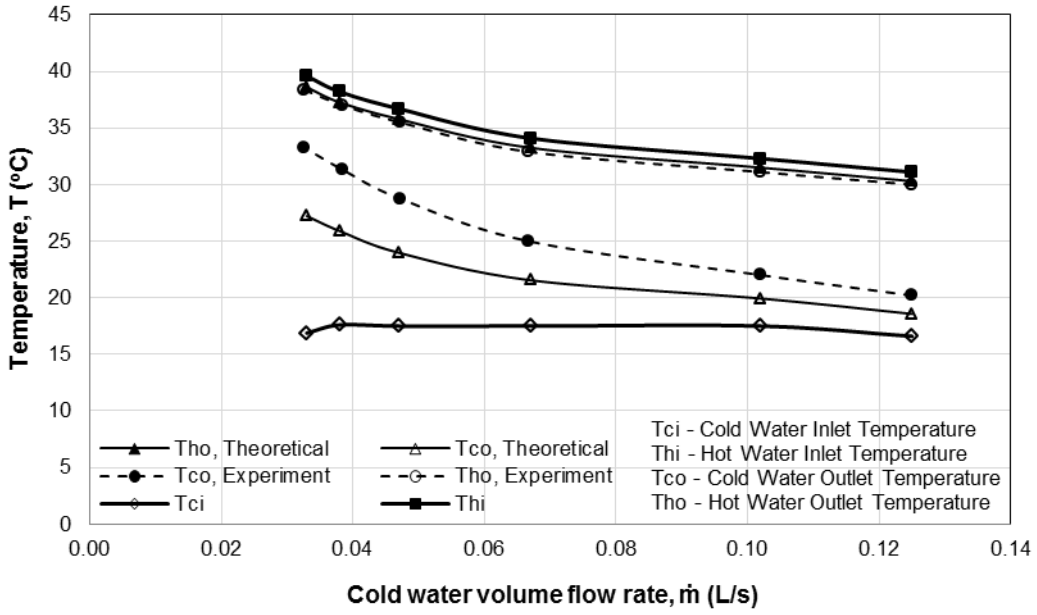

Figure 6.21 The temperatures of cold and hot water with different cold water flow rates

Figure 6.22 shows the temperature differences of cold and hot water both theoretically and experimentally. The temperature difference of cold water decreases with the increase of the cooling water mass flow rates for both experiment and theoretical modelling. This phenomenon is clearly associated with the effects of the mass flow rates, where low cold water mass flow rates would create larger temperature difference and absorb more heat. The hot water shows a constant small temperature difference of approximately 1^{o}C with the variations of cooling water mass flow rates for both experiment and theory. The cold water shows a drastic reduction of temperature difference from the lowest to the highest cold water mass flow rates. This finding results from the effect of different masses of hot and cold water as explained previously based on results in Figure 6.21.

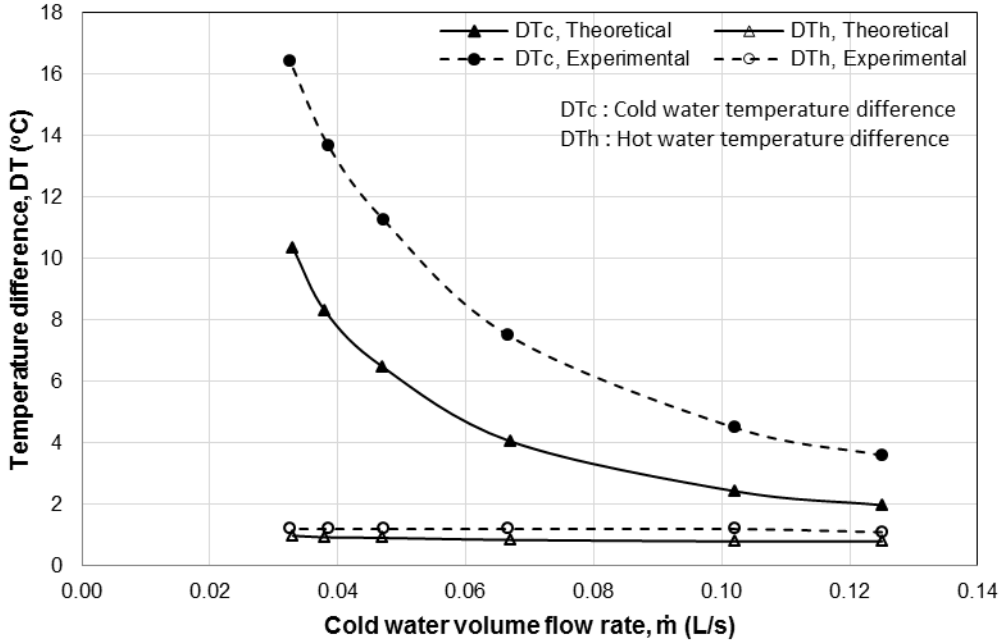

Figure 6.22 The temperature differences of hot and cold water with different cold water flow rates

Figure 6.23 shows the amount of heat extracted by the cooling water and heat transferred from the hot water theoretically and experimentally. Approximately 2kW of heat has been extracted at any instant. Both results show the balance of the heat transfer phenomenon between heat which has been extracted by the cooling water and heat which was transferred from the hot water. The experimental results have proved the validity of the theoretical modelling of the thermosiphon heat exchanger system. The results are related to the obtained velocities as discussed previously. This is understandable, as velocity is one of the parameters determining the quantity of energy produced. On average the results shown that the heat extracted from the system decreases with the increase of the mass flow rates.

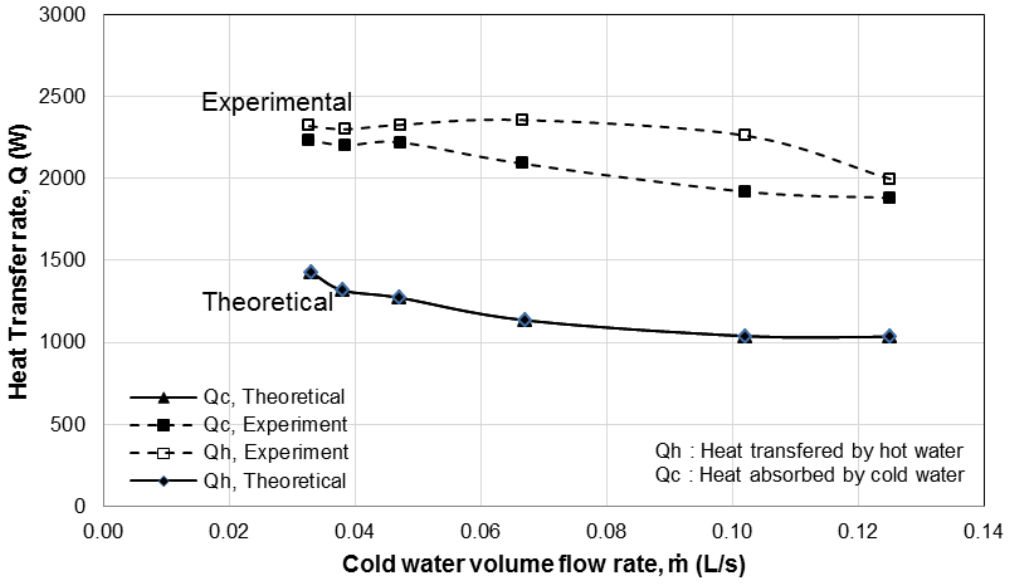

Figure 6.23 The amount of heat extraction with different cold water flow rates

Figure 6.24 shows the estimated effectiveness of the thermosiphon heat exchanger. The effectiveness dropped drastically from 72% at the lowest cold water mass flow rate to 24% at the highest cold water mass flow rate. As explained previously, the effect of cold water velocity relates closely to the temperature difference. Because of buoyancy effects, natural convection occurs. Low velocity causes larger temperature difference and more heat transfer and the heat exchanger become more effective. Higher cold mass flow rate reduces the temperature difference causing less heat transfer and reduced effectiveness.

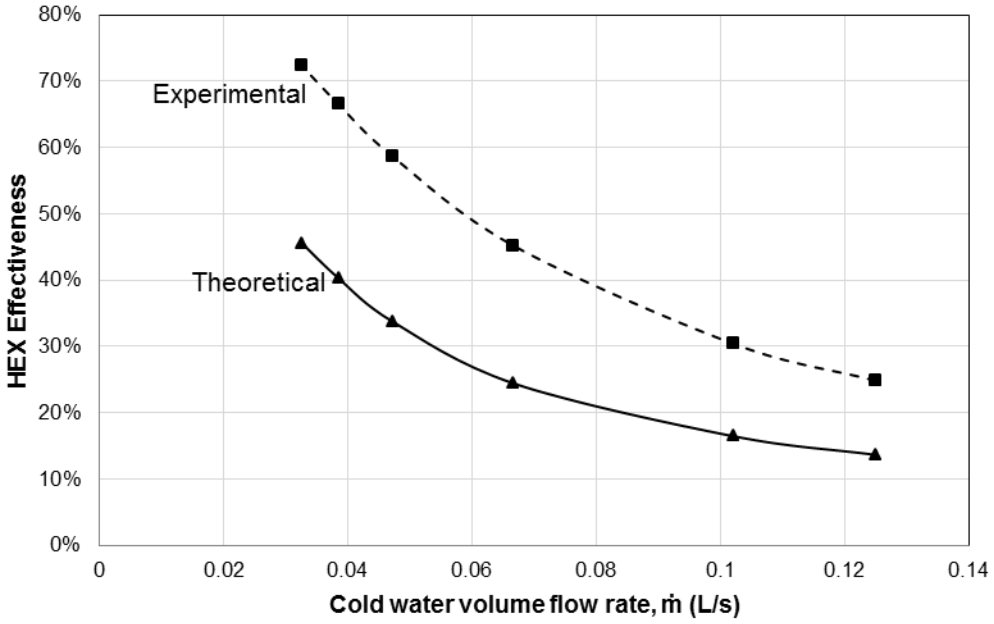

Figure 6.24 The effectiveness of the thermosiphon HEX with variation of cold water flow rates

6.3.2 Summary

A new semi-passive method for extracting heat from hot water using a thermosiphon heat exchanger has been studied theoretically and experimentally. Both theoretical and experiment work has been carried out to explore the concept of a heat extraction system to extract the heat from a solar pond. A prototype thermosiphon system with a coiled heat exchanger has been fabricated and tested in the laboratory. The system was capable of extracting approximately 2kW of heat and has provided positive motivation towards implementing this system for heat extraction from the LCZ or NCZ of solar ponds. The available data will be used to optimise the system and further study to observe thermosiphon heat

exchanger performance in solar ponds is necessary in order to prove the concept beyond this initial result. The use of a thermosiphon as a semi-passive system will result in less complexity of the system and reduce the overall cost of power consumption and maintenance. Measuring the flow rates is only possible using visualisation. Therefore the around 300mm of clear pipe without insulation was used that caused unmeasured heat losses. As a result, the clear section pipe has a higher surface area and insufficient insulation. Due to these reasons, most of the results showed higher value of heat transfer for experimental results than the theoretical predictions.

Chapter 7 - Conclusions and future works

7.1 Introduction

An external heat exchanger for extracting heat from the NCZ of the RMIT solar pond was proposed. Another part of the study was to investigate the use of a thermosiphon heat exchanger as an option for passive heat extraction from a solar pond. The study had the following objectives;

i. To investigate the feasibility of heat extraction from the gradient layer (NCZ) using an external heat exchanger to enhance the overall efficiency of a solar pond.

ii. To examine the possibility of eliminating the pump used in conventional heat extraction by using a thermosiphon based heat exchanger.

As explained in chapter 2, a solar pond is a low cost solar collector as well as a heat storage means for a long period of time. However, the efficiency of solar ponds is limited to between 11% and 15% when using the conventional heat extraction method solely from the LCZ. There has been investigation of extracting heat from the NCZ using an internal heat exchanger. The results were encouraging, but the concept can only be implemented for small scale solar ponds. Therefore, the present study to extract heat from the NCZ using an external heat exchanger was proposed as an alternative to conventional heat extraction only from the LCZ.

7.1.1 The feasibility of the HEX system

A theoretical investigation was carried out to determine the size of heat exchanger required to deliver the heat. Seven units of shell and tube heat exchangers were fabricated. Copper tube of 9.52mm diameter was used as the heat exchanger coil. The HEX system was designed to extract heat multi-layer hot brine from the NCZ using 12V

pumps connected in series. The cold brine from the surface was pumped through the shell heat exchanger to collect heat in stages from HEX 1 to HEX 7. A diffuser was attached to the inlets and outlets of the heat exchangers to force horizontal withdrawal and reinjection of the brine flow. The system operated well and produced substantial temperature difference between the cold inlet to HEX 1 and the hot temperature outlet from HEX 7. This shows that heat extraction from the NCZ using an external heat exchanger is feasible for implementation in working solar ponds.

7.1.2 Efficiency enhancement

Experiments have been carried out in January, February, April and October of 2012. The HEX system was run continuously for periods of seven to eight days to extract heat from the NCZ. The cold heat exchanger fluid mass flow rate was initially set at 0.03 kg/s but reduced to approximately 0.01 kg/s due to sudden expansion and contraction when entering and leaving the shell heat exchanger. The mass flow rate of the hot brine from the NCZ from HEX 1 to HEX 7 was set at 0.03 kg/s in each case. However, most of the flow rates were reduced after some time because of blockage at the diffuser entrance by floating objects in the solar pond. Accumulation of salt inside the pump has also affected the pump performance.

Despite these problems, the HEX system has shown satisfactory performance. In January and February of summer 2012, the effectiveness of the HEX system was between 80% and 84%. On average, 48W/m^2 and 40W/m^2 of heat have been successfully extracted in the months of January and February respectively. This shows that the amount of heat that could be extracted from the NCZ is similar to the amount of heat that is conventionally extracted from the LCZ. Hence, the overall efficiency could be enhanced by up to 50% when compared to a conventional heat extraction solely from the LCZ. Similar results were obtained from the experiments conducted in April. Although the amount of

extracted heat was significantly less due to lower ambient temperature in autumn, a similar percentage of overall efficiency improvement could be achieved.

In October 2012, experiments were conducted with different heat extraction modes to observe the effects on LCZ temperature. The heat was extracted in the following modes;

v. Heat extraction from the NCZ and LCZ connected in series

vi. Heat extraction from the NCZ only

vii. Heat extraction from the LCZ only

viii. Simultaneous heat extraction from the LCZ and NCZ in separate systems

The results showed that heat extraction from the NCZ connected in series with an internal heat exchanger in the LCZ has no adverse effect on LCZ temperature compared to heat removal from the LCZ directly. By extracting heat from the NCZ, the heat transfer fluid was pre-heated prior entering the LCZ. Hence, there was no upward heat loss in the NCZ thus avoiding the effect of cooling the LCZ layer when the temperature difference between heat transfer fluid and surrounding fluid in LCZ was not significant.

7.1.3 Stability effects

The development of convective layers in the salinity gradient layer has been observed during heat extraction studies. The most affected area was between the diffuser of HEX 3 and HEX 6, where a 0.4m thick convective layer developed and another small convective layer was observed at the level of the diffuser of HEX 1. Observations in the month of October showed that a small density difference created a small instability at any instant. This was mainly due to the effect of reinjection of the cooled brine into the same level in the NCZ. The re-injected cooled brine is physically heavier than the surrounding fluid, which tends to cause it to sink to the layer below it. This tends to create a larger

temperature gradient in that particular layer and the layer adjacent to it. The instabilities are unavoidable if the salinity gradient is insufficient to overcome the effects of the larger temperature gradient. This condition promotes a higher heat transfer rate upward and weakens the salinity gradient.

7.1.4 Performance of the passive heat extraction system

A semi-passive thermosiphon heat exchanger driven by buoyancy effects associated with temperature difference and natural convection phenomena has been studied in detail theoretically and experimentally. The main purpose of this study was to investigate the possibility of implementing a semi-passive system which could eliminate or minimise the use of a mechanical pump. A theoretical model has been developed and used for theoretical performance analysis. A prototype thermosiphon heat exchanger has been fabricated and installed in the laboratory. For validation purposes, the theoretical results have been compared with the performance of the thermosiphon heat exchanger prototype in the laboratory. Simple flow visualisation measurements were carried out by injecting dye into the hot water. A Canon video camera and stop watch were used to record the flow. The results showed that, the thermosiphon heat exchanger performed according to the theoretical concept. For hot water temperatures below 70%, the system could extract approximately 2 kW of heat at any instant with appropriate cold water mass flow rates. The results have shown that a thermosiphon heat exchanger could be installed in a working solar pond to extract heat from the NCZ or the LCZ. This could minimise the application of pumps and reduce the operating cost significantly.

7.2 Recommendations for future works

The implementation of heat extraction from the NCZ using an external heat exchanger has shown positive outcomes in enhancing the overall efficiency of a solar pond. The performance of the thermosiphon heat exchanger prototype has produced promising

results in demonstrating a heat extraction system with minimum pump usage. Future studies in this area have been identified and are listed below:

i. Fluid dynamics study on optimisation of the diffuser design to minimise disturbance to the salinity gradient.

ii. Optimisation of a thermosiphon heat exchanger for heat extraction from solar pond.

iii. Experimental study of heat extraction from a salinity gradient solar pond using a thermosiphon heat exchanger.

References

Akabarzadeh, A., J. Andrews and P. Golding (2005). Integration of solar ponds in salinity mitigation schemes to produce low grade heat for industrial process heating, desalination and power. Solar World Congress Bringing Water to the World, Orlando, Florida.

Akbarzadeh, A. and G. Ahmadi (1979). "Computer simulation of the performance of a solar pond in the southern part of Iran." Solar Energy 24: 143-151.

Akbarzadeh, A., J. Andrews and P. Golding (2005). Solar Pond Technologies: A Review and Future Directions. Advance in Solar Energy. 16: 233-294.

Akbarzadeh, A., J. Andrews and P. Golding (2005). Solar Pond Technologies: A review and Future Directions. Advances in Solar Energy, . London, UK, Earthscan. 16: 233–294.

Akbarzadeh, A., P. Johnson and R. Singh (2009). "Examining potential benefits of combining a chimney with a salinity gradient solar pond for production of power in salt affected areas." Solar Energy 83(8): 1345-1359.

Akbarzadeh, A. and P. Manins (1988). "Convective layers generated by dide walls in solar ponds." Solar Energy 41(6): 521-529.

Alagao, F. B., A. Akbarzadeh and P. W. Johnson (1994). "The design, construction, and initial operation of a closed-cycle, salt-gradient solar pond." Solar Energy 53(4): 343-351.

Almanza, R. and R. Castaneda (1993). How to test a liner clay for solar ponds. Proceedings of 3rd International Conference on Progress in Solar Ponds, El Paso Texas, USA.

Almanza, R. and R. Castenada (1993). How to test a liner clay for solar ponds. 3rd International Conference on Progress in Solar POnds, El Paso, Texas, USA.

Anati, D. A. (1987). "Salinity profiles in steady-state solar ponds." Solar Energy 38(3): 159-163.

Anderson, G. C. (1958). "Seasonal Characteristics of Two Saline Lakes in Washington." Limnology and Oceanagraphy 3: 51-68.

Andrews, J. and A. Akbarzadeh (2005). "Enhancing the thermal efficiency of solar ponds by extracting heat from the gradient layer." Solar Energy 78(6): 704-716.

Asif, M. and T. Muneer (2007). "Energy supply, its demand and security issues for developed and emerging economies." Renewable and Sustainable Energy Reviews 11(7): 1388-1413.

Atkinson, J. F., M. Priven and H. Rubin (1993). Examination of flow patterns in the advanced solar pond. 3rd International Conference Progress in Solar Ponds, El Paso, Texas.

Barg, H. P. (1987). Solar Ponds. Advances in Solar Energy Technology. Dordrecht, Holland, D.Reidel Publishing Company. 1: 259-359.

Bemporad, G. A. and H. Rubin (1991). "Internal waves and Kî—¸H instability in thermal layers of the Advanced Solar Pond (ASP)." Solar Energy 46(1): 21-28.

Bemporad, G. A. and H. Rubin (1992). "The onset of thermohaline convection in the advanced solar pond (ASP)." Solar Energy 49(4): 245-255.

Bemporad, G. A. and H. Rubin (1994). "Analysis of the instabilities related to the multiselective injection and withdrawal procedures of the advanced solar pond." Solar Energy 52(6): 533-539.

Bolon, P. (1981). Power from the Dead Sea via solar ponds. Popular Science. New York, Time Mirror Magazine. 218: 84-86.

Bryant, H. C. and I. Colbeck (1977). "A solar pond for London?" Solar Energy 19: 321-322.

Bryant, R. S., R. P. Bowser and L. J. Wittenberg (1979). Construction and initial operation of the Miamisburg salt-gradient solar pond. International Solar Energy Society, Atlanta, Georgia, Pergamon Press Inc.

Chyng, J. P., C. P. Lee and B. J. Huang (2003). "Performance analysis of a solar-assisted heat pump water heater." Solar Energy 74(1): 33-44.

Cohen, Y., W. E. Krumbein, M. Goldberg and M. Shilo (1977). "Solar Lake (Sinai). 1. Physical and chemilcal limnology." Limnology and Oceanography 22(4).

Collins, R. and D. Frederiksen (1989). Alice Spring Solar Pond Project. Alice Spring, Australia, Department of Primary Industries and Energy, Australia.

Date, A. (2012). Solar thermal ebergy collection technology and applications. Solar pond and solar desalination, RMIT University.

Davey, R. R. A. (1968). The Aspendale Solar Pond. Melbourne, Commonwealth Scientific and Industrial Research Organisation, Australia. 15.

Dincer, F. (2011). "The analysis on photovoltaic electricity generation status, potential and policies of

the leading countries in solar energy." Renewable and Sustainable Energy Reviews 15: 713-720.

Drosg, M. (2007). Dealing with Uncertainties : A Guide to Error Analysis. Berlin, Heidelberg, Springer-Verlag Berlin Heidelberg.

Dube, V., A. Akbarzadeh and J. Andrews (2004). "The effects of non-condensable gases on the performance of loop thermosyphon heat exchangers." Applied Thermal Engineering 24: 2439-2451.

Folchitto, S. (1997). Experience with a solar pond at Margherita Di Savoia. International Conference on Solar Energy. New York, USA, ASME: 223-228.

Fynn, R. P. and T. H. Short (1983). Salt Gradient Solar Ponds: Research Progress in Ohio and Future Prospects. 6th International Symposium on Salt. Toronto, The Salt Institute. 2: 431-438.

Fynn, R. P. and T. H. Short (1983). The salt stabilized solar pond for space heating - a practical manual Wooster, Ohio Agricultural Research and Development Center The Ohio State University.

Gasulla, N., Y. Yaakob, J. Leblanc, A. Akbarzadeh and J. L. Cortina (2011). "Brine clarity maintenance in salinity-gradient solar ponds." Solar Energy 85(11): 2894-2902.

Gasulla, N., Y. Yaakob, J. Leblanc, A. Akbarzadeh and J. L. Cortine (2011). "Brine clarity maintainance in salinity gradient solar ponds." Solar Energy 85(11): 2894-2902.

Ghorbani, N., H. Taherian, M. Gorji and H. Mirgolbabaei (2010). "An experimental study of thermal performance of shell and coil heat exchanger." International Communications in Heat and Mass Transfer 37: 775-781.

Golding, P. (1985). Feasibility study on the use of solar ponds for the production process heat. Canberra, Department of Resources and Energy, Australia.

Goode, P. R., J. Qiu, V. Yurchyyshyn, J. Hickey, M. C. Chu, E. Kolbe, C. T. Brwon and S. E. Koonin (2001). "Earthshine observations of the earth's reflectance." Geophysical Research Letters 28(9): 1671-1674.

Goswami, D. Y. and F. Kreith, Eds. (2008). Energy Conversion. Boca Raton, Florida, CRC Press Taylor & Francis Group.

Green, A. A., A. L. M. Joyce and M. Collares-Pereira (1987). The measurement of Radiation Transmission in a Salt-Gradient Solar Pond. 10th Beinnial Congress of International Solar Energy Society. Hamburg, Germany: 13-18.

Harding, G. L. and Y. Zhiqiang (1985). "Thermosiphon circulation in solar water heaters incorporating evacuated tubular collectors and a novel water-in-glass manifold." Solar Energy 34(1): 13-18.

Hawlader, M. N. A. and B. J. Brinkworth (1981). "An analysis of the non-convecting solar pond." Solar Energy 27(3): 195-204.

Hull, J. R. (1979). Physics of the solar pond. PhD, Iowa State University.

Hull, J. R. (1989). Maintainance of brine tranparency in salinity gradient solar ponds. 11th Annual Solar Energy Conference. San Diego, CA, ASME Solar Energy Division.

Hull, J. R. and C. E. Nielsen (1989). "Steady -State Analysis of the rising pond." Solar Energy 42(5): 365-377.

Hull, J. R., C. E. Nielsen and P. Golding (1989). Salinity Gradient Solar Ponds. Boca Raton, Florida, CRC Press, Inc.

Hull, J. R., Nielsen, Carl E., Golding, Peter (1989). Salinity-gradient solar ponds. Boca Raton, Fl, USA, CRC Press.

IEA (2010). 2010 Key World Energy Statistics. Paris, International Energy Agency.

Jaefarzadeh, M. R. (2006). "Heat extraction from a salinity-gradient solar pond using in pond heat exchanger." Applied Thermal Engineering 26(16): 1858-1865.

Kalecsinsky, A. V. (1902). "Ueber die ungarischen warmen und heissen Kochsalzseen als naturerlich Waermeaccumulatoren." Annalen der Physik IV(7): 408-416.

Keren, Y., G. A. Bemporad and H. Rubin (1991). "Basic feasibility experiments related to the advance solar pond (ASP)." ASME Journal of Fluids Engineering 113: 116-123.

Keren, Y., H. Rubin, J. Atkinson, M. Priven and G. A. Bemporad (1993). "Theoretical and experimental comparison of conventional and advanced solar pond performance." Solar Energy 51(4): 255-270.

Kho, T. H., M. N. A. Hawlader, J. C. Ho and N. E. Wijeysundera (1991). "Design and Performance Evaluation of a Solar Pond for Industrial Process Heating." Int. J. Sustainable Energy 10: 83-101.

Koffi, P. M. E., H. Y. Andoh, P. Ghaba, S. Toure and G. Ado (2008). "Theoretical and experimental study of solar water heater with internal exchanger using thermosiphon system." Energy Conversion and Management 49: 2279-2290.

Kooi, C. F. (1979). "The steady state salt gradient solar pond." Solar Energy 23: 37-45.

Kopp, G. and J. L. Lean (2011). A new, lower value of total solar irradiance: Evidence and climate significance. Geophysical Research Letters. 38.

Kumar, A. and V. V. N. Kishore (1999). "Construction and Operational Experience of A 6000 m^2 Solar Pond at Kutch, India." Solar Energy 65(4): 237-249.

Leblanc, J., A. Akbarzadeh, J. Andrews, H. Lu and P. Golding (2011). "Heat extraction methods from salinity-gradient solar ponds and introduction of a novel system of heat extraction for improved efficiency." Solar Energy 85(12): 3103-3142.

Leblanc, J., J. Andrews and A. Akbarzadeh (2010). "Low temperature solar thermal multi effect evaporation desalination systems." Int. J. Energy Res. 34: 393-403.

Lee, Y. and U. Mital (1971). "A Two Phase Closed Thermosyphon." International of Heat and Mass Transfer 15: 1695-1707.

Lesino, G. and L. Saravia (1991). "Solar ponds in hydrometallurgy and salt production." Solar Energy 46(6): 377-382.

Lesino, G., L. Saravia and D. Galli (1990). "Industrial production of sodium sulfate using solar ponds." Solar Energy 45(4): 215-219.

Liao, Y., A. H. P. Swift and R. L. Reid (1988). Determination of critical Froude number for gradient establishment ia a solar pond. Solar Engineering. L. M. Murphy and T. R. Mancini. Denver, CO, Eds: 101-105.

Lim, T. T. (2000). Dye and Smoke Visualisation. Flow Visualisation, Technique and Examples. A. J. Smith and T. T. Lim. Singapore, Imperial College Press: 43-72.

Lu, H. (1994). Monitoring and data Analysis for solar pond operation. Master Thesis, The University of Texas.

Lu, H., J. C. Walton and A. H.P. Swift (2001). "Desalination coupled with salinity-gradient solar ponds." Desalination 136(1-3): 13-23.

Lu, H., A. H. P. Swift, H. D. H. Jr. and J. C. Walton (2004). "Advancements in salinity gradient solar pond technology based on sixteen years of operational experience." ASME Journal of Solar Energy Engineering 126(2): 759 - 767.

Malik, N., A. Date, J. Leblanc, A. Akbarzadeh and B. Meehan (2011). "Monitoring and maintaining the water clarity of salinity gradient solar ponds." Solar Energy 85(11): 2987-2996.

Manins, P. C. (1976). "INTRUSION INTO A STRATIFIED FLUID." Journal of Fluid Mechanics 74(pt 3): 547-560.

Manins, P. C. (1976). "Mixed-region collapse in a stratified fluid." Journal of Fluid Mechanics 77: 177-183.

McVeigh, J. C. (1977). Sun Power An Introduction to the Applications of Solar Energy. Oxford, UK, Robert Maxwell, M.C.

Mehta, A. S., N. Pathak, B. M. Shah and S. D. Gomkale (1988). "Performance analysis of a bittern-based solar pond." Solar Energy 40(5): 469-475.

Mekhilef, S., R. Saidur and A. Safari (2011). "A review on solar energy use in industries." Renewable and Sustainable Energy Reviews 15(4): 1777-1790.

Melack, J. M. and P. Kilham (1972). "Lake Mahega: a mesotropic sulfatochloride lake in western Uganda." African Journal of Tropical Hydrobology and Fisheries 2: 141-150.

Morton, O. (2006). "Solar energy: A new day dawnig?" Nature International weekly journal of science 443: 19-22.

Mulaweh, H. I. A. (2006). "Design and Performance of a Thermosiphon Heat Recovery System." Applied Thermal Energy 26: 471-477.

Myre, E. and R. Shaw (2006). The turbidity tube: Simple and accurate measurement of turbidity in the field, Michigan Technological University: 1-17.

Newell, T. A., R. G. Cowie, J. M. Upper, M. K. Smith and G. L. Cler (1990). "Construction and operation activities at the University of Illinois salt gradient solar pond." Solar Energy 45(4): 231-239.

Nie, Z., L. Bu, M. Zheng and W. Huang (2011). "Experimental study of natural brine solar ponds in Tibet." Solar Energy 85: 1537-1542.

Nielsen, C. E. (1975). "Salt gradient for solar ponds for energy utilization." Environment Conservation 2: 289-292.

Nielsen, C. E. (1980). Design and initial operation of a 400 m^2 solar pond. ISES American Section Annual Meeting Phoenix, Arizona, International Solar Energy Society/AS.

Osdor, A. (1984). Method of trapping and utilizing solar heat. U. S. Patent. U.S.A. 4,462,389: 1-34.

Ould Dah, M. M., M. Ouni, A. Guizani and A. Belghith (2010). "The influence of the heat extraction mode on the performance and stability of a mini solar pond." Applied Energy 87(10): 3005-3010.

Patel, S. M. and C. L. Gupta (1981). Experimental solar pond in a hot humid climate. SunWorld. 5.

Prabhanjan, D. G., T. J. Rennie and G. S. Vijaya Raghavan (2004). "Natural convection heat transfer from helical coiled tubes." International Journal of Thermal Sciences 43(4): 359-365.

Rabl, A. and C. E. Nielsen (1975). "Solar ponds for space heating." Solar Energy 17(1): 1-12.

Reid, R. L., T. J. McLean and C. H. Lai (1985). Feasibility study of a solar pond/IPH/Electrical supply for a food canning plant. 7th ASME-ASES Solar Energy Conference, Knoxville, Tennesse, American Society of Mechanical Engineers.

Rogers, G. F. C. and Y. R. Mayhew (1964). "Heat transfer and pressure loss in helically coiled tubes with turbulent flow." International Journal of Heat and Mass Transfer 7(11): 1207-1216.

Rubin, H. and G. A. Bemporad (1989). "The advanced solar pond (ASP): Basic theoretical aspects." Solar Energy 43(1): 35-44.

Rubin, H. and G. A. Bemporad (1989). "Analysis of turbulent flow in thermal layers of the advanced solar pond (ASP)." Solar Energy 43(1): 25-33.

Schladow, S. G. (1984). "The upper mixed zone of a salt gradient solar pond: Its dynamics, prediction and control." Solar Energy 33(5): 417-426.

Seyboth, K., P. Matschoss, S. Kadner, T. Zwickel, P. Eickemeier, G. Hansen, S. Schlömer and C. v. Stechow (2012). Renewable Energy Sources and Climate Change Mitigation. Special Report of the Intergovernmental Panel on Climate Change. O. Edenhofer, R. P. Madruga and Y. Sokona. New York, Potsdam Institute for Climate Impact Research.

Shah, S. A., T. H. Short and R. P. Fynn (1981). "Modeling and testing a salt gradient solar pond in northeast Ohio." Solar Energy 27(5): 393-401.

Shah, S. A., T. H. Short and R. Peter Fynn (1981). "A solar pond-assisted heat pump for greenhouses." Solar Energy 26(6): 491-496.

Sherman, B. S. and J. Imberger (1991). "Control of a solar pond." Solar Energy 46(2): 71-81.

Shirtcliffe, T. G. L. and R. F. Benseman (1964). "A sun-heated antarctic lake." JOURNAL OF GEOPHYSICAL RESEARCH 69(16).

Silvi, C. (2001). Survey of energy resources 2001-solar energy. London, World Energy Council.

Silvi, C. (2008). "History and future of renewable solar energy." Society for International Development 51: 409-414.

Singh, R., S. Tundee and A. Akbarzadeh (2011). "Electric power generation from solar ponds using combined thermosyphon and thermoelectric modules." Solar Energy 85: 371-378.

Smil, V. (2006). Energy: A Beginner's Guide. Oxford, England, Oneworld Publication.

Solangi, K. H., M. R. Islam, R. Saidur, N. A. Rahim and H. Fayaz (2011). "A review on global solar energy policy." Renewable and Sustainable Energy Reviews 15(4): 2149-2163.

Srinivasan, J. (1990). "Performance of a small solar pond in the tropics." Solar Energy 45(4): 221-230.

Srinivasan, J. (1993). "Solar pond technology." Sadhana 18(1): 39-55.

Srinivasan, P. S., S. S. Nandapukar and F. A. Holland (1970). "Friction factors for coils." Institution of Chemical Engineering Transaction 48: 156-161.

Swift, A. H. and H. Lu (1996). "Applications of salinity gradient solar technologies in the southwest – an overview." Solar Engineering: 237-240.

Swift, A. H. P., R. L. Reid and K. D. McGraw (1988). Operational Strategy and Results for 90 ^{o}C operation of a solar pond for electric power and desalination. 10th Annual ASME Solar Energy Conference, Denver, Colorado, ASME.

Swift, A. H. P., R. L. Reid, M. P. Sewell and W. J. Boegli (1987). Operational Result for 3355 m^2 Solar Pond in El Paso, Texas. Solar Engineering, American Society of Mechanical Engineers. 1: 287-293.

Tabor, H. (1963). "Large area solar collector for power production." Solar Energy 7(4): 189-194.

Tabor, H. (1980). Using solar ponds to store power from the sun. Impact of science on society. 30: 319-328.

Tabor, H. (1981). "Solar Ponds." Solar Energy 27(3): 181-194.

Tabor, H. and R. Matz (1965). A status report on solar pond project. Solar Energy Society Conference. Phoenix, Arizona, USA, Solar Energy Society. 9: 177-182.

Tabor, H. and Z. Weinberger (1981). Non Convecting Solar Ponds. Solar Energy Handbook. J. F. Kreider and F. Kreith. New York, McGraw Hill.

Tabor, H. Z. and B. Doron (1986). Solar Ponds – Lessons Learned from the 150 KW (e) Power Plant at Ein Boqek. ASME solar Energy Div, Anaheim, California.

Tabor, H. Z. and B. Doron (1990). "The Beith Ha'arava 5MW(e) Solar Pond Power Plant (SPPP) - Progress Report." Solar Energy 45(4): 247-253.

Tago, N., K. Morita and M. Sugawara (2006). "Heat extraction characteristics of a single U-tube downhole heat exchanger with square cross section." Heat Mass Transfer 42: 608-616.

Tundee, S., P. Terdtoon, P. Sakulchangsatjatai, R. Singh and A. Akbarzadeh (2010). "Heat extraction from salinity-gradient solar ponds using heat pipe heat exchangers." Solar Energy 84: 1706-1716.

Turner, J. S. (1979). Buoyancy Effects in Fluids. London, Cambridge University Press.

Wang, J. and J. Seyed-Yagoobi (1995). "Effect of water turbidity on thermal performance of a salt-gradient solar pond." Solar Energy 54(5): 301-308.

Wang, Y. F. and A. Akbarzadeh (1983). "A parametric study on solar ponds." Solar Energy 30(6): 555-562.

Wang, Y. F. and Yagoobi (1995). "Effect of water turbidity on thermal performance of salt gradient solar pond." Solar Energy 54(5): 301-308.

Weinberger, H. (1964). "The physics of solar pond." Solar Energy 8(2): 45-56.

Wilson, A. T. and H. W. Wellman (1962). "An Antarctic Lake. A solar Energy Trap." Nature 196(1171).

www.bom.gov.au (2013). Bureau of Meteorology, Australia.

Xu, H. (1990). Laboratory Studies on Dynamical Processes in Salinity Gradient Solar Pond. PhD Thesis, The Ohio State University.

Xu, H., P. Golding and C. E. Nielsen (1987). Prediction of internal stability in a Salt Gradient Solar Pond. International Progress in Solar Ponds, Cuernavaca, Mexico.

Xu, H., P. Golding and A. Swift (1991). Method for monitoring stability within a Salinity Gradient Solar Pond. Solar Engineering 1991. Reno, NV, USA, ASME, Solar Energy Div; Japan Solar Energy Soc; JSME: 75-82.

Xu, H., J. Sandoval, H. Lu, A. Ybarra, P. Golding and A. Swift (1993). "Operating Experience with the El Paso Solar Pond." Proceeding of the3rd International Conference on Progress in Solar Ponds.

Xu, H., A. H. P. Swift and P. Golding (1992). Two Gradient Failure and Repair Events as Experienced at The El Paso Solar Pond. International Solar Energy Conference, Maui, Hawaii, ASME.

Yaakob, Y., A. Date and A. Akbarzadeh (2011). Heat extraction from gradient layer using external heat exchangers to enhance the overall efficiency of solar ponds. IEEE First Conference on Clean Energy and Technology (CET)

Zangrando, F. (1979). Observation and Analysis of a Full Scale Experimental Salt Gradient Solar Pond. PhD, New Mexico.

Zangrando, F. (1980). "A simple method to establish salt gradient solar ponds." Solar Energy 25: 467-470.

Zangrando, F. (1991). "On The Hydrodynamics of Salt Gradient Solar Ponds." Solar Energy 46(6): 323-341.

Zhang, Z. M. and Y. F. Wang (1990). "A study on the thermal storage of the ground beneath solar ponds by computer simulation." Solar Energy 44(5): 243-248.

Appendix A: Calibration of PV pyranometer

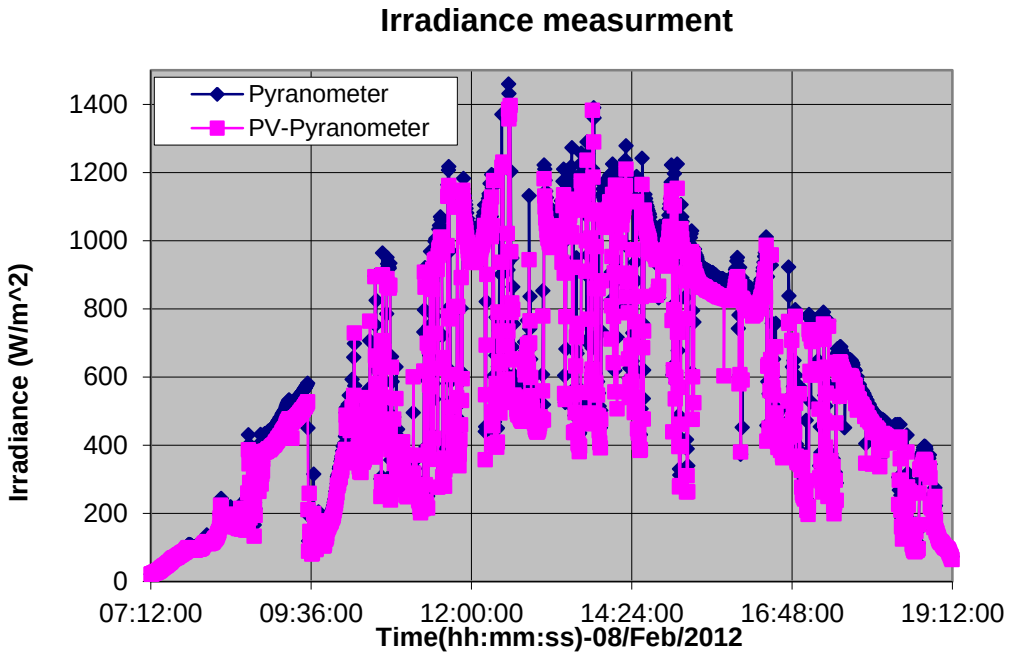

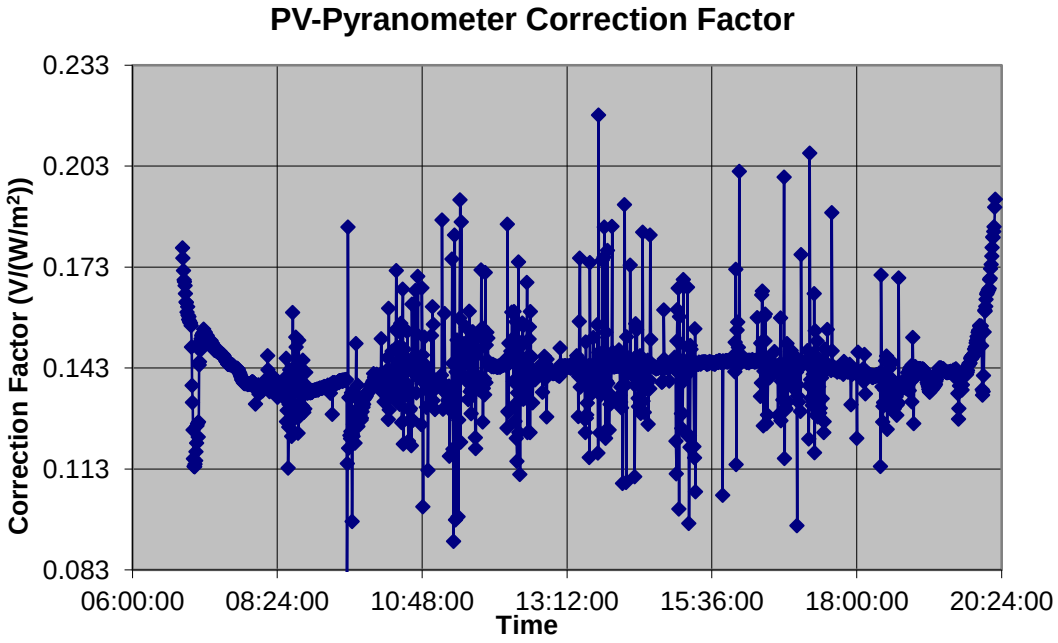

Appendix B: Pump Details

i. Pump Specification

SPECIFICATION

Model	Voltage(V)	Current(mA)	Head(m)	Flow(L/H)	PS
DC40-1225	12	450	2.5	350	flow at zero head

Note: 1. power cord: 0.5m, the positive power line is red, black is negative.

2. long term running is not allowed when blocked;

3. supplying voltage less than 12V.

4. working temperature no more than 60°C, Prior notice required if more than 60°C.

dimension drawing

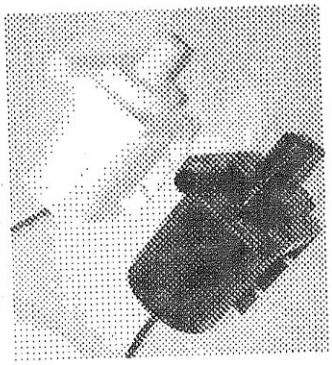

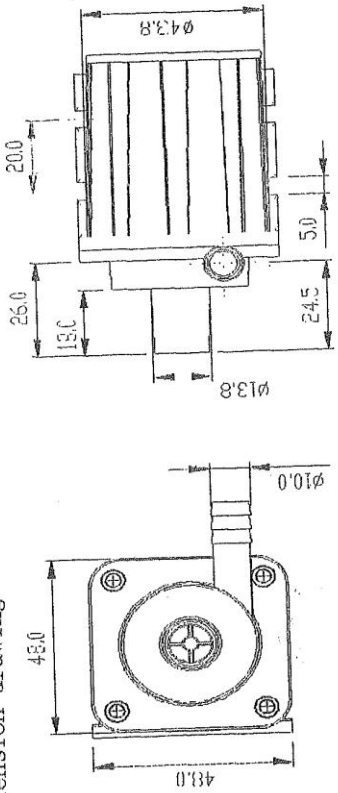

DC40series

ii. Pump performance testing

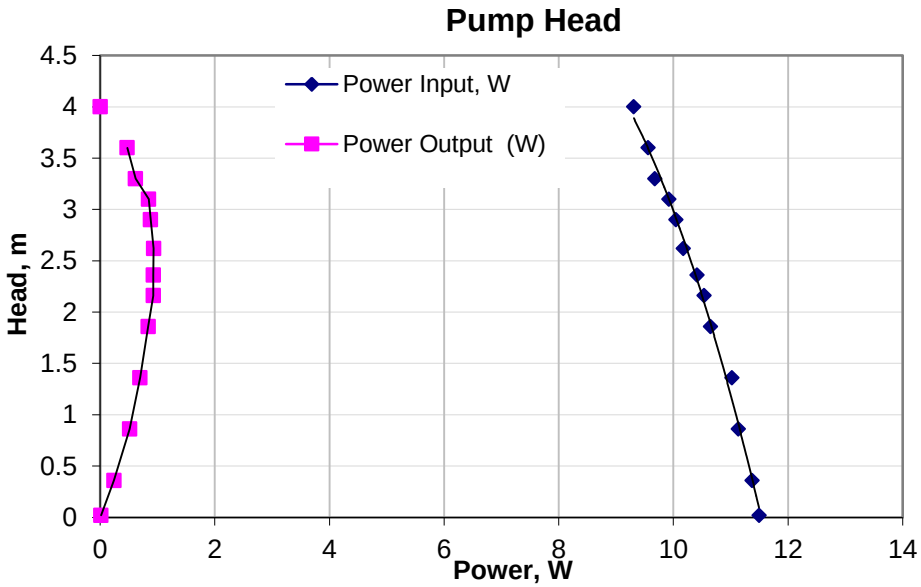

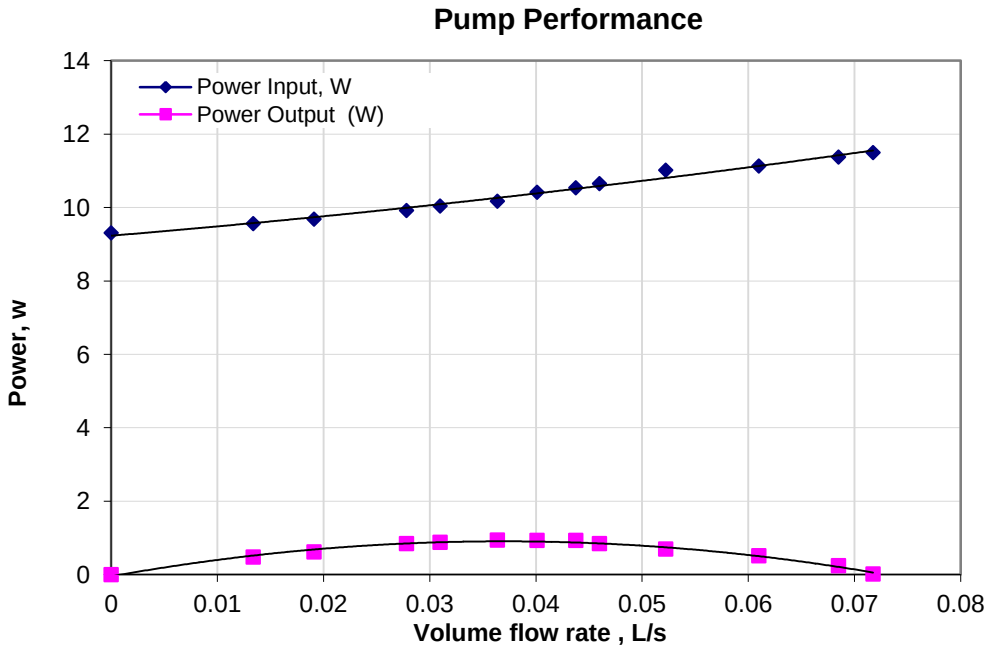

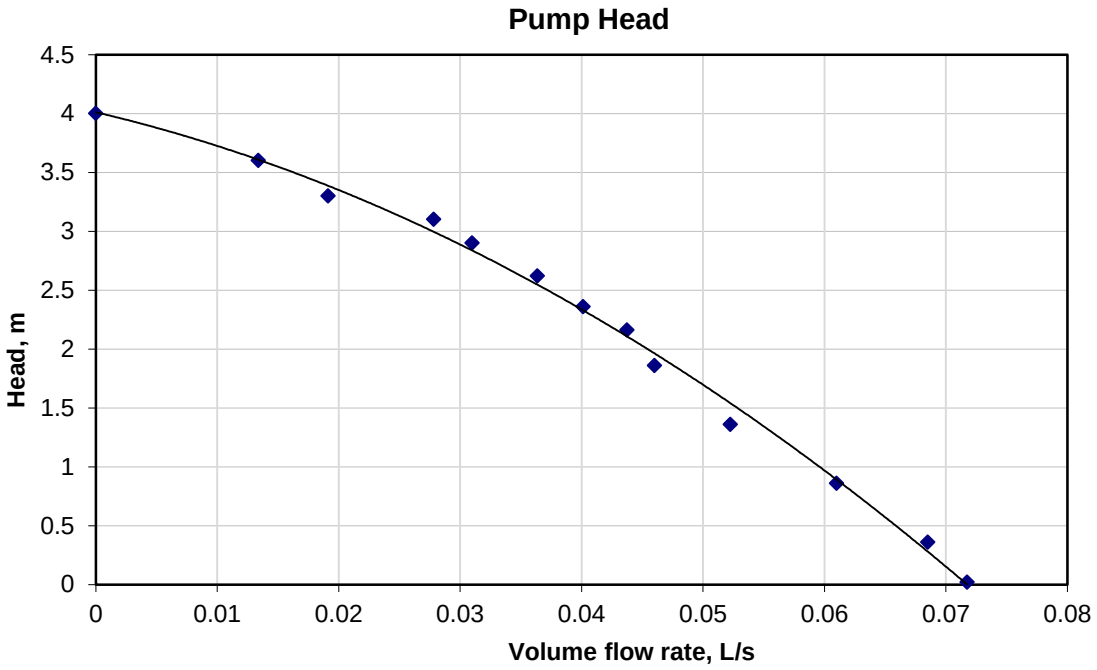
Pump Head
Head, m
4.5
4
3.5
3
2.5
2
1.5
1
0.5
0
0
0.01
0.02
0.03
0.04
0.05
0.06
0.07
0.08
Volume flow rate, L/s

Appendix C: Validation of thermocouples

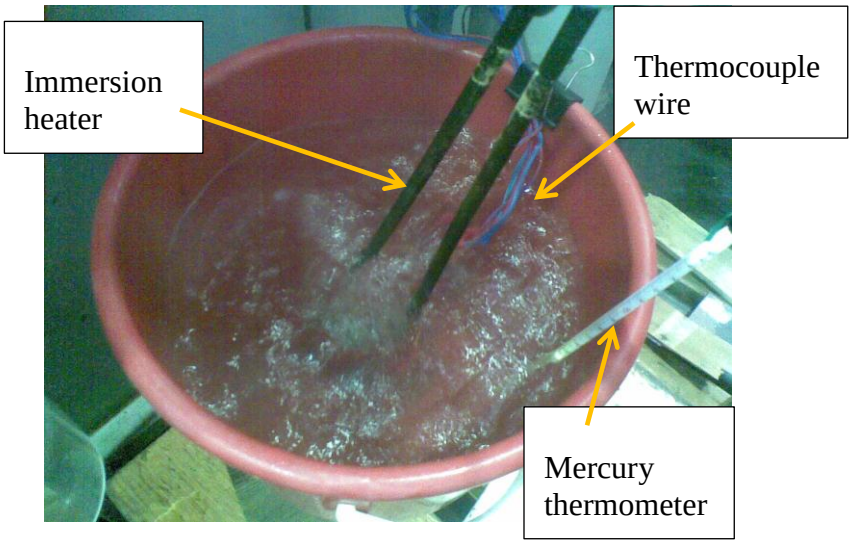

Description: Validation at boiling point using 3kW immersion heater (upper) and temperature reader (lower)

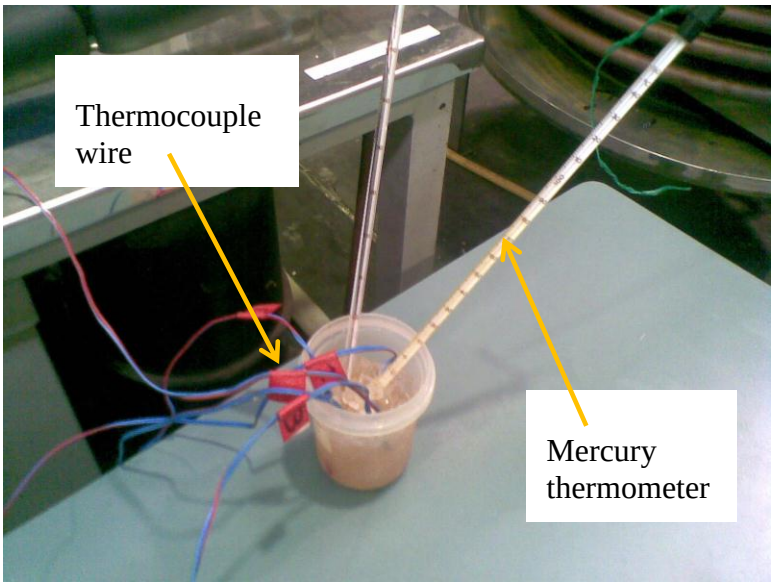

Description: Validation at freezing point using ice cube with manual thermometer (upper) and temperature reader (lower)

Appendix D: Diffuser details

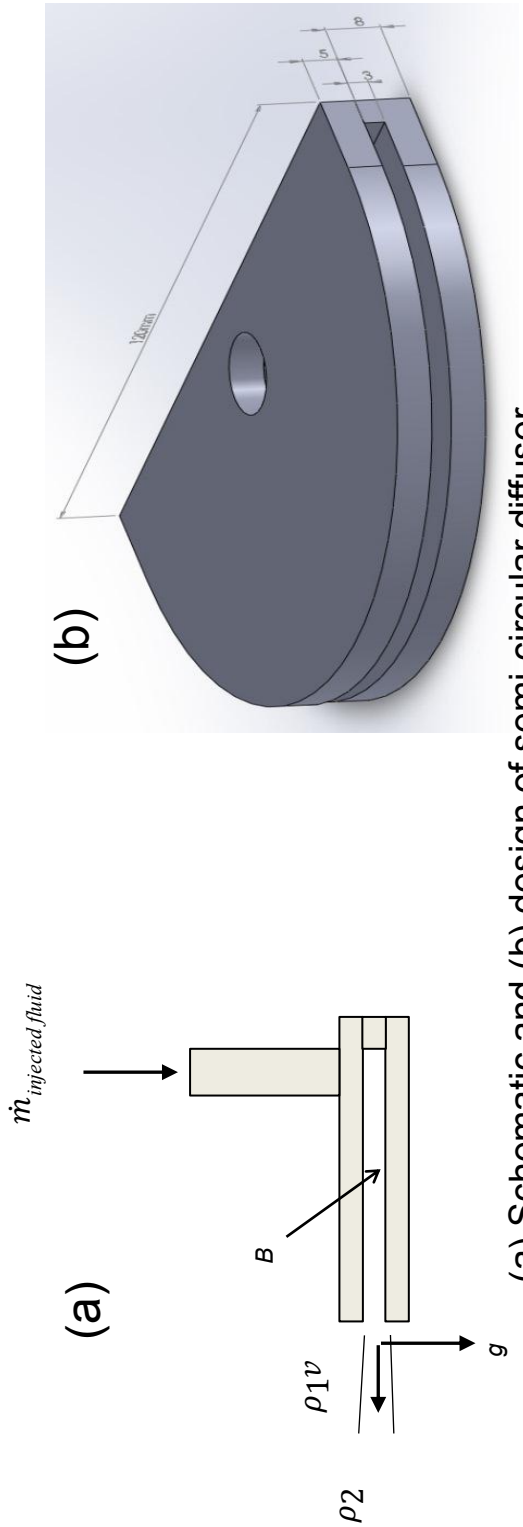

(a) Schematic and (b) design of semi-circular diffuser

Appendix E: Meteorology Data

Daily Global Solar Exposure (MJ/m²)

BUNDOORA (LATROBE UNIVERSITY)

Station Number: 086351 · State: VIC · Opened: 1979 · Status: Open · Latitude: 37.72°S · Longitude: 145.05°E · Elevation: 83 m

2012	Jan	Feb	Mar	Apr	May	Jun	Jul	Aug	Sep	Oct	Nov	Dec
1st	31.6	29.5	6.5	12.8	7.8	7.9	3.4	9.4	13.3	15.6	20.9	25.6
2nd	30.6	27.6	20.3	17.0	5.2	7.2	3.6	8.8	16.0	21.4	20.2	25.7
3rd	22.4	27.4	3.2	15.9	3.9	4.6	6.0	10.1	15.4	22.4	27.4	28.5
4th	27.8	22.8	13.0	17.0	7.0	2.6	6.2	10.3	16.3	22.1	29.3	25.4
5th	31.6	8.4	15.4	16.7	5.4	4.7	6.6	7.7	10.7	21.0	16.0	21.3
6th	31.5	25.5	14.5	13.2	6.4	4.8	4.9	9.0	14.6	7.3	16.5	24.3
7th	13.1	18.1	17.9	13.0	6.0	3.1	8.2	11.1	10.8	16.0	18.4	28.5
8th	15.3	21.5	13.9	9.9	10.6	3.6	7.3	3.0	11.8	15.1	28.7	29.0
9th	18.5	26.8	16.5	8.8	7.4	3.4	6.2	8.1	14.7	20.7	26.2	31.6
10th	15.5	14.5	17.6	10.0	10.3	3.3	2.6	8.3	17.1	15.7	26.1	33.8
11th	23.7	19.6	21.6	13.3	9.1	6.0	6.6	7.4	18.1	8.0	31.0	33.8
12th	19.7	17.6	22.0	15.3	8.2	7.5	2.7	7.2	13.0	12.2	25.6	33.5
13th	20.3	21.5	21.3	15.7	6.0	5.5	5.7	11.9	12.6	13.2	30.5	27.8
14th	15.7	26.5	17.4	13.9	6.0	2.4	5.3	4.3	10.2	24.8	29.8	16.2
15th	31.0	24.1	7.3	15.0	7.1	6.4	6.7	10.3	11.8	12.4	22.8	26.9
16th	31.0	15.5	6.2	7.6	6.3	6.3	6.6	11.9	11.1	10.8	27.1	24.7
17th	28.9	8.1	19.6	13.4	9.4	4.7	8.6	7.2	12.6	17.0	23.8	33.4
18th	24.9	23.9	17.6	13.7	4.9	4.1	7.5	7.5	9.8	20.0	30.0	34.0
19th	31.0	15.3	20.6	7.7	3.4	7.2	7.4	7.0	11.3	23.2	32.0	16.7
20th	9.4	7.0	20.2	9.0	7.3	4.4	4.1	11.9	12.2	25.0	28.8	30.0
21st	17.5	17.9	8.5	11.2	8.7	2.4	8.3	12.1	9.3	21.8	27.5	33.7
22nd	30.4	25.7	19.3	9.5	4.4	4.0	7.0	8.6	19.2	26.1	31.7	33.5
23rd	30.7	25.5	13.0	6.1	8.2	4.5	8.3	10.3	15.7	26.2	30.6	31.3
24th	30.8	25.9	8.3	5.1	4.8	6.2	7.3	9.9	15.4	23.0	29.0	21.1
25th	22.1	25.2	8.2	5.1	2.1	5.1	5.5	11.2	19.8	18.4	28.7	31.3
26th	28.5	22.7	13.1	6.3	5.3	7.6	8.6	11.1	18.7	19.5	26.8	33.8
27th	29.3	3.1	11.6	10.0	4.6	7.2	4.6	14.7	17.9	20.6	24.7	31.5
28th	28.0	4.6	15.5	9.8	4.3	6.8	6.6	14.2	5.1	27.8	31.5	30.3
29th	22.1	9.3	13.4	8.6	4.2	3.4	7.3	14.2	15.6	28.4	32.6	31.5
30th	17.5		17.3	10.8	3.6	6.8	7.6	9.0	16.4	29.1	22.3	34.0
31st	15.4		12.9		8.2		9.3	13.6		20.4		34.0
Highest daily	31.6	29.5	22.0	17.0	10.6	7.9	9.3	14.7	19.8	29.1	32.6	34.0
Lowest daily	9.4	3.1	3.2	5.1	2.1	2.4	2.6	3.0	5.1	7.3	16.0	16.2
Monthly mean	24.1	19.3	14.6	11.4	6.3	5.1	6.3	9.7	13.9	19.5	26.5	28.9

Conversion MJ/m^2 to W/m^2 = $\frac{1x10^6 J}{(24hrs)x(60min)x(60s)}$

Further information

http://www.bom.gov.au/climate/cdo/about/austmaps/solar-radiation-glossary.shtml.

Product code: IDCJAC0016 reference: 14396547 Created on Tue 14 Jan 2014 11:24:53 AM EST

Australian Government
Bureau of Meteorology

Daily Maximum Temperature (degrees Celsius)

BUNDOORA (LATROBE UNIVERSITY)

Station Number: 086351 · State: VIC · Opened: 1979 · Status: Open · Latitude: 37.72°S · Longitude: 145.05°E · Elevation: 83 m

2012	Jan	Feb	Mar	Apr	May	Jun	Jul	Aug	Sep	Oct	Nov	Dec
1st	36.2	23.1	20.5	20.5	21.8	15.6	9.5		14.7	17.2	*15.5*	*28.4*
2nd	38.9	26.7	23.5	24.6	13.2	14.1	11.5	11.8	18.0	23.0	*15.9*	*20.7*
3rd	31.0	27.8		26.0	14.0	12.8	12.6		20.2	26.0	*25.1*	*21.8*
4th	20.9	33.3	26.3	26.6	15.5	13.7	12.3		21.9	30.5	*29.1*	*17.0*
5th	20.2	32.3	21.0	27.1	13.8	11.5	12.1	16.9	20.5	17.2	*26.9*	*16.9*
6th	25.4	23.3		27.5	14.9	13.0	11.3	12.5	18.4	13.0	*21.7*	*20.1*
7th	29.5	20.1	*21.0*	18.5	15.8	12.9	12.8	15.0	14.2	14.5	*19.1*	*31.5*
8th	29.5	21.0	21.0	19.9	20.8	12.5	14.2	11.0	15.5	14.9	*22.6*	*36.9*
9th	24.0	26.2	24.2	14.7	21.0	12.1	15.9	10.6	18.2	17.6	*17.5*	*19.4*
10th	20.0	26.3	20.1	15.5	19.4	11.5	13.5	13.1	19.0	15.4	*19.6*	
11th	17.2	21.6	20.2	18.0	17.1	10.5	15.2	14.1	20.5	12.3	*26.8*	*28.4*
12th	20.2	23.1	24.2	23.0	15.8	15.5	13.2	12.9	20.4	13.5	*26.5*	*34.0*
13th	20.1	24.1	28.8	23.5	12.9	16.2	13.3	15.5	13.4	16.3	*18.7*	*36.1*
14th	19.4	29.4	31.5	24.7	15.8	15.0	14.1	14.7	14.5	23.0	*19.8*	*22.5*
15th	24.8	34.7	28.0	26.5	16.2	15.2	13.6	14.5	15.8	26.0	*18.1*	*24.6*
16th	32.5	33.0	23.2	20.2	15.4	14.5	15.8	14.5	16.1	20.0	*18.5*	*22.2*
17th	33.9	21.5	20.4	24.2	18.0	14.3	15.8	10.5	16.4	16.7	*18.2*	*21.8*
18th	25.0	27.5	21.9	25.4	16.5	15.2	13.4	12.1	16.0	21.5	*18.0*	*28.2*
19th	23.2	30.4	26.8	24.0	13.9	11.9	14.4	12.6	17.4	28.2	*23.6*	*31.8*
20th	20.1	23.0	27.2	22.2	14.5	14.0	14.2	13.4	21.9		*27.8*	*23.2*
21st	27.5	23.7	19.8	23.8	15.2	10.0	15.2	15.8	17.5	18.0	*20.2*	*22.3*
22nd	32.4	26.1	20.0	22.9	16.7	11.2	14.8	21.0	20.3	18.3	*20.6*	*32.0*
23rd	32.1	27.9	17.7	19.3	19.6	13.9	15.4	17.5	19.0	22.5	*24.5*	*38.9*
24th	34.0	36.8	17.5	12.9	14.5	15.2	15.0	12.7	14.4	22.8	*34.4*	*27.5*
25th	25.5		18.0	15.0	14.2	15.0	16.1	12.5	17.8	21.9	*21.8*	*20.7*
26th	23.8	*33.5*	20.0	16.8	15.5	10.8	12.5	14.4	21.5	15.5	*22.0*	*22.9*
27th	30.5		20.1	17.5	14.3	12.7	12.7	14.7	25.3	14.2	*22.4*	*31.2*
28th	33.5	*19.8*	23.2	21.2	13.3	14.5	15.2	17.3	15.5	18.0	*30.7*	*20.8*
29th	35.7	22.0	25.9	15.9	13.4	14.8	11.3	19.3	12.1	28.1	*38.5*	*22.4*
30th	31.6		27.7	18.3	14.2	12.1	12.8	13.3	14.1	31.6	*28.5*	*21.5*
31st	19.0		28.4		16.3		12.8	12.5		28.8		*25.5*
Highest daily	38.9	36.8	31.5	27.5	21.8	16.2	16.1	21.0	25.3	31.6	*38.5*	*38.9*
Lowest daily	17.2	*19.8*	17.5	12.9	12.9	10.0	9.5	10.5	12.1	12.3	*15.5*	*16.9*
Monthly mean	27.0	26.6	23.0	21.2	15.9	13.4	13.6	14.2	17.7	20.2	23.1	25.7

Quality control: 12.3 Done & acceptable, *12.3* Not quality controlled or uncertain, or precise date unknown

Product code: IDCJAC0010 reference: 14396279

Australian Government
Bureau of Meteorology

Appendix F: Uncertainty Analysis

All scientifically relevant quantities must be assigned an uncertainty, as discussed by Manfred Drosg (Drosg 2007). The uncertainty is a statistical measure of data quality. It shows how well the data, i.e., the best estimate, fits the (unknown) true value. However, it does not specify the actual deviation between these two values. No data value is of any use whatsoever in a scientific context without a statement on its uncertainty.

If a data value y has an (absolute) uncertainty Δy, we can get the degree of exactness by dividing Δy by y, thus obtaining a dimensionless quantity, the relative (or fractional or percentage) uncertainty σ_r, (Drosg 2007)

$$\sigma_r = \Delta y / y$$

The absolute uncertainty Δy is not suited for comparisons. In the following example we can see how the absolute uncertainty cannot be used for comparison,

In first case the length of a machine part is measured to be 44.89mm ±0.1mm, and in second case the distance from a point on the earth's surface to a certain point on the moon's surface is known to be 384400 km ±0.001 km; both the absolute uncertainties cannot compared with each other. Thus it is obvious that the quality of a measurement is not necessarily determined by the absolute uncertainties.

The total uncertainty ΔF of a result $F = F(x_1, x_2, x_3, ...)$ is calculated by adding all n individual (independent) uncertainty components ΔF_{xi} in quadrature according to the *law of error propagation*:(Drosg 2007)

$$\Delta F = \sqrt{(\Delta F_{x1})^2 + (\Delta F_{x2})^2 + (\Delta F_{x3})^2 + ...} = \sqrt{\sum_{i=1}^{n} (\partial F / \partial x_i)^2 * (\Delta x_i)^2}$$

The above uncertainty analysis procedure is applied to all the experimental data obtained in this research to estimate the performance and the accompanying uncertainties in the result.

Heat Extraction from NCZ

1. January Experiment

Temperature measurement

Descriptions	Temperature, T, ^{o}C	RTD accuracy	DT500 accuracy	Absolute uncertainty, ΔT	Relative uncertainty, ΔT/T	Remark
		± 0.2 ^{o}C	± 0.1%	±	%	
Tci (HEX 1)	23.7	0.2	0.224	0.300	1.27	Ref 1
Tco (HEX 7)	55	0.2	0.255	0.324	0.59	
T_{LCZ}	60.8	0.3	0.361	0.469	0.77	
Tci (HEX 1)	32.7	0.2	0.233	0.307	0.94	Ref 2
Tco (HEX 7)	56.4	0.2	0.256	0.325	0.58	
T_{LCZ}	61.8	0.2	0.262	0.329	0.53	

Flow rate measurement

Volume, mL	Measuring cylinder accuracy	Time, s	Stop watch accuracy	Absolute uncertainty, Δmdot,mL/s	Ideal mass flow rate, mdot, mL/s	Relative uncertainty Δmdot/mdot
	± 0.02 mL		± 1%	±		± %
265	0.02	13.33	0.1333	0.13	19.9	0.678

HEX temperature difference estimation

Tci	ΔTci	Tco	ΔTco	Absolute uncertainty, ΔDT,Tco-Tci	Ideal DT, (Tco-Tci)	Relative uncertainty, ΔDT/DT
	±		±	±		± %
23.7	0.300	55	0.324	0.44	31.3	1.4
32.7	0.307	56.4	0.325	0.45	23.7	1.9

Solar Pond temperature difference

T_{UCZ}=Tci	ΔT_{UCZ}=Tci	T_{LCZ}	ΔT_{LCZ}	Absolute uncertainty, ΔDT,Tco-Tci	Ideal DT, (Tco-Tci)	Relative uncertainty, ΔDT/DT
	±		±	±		± %
23.7	0.300	60.8	0.469	0.6	37.1	1.5
32.7	0.307	61.8	0.329	0.5	29.1	1.5

Heat Extraction

mdot cold, L/s	Absolute uncertainty, mdot cold	Cp	DT_{HEX}	Absolute uncertainty, DT	Absolute Uncertainty, Qdot cold, ΔW	Ideal value (Qdot=mdot.DT)
	± %			± %	±	
0.0199	0.13	4180	31.3	0.44	0.459	0.6

2. February Experiment

Temperature measurement

Descriptions	Temperature, T, ^{o}C	RTD accuracy	DT500 accuracy	Absolute uncertainty, ΔT	Relative uncertainty, ΔT/T	Remark
		± 0.2 ^{o}C	± 0.1%	±	%	
Tci (HEX 1)	23.27	0.2	0.223	0.300	1.29	Reference 1
Tco (HEX 7)	42.2	0.2	0.242	0.314	0.74	
T_{LCZ}	49.8	0.3	0.350	0.461	0.93	
Tci (HEX 1)	29.4	0.2	0.229	0.304	1.04	Reference 2
Tco (HEX 7)	46.1	0.2	0.246	0.317	0.69	
T_{LCZ}	53	0.2	0.253	0.323	0.61	

Flow rate measurement

Volume, mL	Measuring cylinder accuracy	Time, s	Stop watch accuracy	Absolute uncertainty, Δmdot,mL/s	Ideal mass flow rate, mdot, mL/s	Relative uncertainty, Δmdot/mdot
	± 0.02 mL		± 1%	±		± %
300	0.02	12	0.12	0.12	25.0	0.487

HEX temperature difference estimation

Tci	ΔTci	Tco	ΔTco	Absolute uncertainty, ΔDT,Tco-Tci	Ideal DT, (Tco-Tci)	Relative uncertainty, ΔDT/DT
	±		±	±		± %
23.7	0.300	44	0.314	0.43	20.3	2.1

Solar Pond temperature difference

T_{UCZ}=Tci	ΔT_{UCZ}=Tci	T_{LCZ}	ΔT_{LCZ}	Absolute uncertainty, ΔDT,Tco-Tci	Ideal DT, (Tco-Tci)	Relative uncertainty, ΔDT/DT
	±		±	±		± %
23.7	0.300	49.1	0.461	0.5	25.4	2.2

Heat Extracted

mdot cold, L/s	Absolute uncertainty, mdot cold	Cp	DT_{HEX}	Absolute uncertainty, DT	Absolute Uncertainty, Qdot cold, ΔW	Ideal value (Qdot=mdot.Cp.DT)
	± %			± %	±	
0.0250	0.12	4180	20.3	0.43	0.451	2121.4

3. April Experiment

Temperature measurement

Descriptions	Average Temperature, T, °C	RTD accuracy	DT500 accuracy	Absolute uncertainty, ΔT	Relative uncertainty, ΔT/T
		± 0.2 °C	± 0.1%	±	%
Tci (HEX 1)	15.4	0.2	0.215	0.294	1.91
Tco (HEX 7)	35.1	0.2	0.235	0.309	0.88
T_{LCZ}	40.5	0.3	0.341	0.454	1.12

Flow rate measurement

mdot	Volume, mL	Measuring cylinder accuracy	Time, s	Stop watch accuracy	Absolute uncertainty, Δmdot,mL/s	Ideal mass flow rate, mdot, mL/s
		± 0.02 L		± 1%	±	
HEX_system	394.9	0.02	31.92	0.3192	0.32	12.4
HEX 1	380.2	0.02	12.19	0.1219	0.12	31.2
HEX 2	345.1	0.02	19.53	0.1953	0.20	17.7
HEX 3	362.4	0.02	14.94	0.1494	0.15	24.3
HEX 4	350.2	0.02	11.63	0.1163	0.12	30.1
HEX 5	385.2	0.02	11.3	0.113	0.11	34.1
HEX 6	399.8	0.02	11.11	0.1111	0.11	36.0
HEX 7	505.2	0.02	14.48	0.1448	0.15	34.9

Individual Thi and Tho HEX temperature difference estimation

Descriptions	Thi	RTD accuracy	DT500 accuracy	Absolute uncertainty, ΔT	Relative uncertainty, ΔT/T
		± 0.2 °C	± 0.1%	±	%
HEX 1	23.6	0.2	0.224	0.300	1.271
HEX 2	26.8	0.2	0.227	0.302	1.128
HEX 3	28.2	0.2	0.228	0.303	1.076
HEX 4	32	0.2	0.232	0.306	0.957
HEX 5	31.2	0.2	0.231	0.306	0.980
HEX 6	32.7	0.2	0.233	0.307	0.938
HEX 7	34.4	0.2	0.234	0.308	0.896

Descriptions	Tho	RTD accuracy	DT500 accuracy	Absolute uncertainty, ΔT	Relative uncertainty, ΔT/T
		± 0.2 °C	± 0.1%	±	%
HEX 1	21.8	0.20	0.222	0.299	1.370
HEX 2	20	0.20	0.220	0.297	1.487
HEX 3	22.2	0.20	0.222	0.299	1.347
HEX 4	30.1	0.20	0.230	0.305	1.013
HEX 5	30.8	0.20	0.231	0.305	0.992
HEX 6	31.3	0.20	0.231	0.306	0.977
HEX 7	32.4	0.20	0.232	0.307	0.946

Individual HEX (1-7) temperature difference estimation

Descriptions	Thi	ΔThi	Tho	ΔTho	Absolute uncertainty, ΔDT,Tco-Tci	Ideal DT, (Thi-Tho)
		±		±	±	
HEX 1	23.6	0.300	21.8	0.299	0.423	1.8
HEX 2	26.8	0.302	20	0.297	0.424	6.8
HEX 3	28.2	0.303	22.2	0.299	0.426	6.0
HEX 4	32	0.306	30.1	0.305	0.432	1.9
HEX 5	31.8	0.306	30.8	0.305	0.432	1.0
HEX 6	32.7	0.307	31.3	0.306	0.433	1.4
HEX 7	34.4	0.308	32.4	0.307	0.435	2.0

HEX temperature difference estimation

Tci	ΔTci	Tco	ΔTco	Absolute uncertainty, ΔDT,Tco-Tci	Ideal DT, (Tco-Tci)	Relative uncertainty, ΔDT/DT
	±		±	±		± %
15.4	0.294	35.1	0.309	0.43	19.7	2.2

Solar Pond temperature difference

T_{UCZ}=Tci	ΔT_{UCZ}=Tci	T_{LCZ}	ΔT_{LCZ}	Absolute uncertainty, ΔDT,Tco-Tci	Ideal DT, (Tco-Tci)	Relative uncertainty, ΔDT/DT
	±		±	±		± %
15.4	0.294	40.5	0.454	0.5	25.1	2.2

Heat Extracted

mdot	mdot , mL/s	Absolute uncertainty, mdot	Cp	DT_{HEX}	Absolute uncertainty, DT	Absolute Uncertainty, mdot*DT
		±			±	±
HEX_system	12.37	0.32	4180	19.7	0.42	0.531
HEX 1	31.19	0.12	4180	1.8	0.42	0.442
HEX 2	17.67	0.20	4180	6.8	0.43	0.469
HEX 3	24.26	0.15	4180	6.0	0.43	0.458
HEX 4	30.11	0.12	4180	1.9	0.43	0.448
HEX 5	34.09	0.11	4180	1.0	0.43	0.448
HEX 6	35.99	0.11	4180	1.4	0.43	0.449
HEX 7	34.89	0.15	4180	2.0	0.00	0.146

4. Thermosiphon experiments

Temperature measurement, Tci

Descriptions	Temperature, T, ^{o}C	RTD accuracy	DT800 accuracy	Absolute uncertainty, ΔT	Relative uncertainty, ΔT/T
		± 0.2 ^{o}C	± 0.2%	±	%
mdot1	17	0.2	0.234	0.308	1.81
mdot2	17.6	0.2	0.235	0.309	1.75
mdot3	17.5	0.3	0.235	0.381	2.18
mdot4	17.5	0.2	0.235	0.309	1.76
mdot5	17.5	0.2	0.235	0.309	1.76
mdot6	16.6	0.2	0.233	0.307	1.85

Temperature measurement, Tco

Descriptions	Temperature, T, ^{o}C	RTD accuracy	DT800 accuracy	Absolute uncertainty, ΔT	Relative uncertainty, ΔT/T
		± 0.2 ^{o}C	± 0.2%	±	%
mdot1	33.3	0.2	0.267	0.333	1.00
mdot2	31.3	0.2	0.263	0.330	1.05
mdot3	26.8	0.3	0.254	0.393	1.47
mdot4	25	0.2	0.250	0.320	1.28
mdot5	22	0.2	0.244	0.315	1.43
mdot6	20.2	0.2	0.240	0.313	1.55

Temperature measurement, Thi

mdot	Temperature, T, ^{o}C	RTD accuracy	DT800 accuracy	Absolute uncertainty, ΔT	Relative uncertainty, ΔT/T
		± 0.2 ^{o}C	± 0.2%	±	%
0.033	39.6	0.2	0.279	0.343	0.87
0.038	38.2	0.2	0.276	0.341	0.89
0.047	36.7	0.3	0.273	0.406	1.11
0.067	34.1	0.2	0.268	0.335	0.98
0.102	32.3	0.2	0.265	0.332	1.03
0.125	31.1	0.2	0.262	0.330	1.06

Temperature measurement, Tho

mdot	Temperature, T, ^{o}C	RTD accuracy	DT800 accuracy	Absolute uncertainty, ΔT	Relative uncertainty, ΔT/T
		± 0.2 ^{o}C	± 0.2%	±	%
0.033	38.4	0.2	0.277	0.341	0.89
0.038	37	0.2	0.274	0.339	0.92
0.047	35.5	0.3	0.271	0.404	1.14
0.067	32.9	0.2	0.266	0.333	1.01
0.102	31.1	0.2	0.262	0.330	1.06
0.125	30	0.2	0.260	0.328	1.09

Temperature difference estimation, DTc

mdot	Tci	ΔTci	Tco	ΔTco	Absolute uncertainty, ΔDT	Ideal DT, (Tco-Tci)	Relative uncertainty, ΔDT/DT
	±		±	±			± %
0.033	17.0	0.31	33.3	0.33	0.45	16.3	2.78
0.038	17.6	0.31	31.3	0.33	0.45	13.7	3.30
0.047	17.5	0.38	26.8	0.39	0.55	9.3	5.88
0.067	17.5	0.31	25.0	0.32	0.44	7.5	5.93
0.102	17.5	0.31	22.0	0.32	0.44	4.5	9.81
0.125	16.6	0.31	20.2	0.31	0.44	3.6	12.18

Temperature difference estimation, DTh

mdot	Thi	ΔThi	Tho	ΔTho	Absolute uncertainty, ΔDT	Ideal DT, (Thi-Tho)	Relative uncertainty, ΔDT/DT
		±		±	±		± %
0.033	39.6	0.34	38.4	0.34	0.48	1.2	40.36
0.038	38.2	0.34	37.0	0.34	0.48	1.2	40.09
0.047	36.7	0.41	35.5	0.40	0.57	1.2	47.74
0.067	34.1	0.33	32.9	0.33	0.47	1.2	39.32
0.102	32.3	0.33	31.1	0.33	0.47	1.2	38.98
0.125	31.1	0.33	30.0	0.33	0.47	1.1	42.28

Flow rate measurement

Volume, L	Measuring cylinder accuracy	Time, s	Stop watch accuracy	Absolute uncertainty, Δmdot,L/s	Ideal mass flow rate, mdot, L/s	Relative uncertainty, Δmdot/mdot
	± 0.01 L		± 1%	±		± %
0.69	0.01	21	0.21	0.018	0.033	53.20
0.99	0.01	26	0.26	0.014	0.038	37.44
0.94	0.01	20	0.20	0.015	0.047	31.06
0.86	0.01	15	0.15	0.015	0.057	27.00
0.87	0.01	8.5	0.09	0.015	0.102	14.97
0.84	0.01	6.7	0.07	0.016	0.125	12.47

Hot water velocity, U hot

Description	U hot, m/s	Travel distance, m	Scale accuracy	Time, s	Stop watch accuracy	Video camera accuracy	Absolute uncertainty, ΔU
			± 0.01 m		± 1%	± 1%	±
0.033	0.0580	0.2	0.002	3.45	0.0345	0.00058	0.0173
0.038	0.0580	0.2	0.002	3.45	0.0345	0.00058	0.0173
0.047	0.0595	0.2	0.002	3.36	0.0336	0.00060	0.0173
0.067	0.0602	0.2	0.002	3.32	0.0332	0.00060	0.0173
0.102	0.0578	0.2	0.002	3.46	0.0346	0.00058	0.0173
0.125	0.0557	0.2	0.002	3.59	0.0359	0.00056	0.0173

Heat Extracted, mdot cold

mdot cold, L/s	Absolute uncertainty, mdot cold	Cp	DTc	Absolute uncertainty, DTc	Absolute Uncertainty, Qdot cold, ΔW	Ideal mdot
	±			± %	±	
0.033	0.018	4180	16.3	0.45	0.454	2248.4
0.038	0.014	4180	13.7	0.45	0.452	2176.1
0.047	0.015	4180	9.3	0.55	0.547	1827.1
0.067	0.015	4180	7.5	0.44	0.445	2100.5
0.102	0.015	4180	4.5	0.44	0.442	1918.6
0.125	0.016	4180	3.6	0.44	0.439	1881.0